UNIVERSITÀ DEL SALENTO

FACOLTÀ DI SCIENZE MM. FF. NN.
DIPARTIMENTO DI FISICA

Ph.D. Thesis

COULOMB-FRUSTRATED PHASE-SEPARATION

Carmine Ortix

Advisors: Prof. Matteo Beccaria
Prof. Carlo Di Castro
Dr. José Lorenzana

Contents

A mio padre

Chapter 1

Introduction

A large variety of physical-chemical systems with competing short and long range interactions self organizes in domain patterns [for a review see [1]]. Examples range from ferromagnetic systems [2, 3] to diblock copolymers [4]. Inhomogeneous states display a simple set of predominant morphologies of some degree of regularity like circular droplets ("bubbles") and stripes in two-dimensional (2D) systems [see Fig. 1.1], and layers, cylindrical rods and spherical droplets embedded in a three-dimensional (3D) matrix. The characteristic scale of the domains can vary from mesoscopic scales of hundreds of angstroms as in films of block copolymers [5] to as much of centimeters in ferrofluids [6].

Magnetic domains were first discovered by Weiss who suggested their existence in ferromagnets. He proposed that a large number, typically $10^{12} - 10^{18}$, of atomic magnetic moments were aligned parallel. The direction of alignment varies from domain to domain in a more or less random manner although certain crystallographic axes, namely easy axes, may be preferred by the magnetic moments. The geometrical

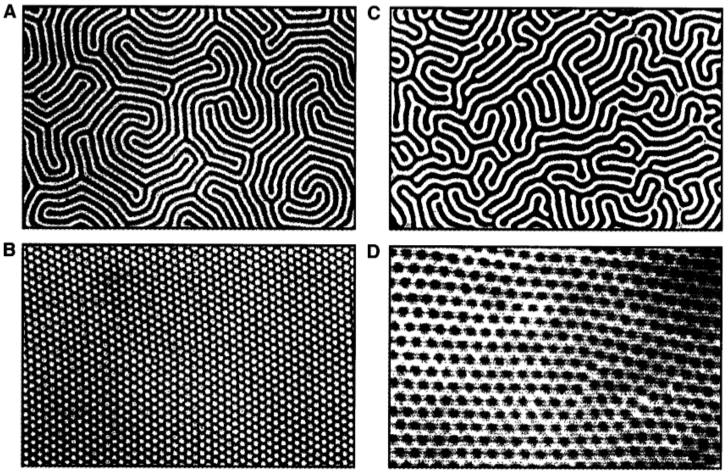

Figure 1.1: Mesoscopic domains in magnetic solid (A,B) and fluid (C,D) films. [Adapted from Ref.[1]].The panel *A* and *C* show stripe phase with labyrinth-like patterns. Bubble phases are shown in *B* and *D*. The period of the domains is in the μm scale.

configurations of the domains were first discussed theoretically by Landau and Lifshitz [7]. Short range forces in a ferromagnet favor one particular direction for the electron spins, up or down in an Ising ferromagnet. However the fully polarized phase has a large energy cost due to the long range dipolar interactions which get minimized when the field generated by the sample is made as small as possible. Domains appear as a compromise where these competing forces are optimized.

From a thermodynamic point of view a density driven first order transition, like the liquid vapor transition, behaves in many aspects analogously to an Ising ferromagnet identifying magnetization with density, and the up and down phases with liquid and vapor. Electrons in a solid can also exhibit first order transitions like the liquid gas transition and are subject, of course, to the long range Coulomb interaction, thus it is natural to ask if domains can appear. To our knowledge the first to suggest this possibility was Nagaev in connections with doped magnetic semiconductors [8]. A similar phenomena has been suggested to occur in neutron star matter [9].

In electronic systems, this idea has gain momentum in recent years due to theoretical and experimental studies in materials like cuprates and manganites. It has become clear that strong electron correlations generally produce a tendency towards phase separation in electron-poor and electron-rich regions [10, 11, 12, 13, 8, 14, 15, 16, 17, 18, 19, 20, 21, 22, 23, 24, 25, 26, 27, 28]. Still, a macroscopic charge imbalance would imply an electrostatic energy cost that grows faster than the volume in the thermodynamic limit. Thus, in analogy with ferromagnetic domains, one can expect charge poor and charge rich domains in order to guarantee large-scale neutrality. In this way, the charge is segregated over some characteristic distance but the average density at large distances is constant. This has been proposed in a variety of electronic systems [13, 8, 15, 16, 29, 30, 31, 32].

From the experimental point of view, the research in the field is in its infancy. There are no good probes of electron density specially at mesoscopic distances. In recent years, a prominent emergent tool has been scanning tunneling microscopy (STM) which allows to sense local variations of the density of states. Hoping that these are coupled to density fluctuations, experimentalist have tried to determine charge variations in different systems. Interesting systems are colossal magnetoresistant manganites. STM experiments in thin films [22] have revealed domains with filamentary and droplike metallic and/or insulating regions in the scale of tens to thousands of nanometers with smooth surfaces [see Fig. 1.2 very similar in morphology to the domains of the classical systems. In addition, percolation of the metallic

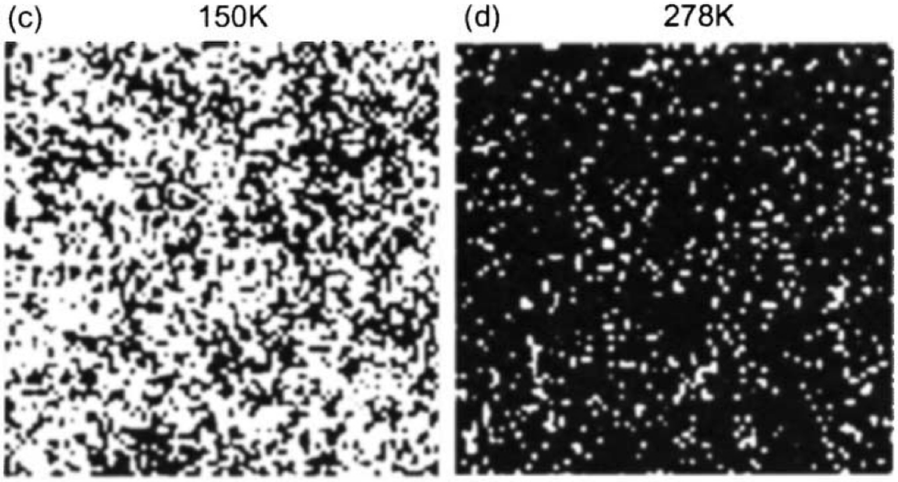

Figure 1.2: Coexisting metallic (white) and insulating (black) domains observed with scanning tunneling spectroscopy in thin films of the perovskite manganite $La_{0.7}Sr_{0.3}MnO_3$ [Adapted from [22]]. The area of the insulating regions grows with temperature approaching the transition from the metallic ferromagnetic low temperature phase to the insulating paramagnetic high temperature phase.

regions is closely correlated to abrupt changes in transport which suggests that frustrated phase separation is at the heart of the colossal magnetoresistence behavior [22, 33]. Interestingly also neutron and X-ray scattering, which couple indirectly to the charge through lattice distortions, has revealed (much smaller) clusters on the nanometer scale, in the bulk.[34, 14, 35, 36]

In cuprates, as in manganites, the situation is complex and different inhomogeneities have been reported at different length scales. At a scale of $\sim 10nm \sim 20$ lattice constants, the system appears to segregate into a pseudogap or underdoped phase with a large gap and a superconducting phase with a smaller gap with smooth interfaces in between [21] [see Fig. 1.3]. This is consistent with Coulomb frustrated phase separation between an underdoped pseudogap phase and an overdoped phase [37]. This scenario has been reproposed on the light of recent neutron scattering

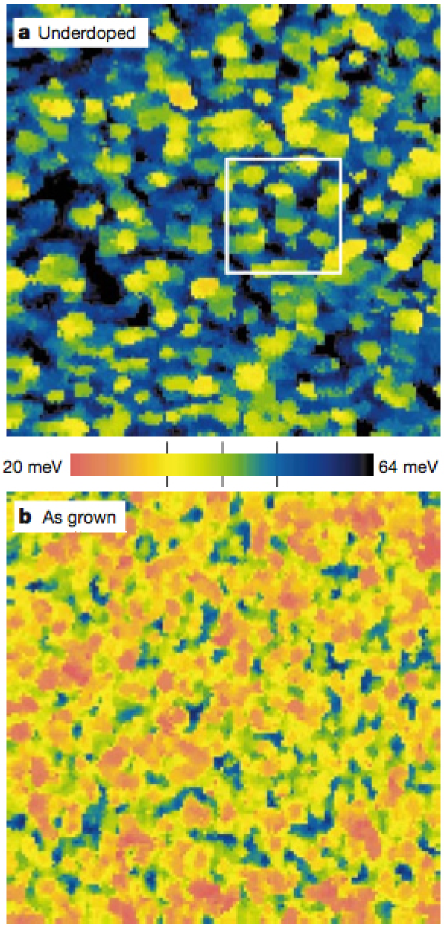

Figure 1.3: Gap maps in the high-temperature superconductor Bi-2212 obtained from scanning tunneling microscopy [Adapted from Ref.[21]]. The top (bottom) panel indicates the map for an underdoped (overdoped) sample. The superconducting nanopatches correspond to smaller gap region.

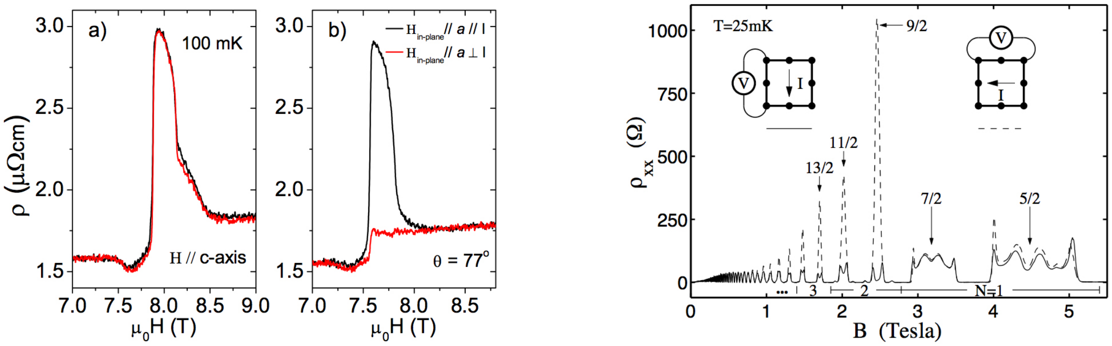

Figure 1.4: Left: The in-plane resistivity tensor in Sr_3 Ru $_2O_7$ [Adapted from Ref.[39]]. Notice the anisotropy in the resistivity occurring when a tilted magnetic field is applied. Right: Anisotropy in the resistivity of an high-mobility GaAs/AlGaAs heterostructure [Adapted from Ref.[40]]. The two traces correspond to different current directions in the sample. The anisotropy is manifested in the high-Landau level $N = 2$ at the filling fraction $\nu = 9/2$.

experiments [38].

Recently a strong transport anisotropy in ultra clean Sr_3 Ru $_2O_7$ samples have been observed in the vicinity of a metamagnetic quantum critical point [39]. From an electronic point of view, this is a layered material and the phenomena can be explained if the system is assumed to segregate in electronic stripe domains which break the C_4 symmetry of the lattice and orient with a small perturbing field generating by a small tilting of the sample with respect to the control field. This is also consistent with the proposal of exotic electronic liquid phase analogue [41] to the intermediate order states of liquid crystals [42]. The idea that the domains in Sr_3 Ru $_2O_7$ are due to frustrated phase separation has already been put forward [43].

The phenomenology of ruthanates has a strong similarity to that observed in GaAs heterostructures. Several magneto-transport anisotropies arise when the Fermi level lies near the middle of a highly excited Landau level [right panel of Fig. 1.4] [40]. It

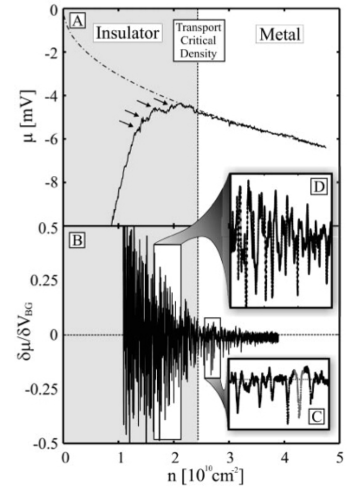

Figure 1.5: Density dependence of the chemical potential (top panel) of a two-dimensional hole gas as obtained in Ref.[18] across the metal-insulator transition. Above the transition density the chemical potential follows the Hartree-Fock prediction. In the insulating side, many small steps arises corresponding to spikes in the inverse electronic compressibility (bottom panel).

has been proposed [44] that in a clean two-dimensional electron gas (2DEG) in high Landau levels, a uniform phase would be unstable against a charge density striped phase where the electron density alternates between zero and full-filling.

Evidences for inhomogeneous states have also been reported in the 2DEG at zero magnetic field. Using a local probe, Ilani and collaborators [18, 17] have shown that close to the still debated Metal-Insulator transition (MIT) [45, 46, 47], mesoscopic inhomogeneities appear. In addition thermodynamic measuraments have shown that close to the MIT the compressibility departs sharply from the predictions of an homogeneous electron gas [48, 49, 50, 51, 17, 18].

Another interesting finding is the appearance of negative spikes in the electronic compressibility [see Fig. 1.5] [18] which indicate that the transition from the homogeneous state to the inhomogeneous state is discontinuous as found theoretically for a metal-insulator striped Coulomb frustrated phase separated state[52, 53]. The main difference between the theoretical result [52] and the experiment [18], is that in Coulomb frustrated phase separation, there is a single large step at the transition from the homogeneous metallic phase to the striped phase whereas Ilani *et al.* find many small steps around the critical density. This behavior is easy to rationalize if one considers that in the presence of disorder, the density will not be uniform in the entire sample. A distribution of critical densities and fragmentation of the large step in many small steps will be naturally produced. The minimum step size will be given by the appearance of a single domain.

This leads us to the problem of disorder, another possible route by itself to charge segregation. As emphasized by Dagotto and collaborators[54, 55] in the context of manganites disorder close to a density driven first order first transition can also induce charge segregation. The physics is well known since the work of Imry and Ma on the random field Ising model. In the case of strong disorder, we expect domains to be much less regular than for Coulomb frustrated phase separation. Interestingly, also irregular patterns have been observed in manganites [56].

It is not clear at the moment which of the two mechanism (quenched disorder or short and long range forces) is dominant to determine each of the anomalous properties of complex electronic systems and more theoretical and experimental work is needed. Probably both mechanism are important but to understand the phenomenology in the clean limit, which is the main objective of this thesis, is certainly a prerequisite to understand the more complex disordered case.

It is also of interest to mention that, even in the absence of quenched disorder, the complexity of the energy landscape of frustrated phase separation models, can make the ordered ground state unreachable leading to a glassy state [57].

As in classical systems, one expects that equilibrium patterns displaying common structural features can be described by simple models which neglect the specific details of the microscopic structure of each system capturing their general properties.

Since domains in these systems have often mesoscopic scales of several lattice constants, general aspects of the phenomena can be analyzed within a coarse grained approach. In this case, tendency to phase separation is recognized by the appearance of anomalies in the electronic contribution to the coarse grained energy of a system. In this thesis we study the formation of electronic inhomogeneities resulting from Coulomb frustrated phase separation considering two kind of anomalies that are often encountered in strongly correlated electronic systems. The first situation is determined by a negative compressibility density region. A notorious example is the uniform electron gas at low density[58] but this feature appears in several other models including the Hubbard model in infinite dimensions [27], the Falicov Kimball model [59], cuprates models [16, 60], manganites models [61, 62, 63], semiconductors heterostructures [64] and in neutron star matter [9]. As we will show in Chapter 2, this feature leads to mesoscopic phase coexistence when long-range Coulomb interactions are taken into account. We are specially interested in the nature of the transition (first or second order) leading to a charge inhomogeneous state which has not been clarified before. A complete discussion will be addressed in Chapter 3. This is a general important question and assumes a relevant importance in metallic systems where the existence of a second-order quantum critical point from a homogeneous phase to an inhomogeneous one can destroy the Fermi liquid behavior [16]. Another possibility is that the inverse electronic compressibility has a point with a Dirac-delta-like negative divergence. This happens when the free energies of two states which are separated by a barrier, cross each other leading to a cusp singularity. An example is also provided by the uniform electron gas. Indeed, numerical simulations showed that in a uniform electron gas, the Wigner crystal and the Fermi liquid homogeneous phase free energies cross at some density [65]. The same feature appears in several models including manganites [66, 28]. In Chapter 2, we show that for weak Coulomb interactions, a universal picture can be achieved and the main properties of inhomogeneous states are irrespective of the specific modeling of the competing phases. On the contrary, at strong Coulomb couplings, the phenomenology of mesoscopic domains strongly depends upon the particular anomaly in the compressibility and two universality classes then arises [67]. In the negative compressibility class (Chapter 3), the transition is generically first order both in three- and two-dimensional systems except for a liquid-gas-like critical point where the transition is driven by a charge-susceptibility divergence [68]. The scenario changes when strong anisotropies are taken into account. Indeed, if charge modulations are restricted to a preferential direction, both first-order and second-order transitions are allowed separated by a tricritical point. The phenomenology of the systems with a cusp singularity, instead, points to a major role covered by the system dimensionality. Two-dimensional systems displays a more pronounced tendency towards phase separation than three-dimensional ones [69].

In the inhomogeneous phase region, the typical size of the domains, are determined by the competition between the long-range Coulomb interaction and the surface energy. The latter is usually determined by short-range effects. We show in Chapter 4 how to extend the concept of surface energy in three-dimensional Coulomb systems. We show that the inclusion of long-range forces leads to a new term due to the interaction between the local electric field at the interface with the dipole layer.

Chapter 2

Modeling Coulomb-frustrated phase separation

In this chapter we discuss two different mechanisms producing tendency towards phase separation (Sec. 2.1) and introduce the related coarse grained models of Coulomb frustrated phase separation (Sec. 2.2). In Sec. 2.3 we discuss the basic length scales of the problem leaving Sec. 2.4 for a discussion of the main properties of phase-segregated states for weak Coulomb interaction where a unified picture can be achieved. A large portion of this chapter has appeared in Ref. [67].

2.1 The scenarios behind mesoscopic phase separation

The tendency towards a phase segregated state of matter is manifested by a thermodynamic instability of the homogeneous phase of a system. Usually, thermodynamic stability criteria are formulated by referring to the availability [70, 71] of a system immersed in a bath of fixed temperature T_0 and subject to an external pressure p_0 defined as: $A = U - T_0 S + p_0 V$ where S and V indicates respectively the entropy and the volume of the system alone and U is its internal energy. In a thermodynamic equilibrium state A takes a minimum. The pressure and temperature of the system then satisfy $T = T_0$ and $p = p_0$. This means that the system is in equilibrium with the bath and cannot act as a source of work for an ideal Carnot machine. Thus, deviations for any infinitesimal change from the equilibrium state must be positive. By working at constant temperature this implies

$$\delta A = \frac{1}{2}\frac{1}{k_T V}\delta V^2 > 0 \tag{2.1}$$

as easily follows by expanding in a Taylor series the internal energy U to second order around the equilibrium point. Notice that we introduced the isotherm compressibility as $k_T = -(\partial V/\partial p)_T/V$ to emphasize that, at fixed temperature, a positive compressibility is a necessary condition to guarantee the stability of the system in its homogeneous phase. In the following we will introduce two possible scenarios where the appearance of a negative compressibility instability drives the system towards the phase segregation mechanism.

- *Negative compressibility density region*

Let us begin by assuming the density dependence of the free energy density $f(n)$ and its first derivative to be continuous everywhere. In the unstable negative compressibility region, the inclusion of higher order terms in the internal energy expansion [71] provides a double-well form as shown schematically in Fig. 2.1. In a finite window of

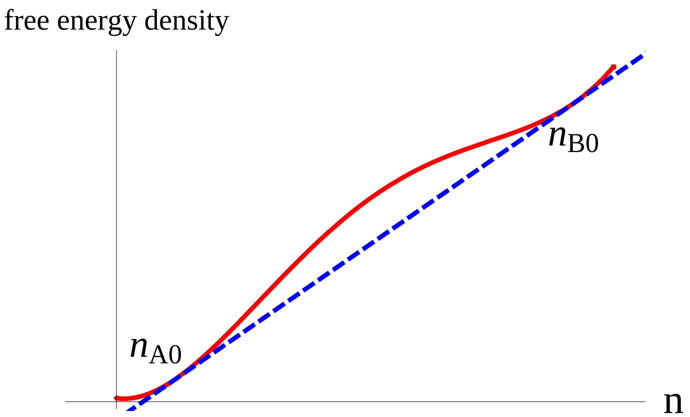

Figure 2.1: Sketch of the free energy density of a system unstable towards phase separation with a negative compressibility density region. The dashed line indicates the energy of a phase separated state with local density composition $n_{A\,0}$ and $n_{B\,0}$.

densities, the negative inverse short-range compressibility [1] $\kappa^{-1} = \partial^2 f/\partial n^2$ yields the system to be locally unstable against spinodal decomposition [42]. Outside this "miscibility" gap [72], whose extremes correspond to the spinodal densities with $\kappa^{-1} = 0$, the homogeneous phase of the system is locally stable because of the positiveness of the curvature of the free energy. Now, let us assume that we are dealing with an ideal neutral system of average density $\overline{n} = N/V$. We want to show that, in a certain range of densities, the energy of the system can be lowered by segregation in two macroscopic regions with local densities $n_{A\,0}$ and $n_{B\,0}$ with $n_{B\,0} > \overline{n} > n_{A\,0}$. The total free energy density then reads:

$$f_{PS} = (1-\nu)\, f(n_{A\,0}) + \nu f(n_{B\,0}) \tag{2.2}$$

---

[1] We caution that hereafter we will refer to the short-range compressibility κ that is related to the usual isotherm compressibility k_T through $\kappa = k_T n^2$.

where ν is the volume fraction in the high density $n_{B\,0}$ phase and the additional constraint

$$\overline{n} = (1-\nu)\, n_{A\,0} + \nu n_{B\,0} \tag{2.3}$$

relates the local densities of the coexisting phases to the average density of the system. Minimization of the phase separated free energy Eq. (2.2) under the condition Eq. (2.3) with respect to $n_{A\,0}$ and $n_{B\,0}$ gives:

$$\mu(n_{B\,0}) \equiv \mu(n_{A\,0}) \equiv \frac{f\,(n_{B\,0}) - f\,(n_{A\,0})}{n_{B\,0} - n_{A\,0}} \tag{2.4}$$

where $\mu = \partial f/\partial n$ indicates the chemical potential of the homogeneous phase. The solution to these equations can be find graphically with the Maxwell or "tangent" construction that is illustrated schematically with the dashed line in Fig. 2.1. The line connecting the two local densities is tangential to the free energy of the homogeneous phase (the full line of Fig. 2.1) and determines $n_{A\,0}$ and $n_{B\,0}$. The free energy of the mixture is given by the value of the line at $\overline{n}$ and is obviously lower than the uniform energy $f(\overline{n})$ in all the range $n_{A\,0} < \overline{n} < n_{B\,0}$. The coexistence equations do not change if a constant is added to the free energies. They are also invariant with respect to the addition of a term linear in density $\mu_0 n$ since it has the only effect to shift the origin of the chemical potential scale. This invariance also persists in the presence of the Coulomb interactions and will be used to simplify the models defined in Sec. 2.2.1. Between the spinodal points and the Maxwell construction densities, a "metastable" region of densities forms, where the homogeneous state of the system is globally unstable because the total free energy density of a phase separated state has lower energy but is locally stable to small density fluctuations. We will augment a free energy of this kind with the long-range Coulomb interaction in Sec. 2.2.1.

- *Dirac-delta-like negative compressibility divergence*

Along a different route, we assume that the minimal free energy of a homogeneous phase has an upward cusp singularity at a reference density n_c and, as a result, a Dirac-delta-like negative divergence in the short-range compressibility κ (see Fig. 2.2). This occurs in systems undergoing a putative direct density driven first-order phase transition [73, 72], in which case the system switches at n_c from one A-phase to another B-phase not continuously connected to the first one in the space of the macroscopic thermodynamic variables of the system. The negative divergence of the compressibility at the reference density n_c drives the system towards phase segregation. Indeed in the neutral case the free energy of a phase separated state as ruled by the Maxwell construction Eq. (2.4) represents a minimal free energy. An important feature differentiating the cusp singularity scenario depicted in Fig. 2.2 from the negative compressibility density region case, is the absence of a miscibility gap (except for the reference density n_c) unstable towards spinodal decomposition. Mixed scenarios in which the cusp singularity is accompanied by a density region unstable towards spinodal decomposition are possible but will not be considered in this thesis.

One can capture the above depicted situations with tendency towards phase segregation, by expanding the free energy around a reference density n_c as

$$f_\gamma = \alpha \left| n - n_c \right|^\gamma + \beta \left(n - n_c \right)^{2\gamma} \tag{2.5}$$

where we have subtracted the constant and the linear term corresponding to the Maxwell-construction line according to the previous discussion. Obviously we need $\alpha < 0$ for the tendency to phase separation to occur and $\beta > 0$ is essential to provide

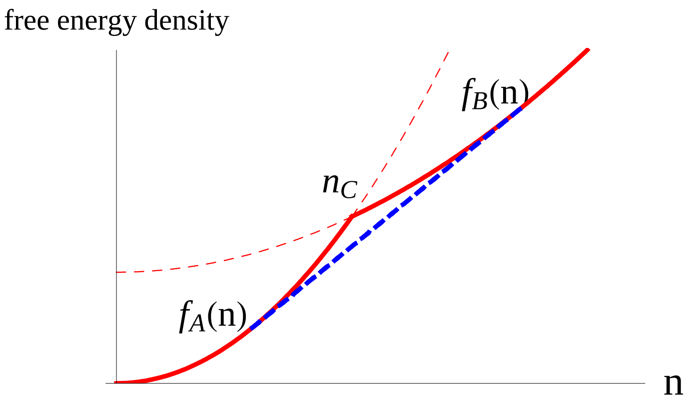

Figure 2.2: Sketch of the behavior of the free energy of a system with a cusp singularity at n_c. The system switches from an A-phase to a B-phase with an upward cusp singularity in the total free energy. The thin dashed lines indicate the metastable density regions of the two competing phases. Finally the thick dashed line is the free energy of the phase separated state as ruled by the Maxwell construction.

a double-well form of the free energy. Finally $\gamma = 2$ indicates a system with a negative compressibility density region whereas $\gamma = 1$ corresponds to the cusp singularity model. Notice that in the free energy expansion Eq. (2.5) we are assuming the same short-range compressibility κ for either $n > n_c$ and $n < n_c$. Of course, one can also consider asymmetric situations by adding cubic terms. Such asymmetry does not change the physics substantially and will be neglected for simplicity. The exception is the important case of an incompressible "insulating" phase coexisting with a compressible "metallic" phase. This limiting case constitutes a different universality class and will be discussed to some extent in Chapter 5. A full treatment can be found in Ref.[31] in three-dimensional systems and in Ref.[52, 53] in two-dimensional systems.

In the Maxwell-construction picture, the behavior of both $\gamma = 1$ and $\gamma = 2$ systems is identical. The local densities of the coexisting regions are determined by the minima of the double-well $n_{A\,0} = n_c - \Delta n_0/2$ and $n_{B\,0} = n_c + \Delta n_0/2$ ($\Delta n_0 = 2\left[|\alpha/(2\beta)\right]^{1/\gamma}$).

Because of the segregation at local densities different from the average one $\overline{n}$, the systems acquires a phase separation energy gain equal to the height of the double-well barrier $f_0 = \alpha^2/(4\beta)$ for $\overline{n} = n_c$. This gives the scale for the typical phase separation energy gain which plays a fundamental role in this thesis.

2.2 Coarse grained models of Coulomb-frustrated phase separation

Since now, we have dealt with ideal neutral systems where macroscopic phase separation is determined by the Maxwell construction. In electronic systems, this behavior is drastically changed by the presence of the long-range Coulomb interaction. There are several ways of introducing charging effects in the phase coexistence phenomenon. For example the electronic charge density can be coupled to the square of an order parameter as relevant in systems with Jahn-Teller interactions [74]. In this section, we introduce two models that are able to provide a full analysis of Coulomb frustrated phase separation in systems where tendency towards charge segregation is induced respectively by a Dirac-delta-like negative divergence in the short-range electronic compressibility [$\gamma = 1$ in Eq. (2.5)] and by a negative compressibility density region [$\gamma = 2$ in Eq. (2.5)]. The "fluid" of the previous section is now considered to be charged. Thus the models are supplemented by the long-range Coulomb interaction. A rigid background is added to ensure charge neutrality.

2.2.1 The negative compressibility model

Coulomb frustrated phase separation in systems with a negative compressibility density range can be analyzed by introducing a model where the electronic charge density plays the role of a scalar order parameter in a analogous way as the liquid-gas transition of classical fluids. The Hamiltonian reads:

$$H_2 = \int d^D x \left[\alpha \Delta n^2 + \beta \Delta n^4 + c |\nabla n(\mathbf{x})|^2 + \frac{e^2}{2\varepsilon_0} \int d^D x' \frac{[n(\mathbf{x}) - \overline{n}]\,[n(\mathbf{x}') - \overline{n}]}{|\mathbf{x} - \mathbf{x}'|} \right] \tag{2.6}$$

Here ε_0 is the dielectric constant due to the degrees of freedom not included in the model, $\overline{n}$ is the average charge coinciding with minus the density of the rigid background to ensure charge neutrality and $\Delta n = n - n_c$ is the electronic density deviation from the reference density. The reference density can be fine tuned so as to eliminate a small cubic term. Finally the gradient term models the surface energy of smooth interfaces and is parameterized by the stiffness constant c. This model (or closely related variants) has been used to describe inhomogeneities in a variety of systems [57, 75, 15, 76, 4] including mixtures of block copolymers [4], charged colloids in polymeric solutions [75] and electronic systems [15, 57]. A full treatment of the model Eq. (2.6) in the case of D-dimensional systems subject to a weak D-dimensional Coulomb interaction has been provided by Muratov [32].

Eq. (2.6) has several free parameters ($\alpha\,, \beta\,, c\,, etc.$). For the future discussion, it is useful to define also a dimensionless form where the parameter space is drastically reduced. We thus measure lengths in units of $\xi = \sqrt{2c/\alpha}$, and define a dimensionless density $\phi(x) = 2\Delta n(x)/\Delta n^0$ and measure energy in units of $f_0 \xi^D$. Thus, apart from an irrelevant constant, we are left with the following hamiltonian:

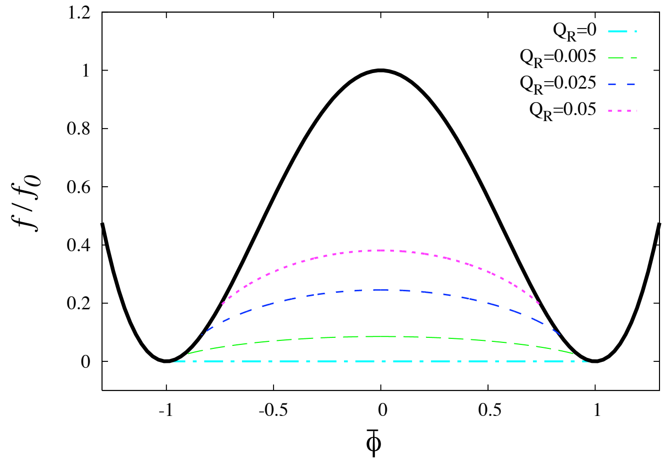

Figure 2.3: Behavior of the free energy densities for electronic uniform phases Eq. (2.7). The dashed lines are the exact energies of layered inhomogeneities for different values of the frustrating parameter. The short-long dashed line corresponds to the Maxwell construction ($Q_R = 0$).

$$\widetilde{H}_2 = \int d^D x \left[\left(\phi(\mathbf{x})^2 - 1\right)^2 + |\nabla\phi(\mathbf{x})|^2 + \frac{Q_R^2}{2} \int d^D x' \frac{\left[\phi\left(\mathbf{x}\right) - \overline{\phi}\right]\left[\phi\left(\mathbf{x}'\right) - \overline{\phi}\right]}{|\mathbf{x} - \mathbf{x}'|} \right] \quad (2.7)$$

with $\overline{\phi} = 2(\overline{n} - n_c)/\Delta n^0$ and Q_R^2 a rescaled dimensionless Coulomb coupling given by:

$$Q_R^2 = \frac{e^2}{\varepsilon_0} \frac{2\,\xi^{D-1}}{|\alpha|}.$$

We see that the parameter space can be reduced to only two parameters, the dimensionless global density $\overline{\phi}$ and the renormalized coupling Q_R^2. The solution of this model will be discussed in Chapter 3.

2.2.2 The cusp singularity model

To analyze Coulomb frustrated phase separation in systems with a Dirac-delta-like negative compressibility divergence ($\gamma = 1$), it is convenient to introduce an auxiliary field s linearly coupled to the charge and analogous to a Hubbard-Stratonovich variable. Two versions of the model are possible which lead to similar results: s can be taken as a soft spin [73] or a conventional Ising spin with $s = \pm 1$ [69] where the sign distinguishes the two competing phases. We take the latter model which is more straightforward to analyze. It consists of a ferromagnetic Ising model linearly coupled to the local charge:

$$\begin{aligned} H_1 &= -J \sum_{<ij>} (s_i s_j - 1) - |\alpha| \sum_i s_i (N_i - N_c) + \frac{\beta}{a^D} \sum_i (N_i - N_c)^2 \\ &\quad + \frac{e^2}{2\varepsilon_0} \sum_{ij} \frac{\left(N_i - \overline{N}\right)\left(N_j - \overline{N}\right)}{r_{ij}} \end{aligned} \tag{2.8}$$

where $s_i = \pm 1$, the index i runs over the sites of a hypercubic lattice of dimension $D = 2, 3$ with lattice constant a, the N's are dimensionless numbers of particles per site and $\overline{N}$ their average value. The soft version replaces the Ising part with a double well potential [73].

We have written the model on the lattice for clarity but we are interested on the continuum limit of this model with $n(\mathbf{x}) \equiv N_i/a^D$. Uniform phases correspond to a ferromagnetic state in s. Inserting the two possible values of s in Eq. (2.8), one obtains that uniform phases are described by Eq. (2.5) with $\gamma = 1$, i.e. two intersecting parabolas with minima at $\pm\Delta n_0/2$ and a crossing point at n_c (the full lines in Fig. 2.4). In the hard spin case, domain walls of the Ising order parameter are sharp by construction with a surface tension $\sigma = 2J/a^{D-1}$, thus the Ising term can be written as $\sigma\Sigma$ with Σ the total surface of interface among the two phases.

To provide a dimensionless form of the model Eq. (2.8), it is convenient to define, analogously to the negative compressibility model Eq. (2.6), the unit length scale ξ defined as $\xi \equiv 4\sigma\beta/\alpha^2$. This represents the size that inhomogeneities should have

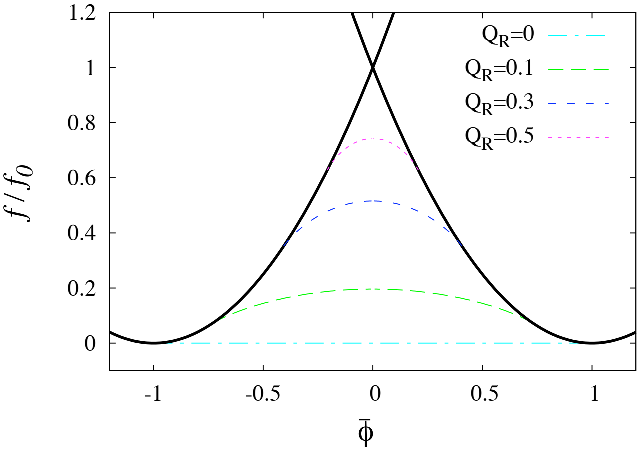

Figure 2.4: Behavior of the free energy densities for the electronic uniform phases Eq. (2.9) and $D = 2$. The dashed lines are the exact energies of stripe inhomogeneities for different values of the frustrating parameter. The short-long dashed line corresponds to the Maxwell construction ($Q_R = 0$).

for the total interface energy to be of the same order as the phase separation energy density gain $\alpha^2/(4\beta)$. As before, we measure the energy in units of $\xi^D\alpha^2/(4\beta)$, lengths in units of ξ and surfaces in units of ξ^{D-1}. In these units $\sigma \equiv 1$ and apart from an irrelevant constant one obtains the following dimensionless hamiltonian:

$$\widetilde{H}_1 = \Sigma + \int d^Dx[\phi(\mathbf{x}) - s(\mathbf{x})]^2 + \frac{Q_R^2}{2}\int d^Dx \int d^Dx' \frac{\left[\phi\left(\mathbf{x}\right) - \overline{\phi}\right]\left[\phi\left(\mathbf{x}'\right) - \overline{\phi}\right]}{|\mathbf{x} - \mathbf{x}'|} \tag{2.9}$$

where

$$Q_R^2 = \frac{e^2}{\varepsilon_0}\frac{\xi^{D-1}}{\beta}$$

As for the model Eq. (2.7), the parameter space is determined by the two dimensionless parameters $\overline{\phi}$ and Q_R. The exact solution for layered inhomogeneities in three-dimensional systems and striped states in two dimensions will be provided in Chapter 5.

2.3 Typical length scales

In the absence of the Coulomb interaction, both models Eqs. (2.7), (2.9) are subject to ordinary phase separation in a range of global densities $|\overline{\phi}| < 1$ as determined by the Maxwell construction shown by the short-long dashed lines in Figs. 2.3, 2.4. The phase-separated state is made up of macroscopic domains with constant local densities $\phi = \pm 1$.

For $Q_R \neq 0$, macroscopic phase separation is precluded since the Coulomb cost grows faster than the volume in the thermodynamic limit and mesoscale domains appear. This follows immediately by dimensional analysis of the models. Indeed, taking $\phi \sim 1$ in the last term of Eqs. (2.7), (2.9), the Coulomb energy density per domain of typical size l_d can be evaluated as:

$$f_{lr} = Q_R^2 \tilde{l}_d^{D-1}$$

where we have defined $\tilde{l}_d \equiv l_d/\xi$ and the integrals have been evaluated in a volume of order $\tilde{l}_d^D$. As anticipated, f_{lr} diverges for $\tilde{l}_d \to \infty$ reflecting the fact that a macroscopic phase separation is avoided in electronic systems. In a mesoscopically phase separated state, a large number of small inhomogeneities minimize the Coulomb energy but they cost too much energy for the system to form domain walls. Indeed the surface energy density goes as:

$$f_\sigma \sim \tilde{l}_d^{-1} \tag{2.10}$$

The competition between interface and charging effects (shown schematically in Fig. 2.5) determines the typical size of the inhomogeneities. The two terms are

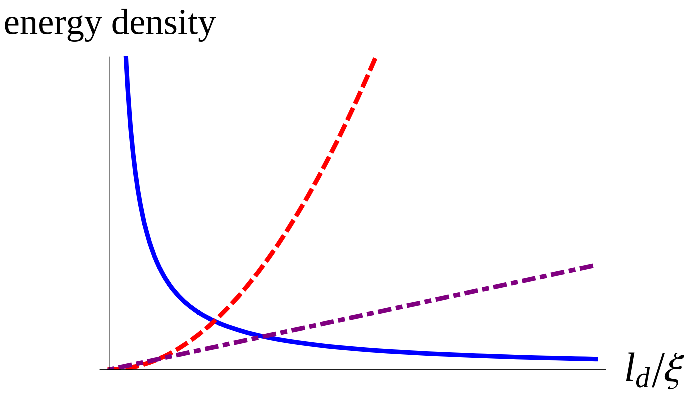

Figure 2.5: Sketch of the competition between interface and charging effects in a mesoscopic phase separated state. The full line shows the behavior of the surface energy while the dashed and the dotted-dashed line indicates the contribution of the Coulomb energy respectively in two- and three-dimensional systems.

optimized at a scale:

$$\tilde{l}_d^D = \frac{1}{Q_R^2}. \tag{2.11}$$

Another important length scale is the screening length of the Coulomb interaction that can be defined for two- and three-dimensional systems as:

$$l_s^{D-1} = \left[\frac{2^{D-1}\pi e^2 \kappa}{\varepsilon_0}\right]^{-1} \tag{2.12}$$

where κ is the characteristic short-range electronic compressibility of the competing homogeneous phases:

$$\kappa = (2\beta)^{-1} \qquad (\gamma = 1) \tag{2.13}$$

$$\kappa = (2|\alpha|)^{-1} \qquad (\gamma = 2) \tag{2.14}$$

For both the above presented models, the characteristic screening length in units of

ξ is given by:

$$\tilde{l}_s^{D-1} \equiv \frac{1}{2^{D-2}\pi Q_R^2} \qquad (\gamma = 1) \tag{2.15}$$

$$\tilde{l}_s^{D-1} \equiv \frac{1}{2^{D-3}\pi Q_R^2} \qquad (\gamma = 2) \tag{2.16}$$

From Eq. (2.11),(2.15),(2.16) it turns out that at weak frustration ($Q_R << 1$) we have the following hierarchy of scales [32]:

$$l_s >> l_d >> \xi. \tag{2.17}$$

This separation of lengths allows for a unified treatment of the frustrated phase separation mechanism at weak frustration that will be discussed in the following section.

On the contrary, at strong frustration we expect the behavior of the models Eqs. (2.7), (2.9) to be radically different leading to two "universality" classes [67]. This can be qualitatively anticipated by considering the $Q_R \to \infty$ limit where only uniform phases are allowed. For the $\gamma = 2$ case, the behavior is analytic as a function of the density whereas for $\gamma = 1$ one has a first-order phase transition at $\overline{n} = n_c$.

2.4 The weak coupling regime

In the weak frustration regime, the effect of long-range forces can be considered as a small perturbation upon the ordinary phase separation mechanism. Thus, mixed states are expected to appear with local densities close to the two minima of the double-well. For systems with $\gamma = 2$, frustrated phase separation can be analyzed by expanding quadratically the free energy around the two densities $\phi = \pm 1$ [2]. Then,

---

[2] For the range of validity of the quadratic expansion of the $\gamma = 2$ model see Appendix C.

the bulk free energies become the same as for the $\gamma = 1$ model. In addition, the hierarchy of length scales Eq. (2.17) for $Q_R << 1$ allows to consider the interface as sharp. A surface tension can be defined by neglecting long-range effects in the interface scale ξ and computing the excess energy of an isolated interface [32]. At this point, the two models become equivalent and the phenomenology of mixed states is depicted in a universal fashion. In addition, a mesoscopically phase separated state can be assumed to be similar to the macroscopically phase separated state of neutral fluids. Thus, the local variation of the charge density inside the domains can be approximately neglected and we can refer to a uniform density approximation (UDA) [29, 30, 31, 52, 69] in which the local density inside the domains can be assumed constant. This also follows from Eq. (2.17) since l_s represents the scale at which the electrostatics imposes charge variations and is much larger than the inhomogeneity scale l_d. We will show in the following chapters, that the UDA gives very accurate results for both two- and three-dimensional systems even beyond the expected range of validity. The low ($n < n_c$) and high ($n > n_c$) density phase will be termed respectively A and B. Defining $\tilde{f} \equiv f/f_0$ the free energy density of a phase separated state can be put as:

$$\tilde{f} = (1-\nu)\,\tilde{f}_A\left(\phi_A\right) + \nu \tilde{f}_B\left(\phi_B\right) + e_{mix} \tag{2.18}$$

ν indicates the volume fraction of the B-phase domains and

$$\begin{aligned} \tilde{f}_A &= \left[\phi_A + 1\right]^2 \\ \tilde{f}_B &= \left[\phi_B - 1\right]^2 \end{aligned}$$

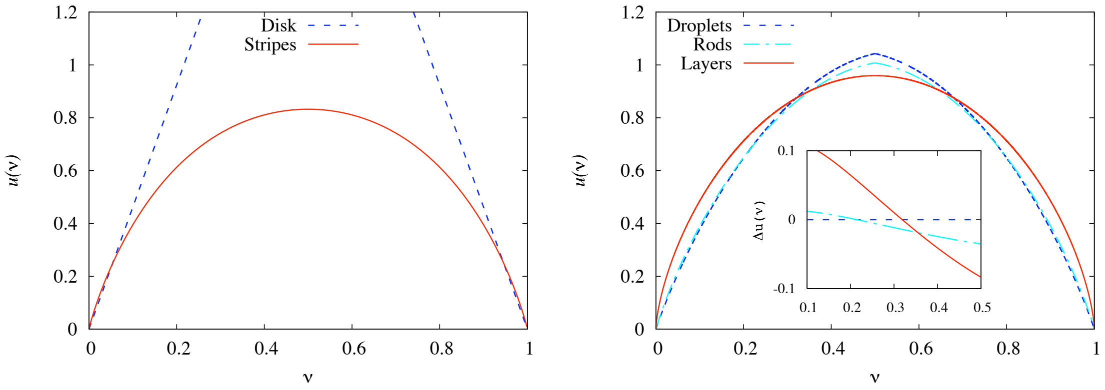

Figure 2.6: The left (right) panel shows the function $u(\nu)$ in two- (three-) dimensional systems for stripes and disks (layers, rods and droplets). For the disk, droplet and rod inhomogeneities, the mixing energy has been computed referring to B-phase inhomogeneities for $\nu < \frac{1}{2}$ while A-phase droplets and rods has been considered for $\nu > \frac{1}{2}$. The inset in the right panel shows the difference in u with respect to the droplet geometry to resolve the crossings between the different morphologies.

Finally, e_{mix} represents the additional energetic cost to form inhomogeneities due to the long-range Coulomb interaction and the interface boundary energy. For a given geometry, it is determined by adding the Coulomb cost and the surface energy cost and optimizing with respect to the dimension of the inhomogeneities as discussed in Appendix B. By the means of the charge-neutrality constraint $\overline{\phi} = (1-\nu)\,\phi_A + \nu\phi_B$, it is possible to eliminate the local densities ϕ_A and ϕ_B in favor of $\overline{\phi}$ and the density deviation $\phi_B - \phi_A$. The mixing energy can be then cast in the suitable simple form:

$$e_{mix} = Q_R^{2/D}\left(\phi_B - \phi_A\right)^{2/D} u(\nu). \tag{2.19}$$

The dependence of the mixed state (MS) free energy upon the morphology of the domains is stored in the function $u(\nu)$. In analogy with the set of morphological structures displayed in classical systems [1], we account in the following for periodic striped structures and disks in two-dimensional systems. Alternating layers, cylindrical rods and spherical droplets are instead considered in three-dimensional systems. In the latter case, $u\left(\nu\right)$ can be easily obtained computing the macroscopic electric field generated by the charged coexisting domains. For rod-like and droplet-like inhomogeneities, this can be achieved by referring to the Wigner-Seitz-approximation (WSA)[77, 13, 58] in which the system is divided respectively in slightly overlapping cylindrical and spherical cells. In Appendix B, we will address a detailed evaluation of these functions. They can be put as:

$$\begin{aligned}
u\left(\nu\right) &= 3^{5/3}{\frac{\pi}{10}}^{1/3}\nu\left[2-3\nu^{1/3}+\nu\right]^{1/3} && \textit{Droplets} \qquad (2.20)\\
u\left(\nu\right) &= 3\nu^{1/3}\left[-\pi\nu^{2}\log\sqrt{\nu}-\frac{\pi}{2}\nu^{2}+\frac{\pi}{2}\nu^{3}\right]^{1/3} && \textit{Rods} \qquad (2.21)\\
u\left(\nu\right) &= {\frac{\pi}{2}}^{1/3}\left[3\nu\left(1-\nu\right)\right]^{2/3} && \textit{Layers} \qquad (2.22)
\end{aligned}$$

These functions appear also in the theory of diblock copolymers [4]. In the right panel of Fig. 2.6, we plot $u(\nu)$ for the different geometries in three-dimensional systems. In the two-dimensional case, we can refer to an approximated evaluation of u where the Coulomb energy cost coincides with the self-energy of a neutral Wigner-Seitz cell *i.e.* neglecting the Coulomb interaction among different cells [52]. The approximated expressions for disks and stripes are given by [c.f. Appendix B]:

$$\begin{aligned}
u\left(\nu\right) &= \frac{8}{\sqrt{3}}\nu && \textit{Disks} \qquad (2.23)\\
u\left(\nu\right) &= 2\sqrt{2}\nu\left(1-\nu\right)\left[-\log\nu\left(1-\nu\right)\right]^{1/2} && \textit{Stripes} \qquad (2.24)
\end{aligned}$$

and are shown in the left panel of Fig. 2.6. The advantage of the UDA approximation is that the mixing energy, that encloses long-range force effects, can be computed independently from the specific modeling of the homogeneous phases free energy. These functions are valid whatever form one choses for $f_{A/B}$.

As shown in Fig. 2.6, droplet-like or disk inhomogeneities are preferred for low volume fractions of the minority phase ($\nu \sim 0$ or $\nu \sim 1$). On the contrary, stripes and layers appear for $\nu \sim \frac{1}{2}$. At intermediate values of ν in three dimensional systems, one finds cylindrical rods. In the diblock copolymer context the control parameter is the volume fraction ν. Here instead the control parameter is the global density $\overline{\phi}$. However for $Q_R << 1$, the volume fraction increases nearly linearly with the global density and the two parameters are practically equivalent. From Fig. 2.6 one sees that there will be a series of morphological transitions that connect droplet states near the homogeneous-MS transitions to the striped mixed state at $\overline{\phi} \sim 0$. In the present approximation, they appear as first order however consideration of more complicated geometries and charge relaxation effects can change this to a smooth evolution of inhomogeneities that could also include "fingering" and elongation of the domains as in classical systems [1]. The stripe and rod phases are expected to behave as a glass in quench experiments [57] with labyrinth-like patterns.

As discussed in Sec. 2.1, f_0 determines the typical scale of phase separation energy gain. e_{mix} is the energy cost due to frustration measured in unit of f_0. To get a typical scale for the energy cost, we evaluate Eq. (2.19) at $\nu = 1/2$ and $\phi_B - \phi_A = 2$ (Maxwell construction). Apart from numerical factors this allows to give another physical interpretation to the frustration parameter:

$$Q_R = \left(\frac{\text{Typical mixing energy cost}}{\text{Typical phase separation energy gain}} \right)^{D/2} .$$

In Fig. 2.4, we show with dashed lines the typical behavior of mixed state free energies at different values of Q_R. These results are exact but the results within the UDA approximation at weak coupling are practically identical [see Chapter 5

]. An interesting property of mixed states is that they present the “wrong” curvature, that is, the electronic compressibility $\partial^2 f_e/\partial\phi^2$ is negative. Generally, this does not imply a thermodynamic instability since the usual stability condition of positive compressibility must be formulated for the global neutral system thus including the background compressibility. Since in our models, the inverse background compressibility is assumed to be an infinite positive number (the background density is fixed to the uniform average value $\overline{\phi}$), it follows from this point of view that the system is in a stable mixed state. In solid state systems, the background represents the positive ionic lattice that compensates the electronic fluid. In general, the compressibility of the former can be neglected but when the electronic inverse compressibility becomes very large and negative, they may compete. This will be discussed in Chapter 5.

An important difference with ordinary phase separation resides in the behavior of the local densities of the domains. In unfrustrated phase separation, the two phases have a constant density independently of the global density. In frustrated phase separation, the local density of the domains decreases with an increase of the global density [29, 31]. This can have important consequences in physical systems undergoing Coulomb frustrated phase separation. For example, the puzzling maximum of the Curie temperature in the three-dimensional perovskite manganite $\mathrm{La}_{1-x}\mathrm{Ca}_x\mathrm{MnO}_3$ at $x = 0.35$ Ca doping [78], not predicted by the conventional double-exchange mechanism [79, 80, 81], can be explained [30] by assuming that the Curie temperature is an increasing function of the local density, rather than the global density controlled by doping.

Chapter 3

Domain pattern formation in systems with negative compressibility

In this chapter, we analyze the phenomenology of domain pattern formation in systems with negative compressibility from weak to strong coupling by means of the paradigmatic model of Coulomb-frustrated phase separation introduced in Chapter 2. Using a combination of numerical techniques and exact asymptotic expansions, we are able to derive the phase diagram of three-dimensional systems (Sec. 3.2) both in absence (Sec. 3.2.1) and in presence (Sec. 3.2.2) of strong anisotropies. These results,appeared in Ref.[68], can be interpreted as a mean-field description of a parameter (e.g. temperature) driven phase transition to charge inhomogeneous states near a critical point (Sec. 3.3). A discussion of the nature of the transition in two-dimensional systems embedded in the three-dimensional Coulomb interaction is reported in Sec. 3.4.

3.1 General considerations

As discussed in Chapter 2, domain pattern formation in systems with a negative short-range electronic compressibility density region can be analyzed within the model Eq. (2.7) that we recall for the reader's convenience:

$$\widetilde{H}_2 = \int d^D x \left[\phi(\mathbf{x})^2 - 1\right]^2 + |\nabla\phi(\mathbf{x})|^2 + \frac{Q_R^2}{2}\int d^D x \int d^D x' \frac{\left[\phi\left(\mathbf{x}\right) - \overline{\phi}\right]\left[\phi\left(\mathbf{x}'\right) - \overline{\phi}\right]}{|\mathbf{x} - \mathbf{x}'|} \tag{3.1}$$

The hierarchy of length scales $\xi << l_d << l_s$ [see Chapter 2] of the weak coupling regime, allows to treat the model within a sharp-interface approach. In this case, strongly anharmonic mixed states appear with finite wave-amplitudes at the transition. On the contrary, in the strong coupling regime, the separation of length scales is no longer valid and a sharp interface treatment is unreliable. The prominent role of smooth interfaces leads to a very different mechanism for the creation of charge inhomogeneities as will be shown below. Indeed computing the static response to an external field in momentum space, one obtains the following charge susceptibility:

$$\chi(\mathbf{k}) = \left[|\mathbf{k}|^2 + \frac{Q_R^2}{2}v(\mathbf{k}) - 2 + 6\overline{\phi}^2\right]^{-1} \tag{3.2}$$

We remind that the system is considered to be D-dimensional but embedded in the usual three dimensional Coulomb interaction. Thus:

$$v(\mathbf{k}) = \frac{2^{D-1}\pi}{|\mathbf{k}|^{D-1}}.$$

as follows from the effective Poisson equation for the 3D Coulomb interaction in two and three dimensional systems [c.f. Appendix A] [82, 52]. The charge susceptibility has a peak at

$$k_0 = \left[(D-1)\ 2^{D-3}\pi Q_R^2\right]^{1/(D+1)} \tag{3.3}$$

determined by the competition between interface and charging effects. It diverges as Q_R approaches a Gaussian instability line Q_{Rg} from above where,

$$Q_{Rg} = \frac{1}{\sqrt{2\pi}}\left[1-3\overline{\phi}^2\right] \qquad 3D \tag{3.4}$$

$$Q_{Rg} = \sqrt{\frac{4\sqrt{2}}{3\sqrt{3}\pi}}\left[1-3\overline{\phi}^2\right]^{3/4} \qquad 2D \tag{3.5}$$

For values of Q_R greater than $Q_{R0} = 1/\sqrt{2\pi}$ in 3D and $Q_{R0} = \sqrt{4\sqrt{2}/(3\sqrt{3}\pi)}$ in 2D, the charge susceptibility turns out to be positive in the whole **k**-space and in the entire region of global densities $-1 < \overline{\phi} < 1$. This ensures thermodynamic stability of the homogeneous phase against small amplitude inhomogeneity. The divergence of the charge susceptibility at Q_{Rg}, indicates an instability of the homogeneous phase towards a sinusoidal charge density wave (SCDW) with vanishing wave amplitude and direction chosen by spontaneous symmetry breaking. This is analog to spinodal decomposition in neutral systems [42]. The correspondent second-order phase transition is referred as the “microphase” separation transition in classical systems [1, 32, 4]. A similar mechanism has been proposed in cuprates predicting charge ordering instabilities and other anomalous properties in accord with experiment [16].

So far, the crossover from the strongly anharmonic inhomogeneous state expected at weak coupling to the SCDW appearing at the Gaussian instability line, has not yet been addressed and we will account for in the following section in the case of three-dimensional systems.

3.2 The phase diagram of 3D systems

In this section, we derive the full phase diagram of 3D systems from the limit of zero frustration up to the strong frustration regime. We will first consider the simple case of isotropic systems. To account for strong anistropic systems one should consider an anisotropy in the gradient term that will be discussed in Sec. 3.2.2.

3.2.1 Isotropic systems

In our following analysis we will look for periodic textures. We can thus introduce a Bravais basis $\{\mathbf{a_1}, \mathbf{a_2}, \mathbf{a_3}\}$ for which the periodicity of the density can be expressed as

$$\phi\left(\mathbf{r} + m_1\mathbf{a_1} + m_2\mathbf{a_2} + m_3\mathbf{a_3}\right) = \phi\left(\mathbf{r}\right)$$

with m_1, m_2, m_3 real integers. In the dual momentum space, the wavevectors $\mathbf{G}$ will form a reciprocal lattice with primitive wave-vectors $\{\mathbf{b_1}, \mathbf{b_2}, \mathbf{b_3}\}$ determined by:

$$\mathbf{a}_i \cdot \mathbf{b}_j = 2\pi\delta_{i,j} \qquad\qquad i, j = 1, 2, 3$$

The Fourier decomposition of the density can be put as:

$$\phi\left(\mathbf{x}\right) = \frac{1}{V}\sum_{\mathbf{G}} \phi_{\mathbf{G}}\, e^{i\mathbf{G}\cdot\mathbf{x}} \tag{3.6}$$

where V indicates the unit cell volume of the periodic texture. For a charge inhomogeneous state to be stabilized, we must require that its free energy must be lower than the one of homogeneous phase $\left[\overline{\phi}^2 - 1\right]^2$ [c.f. Eq. (3.1)]. It is thus convenient to refer to the difference of free energy density between a charge inhomogeneous state and a homogeneous phase whose Fourier decomposition comes out:

$$\begin{aligned}\frac{\delta F}{V} &= \frac{1}{V^2}\sum_{\mathbf{G}\neq 0}\phi_{\mathbf{G}}\chi^{-1}(\mathbf{G})\,\phi_{-\mathbf{G}}+\frac{1}{V^3}\sum_{\mathbf{G}_1,\mathbf{G}_2,\mathbf{G}_3\neq 0}4\overline{\phi}\,\phi_{\mathbf{G}_1}\phi_{\mathbf{G}_2}\phi_{\mathbf{G}_3}\delta(\mathbf{G}_1+\mathbf{G}_2+\mathbf{G}_3,0)+\\ &\quad+\frac{1}{V^4}\sum_{\mathbf{G}_1,\mathbf{G}_2,\mathbf{G}_3,\mathbf{G}_4\neq 0}\phi_{\mathbf{G}_1}\phi_{\mathbf{G}_2}\phi_{\mathbf{G}_3}\phi_{\mathbf{G}_4}\delta(\mathbf{G}_1+\mathbf{G}_2+\mathbf{G}_3+\mathbf{G}_4,0) \qquad (3.7)\end{aligned}$$

where we remind that the $G = 0$ component of the Coulomb interaction cancels in order to satisfy the electroneutrality constraint $\langle\phi(\mathbf{x})\rangle = \overline{\phi}$ that in momentum space reads $\phi_{\mathbf{G}=\mathbf{0}} = V\overline{\phi}$.

The presence of a self-generated cubic term in Eq. (3.7) calls for the possibility of first-order transitions. This is a widely common behavior in mean field theory of phase transitions and occurs for example in the isotropic-nematic and in the liquid-solid transitions [42]. Rigorously, to capture first-order transitions, one should account for all vectors $\mathbf{G}$ of a given reciprocal lattice in Eq. (3.7) and for all possible choices for the reciprocal lattice. Thus a complete discussion requires a minimization of the free energy density with respect to $\phi_{\mathbf{G}}$ for all possible reciprocal lattice candidates. A different route, however, can be kept if one refers to the strong-coupling regime. In this case, we will assume that the transition will be at most weakly first-order which can be checked *a posteriori*. We keep only wave-vectors of a given magnitude and we assume that the magnitude of the wave vector is determined by the maximum of the charge susceptibility in the uniform phase[1]. This makes a close connection between our discussion and the liquid-solid transition theory [42, 83] where the typical wave-vector is fixed by the static structure function peak in the liquid phase. In addition, because of the isotropy, the amplitudes of the Fourier components $\phi_{\mathbf{G}}$ will depend

---

[1] A variational determination of the optimal G would lead to the same condition.

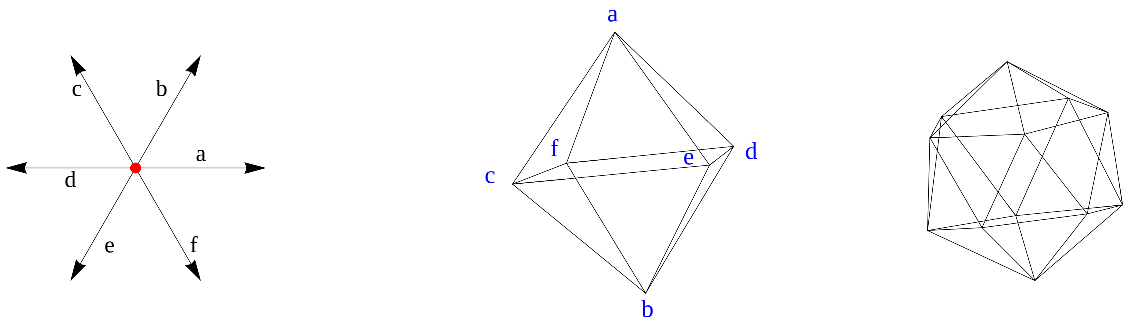

Figure 3.1: Left panel: The six shortest vectors of triangular lattice forming the equilateral triangle a, c, e and its inverted image b, d, f. Central panel: The octahedron in which the $m = 12$ shortest vectors of a FCC reciprocal lattice can be rearranged. The square a, b, c, d is planar while a, b, c, f is a non-planar diamond. Right panel: An icosahedron. It is straightforward to show that for a triangular lattice $\{p, q\} = \{1, 0\}$ whereas for a FCC and a icosahedral lattice $\{p, q\} = \{2, 2\}$.

only upon the magnitude of $\mathbf{G}$ [83]. As a consequence, the free energy Eq. (3.7) comes out in our strong coupling assumption:

$$\frac{\delta F}{V} = \chi^{-1}(G)\,\phi_G^2 \sum_{\mathbf{G}} 1 + 4\,\overline{\phi}\,\phi_G^3 \sum_{\mathbf{G_1},\mathbf{G_2},\mathbf{G_3}} \delta_{\mathbf{G_1}+\mathbf{G_2}+\mathbf{G_3},0} + \phi_G^4 \sum_{\mathbf{G_1},\mathbf{G_2},\mathbf{G_3},\mathbf{G_4}} \delta_{\mathbf{G_1}+\mathbf{G_2}+\mathbf{G_3}+\mathbf{G_4},0} \tag{3.8}$$

where the sums over the momenta are constrained by $|\mathbf{G}_i| = G$. Obviously, the quadratic contribution $\propto \phi_G^2$ is determined by the number $m = \sum_{\mathbf{G}} 1$ of reciprocal lattice vectors with G magnitude. The key point is that to have an energetic advantage from the cubic term of Eq. (3.8), which in turn leads to a first-order transition, we need triads of wave-vectors of equal magnitude that add to zero thus forming an equilateral triangle so that the Kronecker δ is fulfilled. This cannot be realized by a one-dimensional reciprocal lattice for which $m = 2$. An additional translational symmetry breaking is at least needed leading to consider reciprocal lattices with dimension $d > 1$. As stated in Ref.[42], there are only three distinct sets of equal length vectors $\mathbf{G}$ containing closed equilateral triangles and both $\mathbf{G}$ and $-\mathbf{G}$ that form symmetric structures. The first set consists in the $m = 6$ edge vectors of an equilateral triangle and its opposite image that can be formed by a triangular reciprocal lattice [left panel of Fig. 3.1]. The second set consists in the $m = 12$ edge vectors of an octahedron [center panel of Fig. 3.1]. These vectors can be translated so that their tails are at the origin and their heads are on the surface of a sphere of G radius. In this form, the latter set corresponds to a face-centered-cubic (FCC) lattice. The latter possibility consists in the set of the $m = 30$ edges of an icosahedron [right panel of Fig. 3.1] that can be formed by the shortest vectors of an icosahedral reciprocal lattice.

For all sets of wave-vectors, it is possible to compute the free energy Eq. (3.8) upon introducing the number p of equilateral triangles and the number q of non-planar diamonds to which each vectors belongs. A detailed derivation is presented in Appendix E. We finally obtain a Landau free energy expansion in the order parameter ϕ_G that reads [2]:

$$\frac{\delta F}{V} = \chi^{-1}\left(G\right) m\phi_G^2 + 8\overline{\phi}\, p\, m\phi_G^3 + \phi_G^4\left[3m\left(m-1\right) + 6qm\right] \tag{3.9}$$

Upon minimizing with respect to the wave-amplitude ϕ_G and requiring $\delta F = 0$, we determine the first-order transition line:

$$Q_{R_t} = Q_{R\,g} + Q_{R\,0}\frac{8p^2\overline{\phi}^2}{\left[3\left(m-1\right)+6q\right]} \tag{3.10}$$

---

[2] We caution that Eq. (3.9) differs from the result reported in Ref.[42]. We are in debt with T.C. Lubensky for confirming us that the result in the book has to be modified.

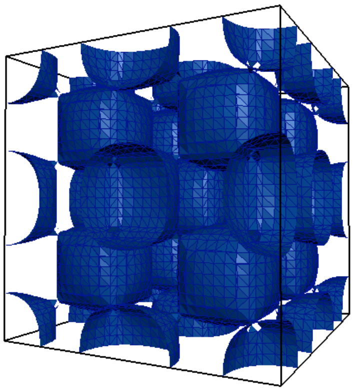

Figure 3.2: Constant density plot of the density deviation $\phi(\mathbf{x}) - \overline{\phi}$ rescaled by the transition wave-amplitude factor, at the transition to a nucleated BCC lattice. The panel shows a cell with size $-2\sqrt{2}\pi/G < \{x, y, z\} < 2\sqrt{2}\pi/G$. The structures enclosed by the surface represent electron-rich (electron-poor) region for $\overline{\phi} < 0$ ($\overline{\phi} > 0$).

The jump in the order parameter at the transition $\phi_G = -4p\overline{\phi}/\left[3(m-1) + 6q\right]$ goes to zero at $\overline{\phi} = 0$ confirming that the transition is weakly first-order with the Gaussian line (the dotted line in Fig. 3.5) playing the role of the limit of metastability of the homogeneous phase.

Decreasing Q_R the first inhomogeneous structure to become stable is the FCC reciprocal lattice defined by the 12 wave-vectors $\mathbf{G}/G = 1/\sqrt{2}\left[(\pm1, \pm1, 0), (\pm1, 0, \pm1), (0, \pm1, \pm1)\right]$. The FCC lattice in the dual space gives rise in the 3D real space to a BCC crystal of inhomogeneities shown in Fig. 3.2. At the BCC lattice points $\mathbf{x}_L = \sqrt{2}\pi/G\left[(\pm1, \pm1, \pm1), (0, 0, 0)\right]$, the full constructive interference between the sinusoidal charge density waves components of the density modulation implies that $\phi(\mathbf{x}_L) = \overline{\phi} + 12\,\phi_G$. Notice that since the transition wave amplitude has the opposite sign of the global density $\overline{\phi}$, the charged domains will represent overcompensated or undercompensated region respectively for $\overline{\phi} < 0$ and $\overline{\phi} > 0$.

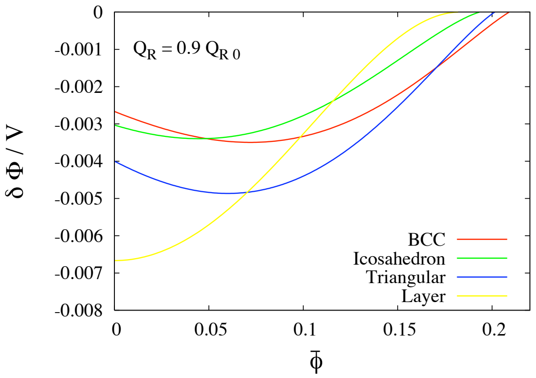

Figure 3.3: Behavior of the free energies Eq. (3.9) for the different reciprocal lattices discussed in the text as a function of the global density at fixed Coulomb coupling. Crossing between the different lines determine the morphological transitions. Notice that the icosahedron reciprocal lattice corresponding to the icosahedral quasicrystal is never favorable.

The first-order homogeneous-BCC transition line is given by:

$$\frac{Q_{R_t}}{Q_{R0}} = 1 - 3\overline{\phi}^2 + \frac{32}{45}\overline{\phi}^2 \tag{3.11}$$

and is shown with the red thin full line in Fig. 3.5. It terminates at a liquid-gas-like critical point $(\overline{\phi}, Q_R) = (0, Q_{R0})$(the black circle in Fig. 3.5) where the transition is second-order-like and driven by the charge susceptibility divergence as easily follows by considering that the cubic term of Eq. (3.7) vanishes at $\overline{\phi} = 0$. Thus at the critical point the spinodal decomposition mechanism enters into play and leads to SCDW.

Below the first-order transition line, there is a tendency towards a morphological change of the inhomogeneities. Close to Q_{R0}, only the structures previously identified are expected to compete. Therefore we can obtain the full phase diagram around this point. In Fig. 3.3 we show the behavior of the free energies Eq. (3.9) for the reciprocal lattice candidates as a function of the average density $\overline{\phi}$ and fixed coupling strength. Starting from the BCC-lattice region of stability at large $\overline{\phi}$, we

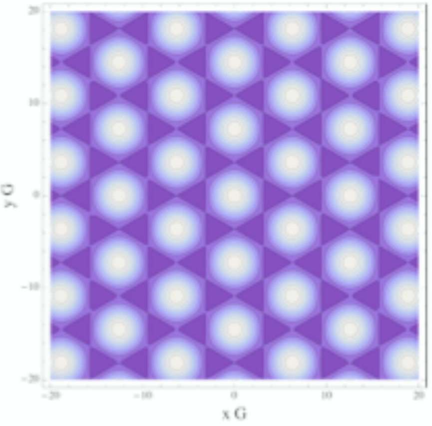

Figure 3.4: Contour plot of the rescaled density deviation $\left[\phi\left(\mathbf{x}\right)-\overline{\phi}\right]/\phi_G$ in the two-dimensional modulation plane of rod-like inhomogeneities. The white spots corresponds to the lattice points of a triangular lattice where the sinusoidal charge density waves are "in-phase" and $\phi\left(\mathbf{x}\right)=\overline{\phi}+6\phi_G$. In the purple areas the density value is more close to its average value.

find a first-order morphological transition leading to rigid rod-like inhomogeneities for which the modulation occurs in a selected plane and the translational symmetry is preserved in a spontaneously chosen direction. The two-dimensional modulation is specified by the triangular reciprocal lattice defined the six wave-vectors $\mathbf{G}/G = \left(\pm\cos\pi/3, \pm\sin\pi/3\right), \left(\pm 1, 0\right)$ and is shown in Fig. 3.4. The appearance of rod-like domains in a triangular lattice is reminiscent of type II superconductors where above the lower magnetic critical field H_{c_1} "normal" state vorteces form the Abrikosov vortex lattice [84]. It is worth noticing that the same feature appears in the twist-grain-boundary (TGB) phase of liquid crystals [42].

By further decreasing the global density, we find a subsequent first-order morphological transition that restores the translational symmetry in an additional direction and leads to layered structures. This state can be interpreted as a *smectic* electronic

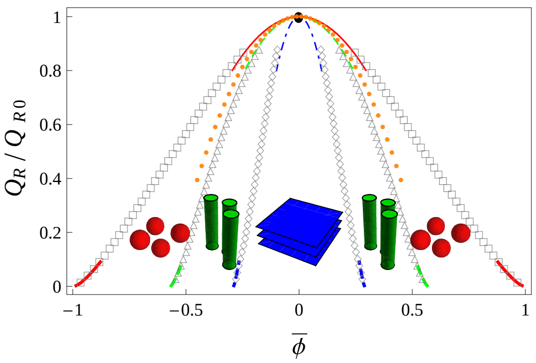

Figure 3.5: The full phase diagram in three-dimensional isotropic systems. The small dots indicates the Gaussian instability line Q_{Rg}. The thin and thicks lines represent first-order transitions in the strong-coupling approximation and in the UDA . Full lines indicates the transition from homogeneous to droplet-like inhomogeneities while dashed and dotted-dashed lines the morphological transition from droplets to rods and from rods to layers. Finally the □, △ and ♢ points are the results from discrete numerical minimization.

liquid phase that possesses orientational order and breaks the translational symmetry only in one direction. Possibly, fluctuations of the stripe order can restore the translational symmetry [85] thus leading to a *nematic* phase.

By determining crossings of the free energies as in Fig. 3.3 at different coupling strength, we obtain the first-order morphological transition lines sketched with the thin lines in Fig. 3.5. The icosahedral structure never becomes favorable according to our analysis. This interesting structure corresponds to a quasicrystal in real space. Here we would notice that with the inclusion of higher order harmonics at weaker couplings, the icosahedral quasicrystal and other structures could be stabilized in a narrow range of global densities. It can also happen that the first-order-like abrupt changes of the inhomogeneity structure could be substituted by a more smooth evolution as found in classical systems [1].

For $Q_R << Q_{R0}$ the weakly first-order transition Eq. (3.11) cannot be correct since the inhomogeneous region must converge to the Maxwell construction phase separation density range $-1 < \overline{\phi} < 1$ whereas Eq. (3.11) predicts a narrower range. Indeed by decreasing the Coulomb coupling from Q_{R0} along the transition line, the jump in the chemical potential is more abrupt and the weak first order character of the transition is lost calling for a computation with more harmonics.

For small Q_R the separation of length scales ($\xi << l_d << l_s$) discussed in Chapter 2 allows to treat the problem within the Uniform-Density-Approximation. We have refined the latter approximation by a direct evaluation of the free energy excess of an isolated domain wall. Interestingly we find that one can extend the range of applicability of the latter approximation by taking into account the density dependence of the surface energy and the interaction of the dipole layer formed at the interface with the local electric field. Details will be presented in Chapter 4. Within the refined UDA, we find the same transitions as in strong coupling but now the inhomogeneities form sharply defined spherical droplets, cylindrical rods and layers. The transition lines in this approximation are shown with the thick lines in Fig. 3.5.

In order to study the crossover from the weak to the strong-coupling regime, we have numerically minimized a discretized version of the model Eq. (3.1) in the Wigner-Seitz approximation [13, 77, 58]. For rod-like and droplet-like inhomogeneities we assumed respectively cylindrical and spherical shape to reduce the minimization procedure to a one-dimensional effective problem in the radial direction alone. This is a reasonable approximation if the typical size of the domains is much lower of their typical distance [77, 58] as indeed found by decreasing the coupling strength. The

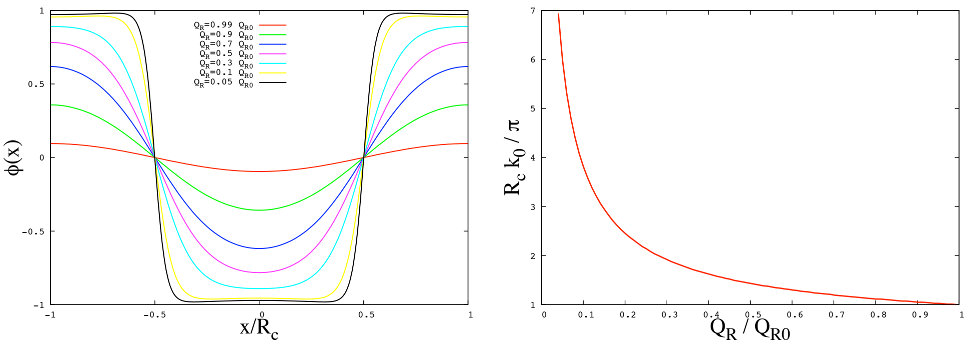

Figure 3.6: Left panel: Behavior of the charge density modulation for different values of the dimensionless coupling Q_R for $\overline{\phi} = 0$. Near the Gaussian instability the modulation corresponds SCDW (red-line). As Q_R decreases more harmonic plays a relevant role and the charge modulation assumes the characteristic of a non-harmonic "layered" structure. For $Q_R \to 0$ the modulation is made by layer of $\phi \sim \pm 1$ (black line) and converges to the Maxwell construction. Right panel: Evolution of the periodicity of the charge density wave measured in unit of the periodicity of the SCDW at $Q_R = Q_{R0}$.

resulting transition line are sketched with the $\square$,$\triangle$ and $\diamondsuit$ points in Fig. 3.5 [3].

Finally we study how the anharmonic behavior of the inhomogeneities is build up into the systems as the coupling strength Q_R is decreased. We show the behavior below the critical SCDW point, but the same feature appears in the whole phase diagram. The evolution of the SCDW at $\overline{\phi} = 0$ as the Coulomb coupling is decreased is shown in the left panel of Fig. 3.6. The SCDW smootly evolves into an anharmonic charge density wave that has as a limiting case a macroscopically phase separated state at $Q_R = 0$ in which the periodicity of the charge density wave becomes of the order of the system typical size. The evolution of the modulation half-periodicity R_c with Q_R is shown in the right panel of Fig. 3.6. The Fourier components behaves

---

[3] Since the free energies of the different morphological structures are very close in energy, we applied a finite size scaling analysis to correctly determine the first-order morphological transition lines.

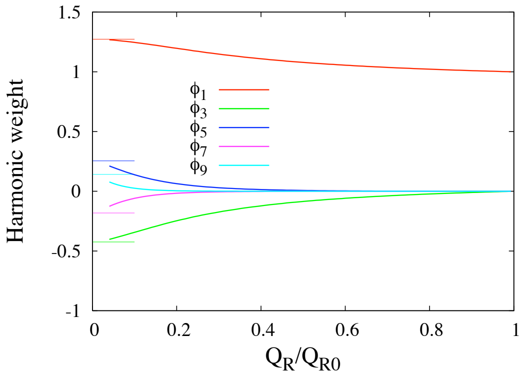

Figure 3.7: Evolution of the harmonic weights $\phi_m / \sum_{m'} \phi_{m'}$ as a function of the dimensionless coupling Q_R. The horizontal lines indicates the weights for a layered structure of $\phi = \pm 1$. The even components $\phi_m \equiv 0$ due to the odd symmetry of the charge density wave at $x = \pm R_c/2$.

as $\phi_{\mathbf{G}} = V \sum_m \delta\left(\mathbf{G} - mG\right) \phi_m/2$ and their evolution is shown in Fig. 3.7. Close to the critical point they behaves as $\phi_m \sim (Q_R - Q_{R0})^{m/2}$ as follows by considering that ϕ_m couples with ϕ_1^m in the quartic term of Eq. (3.1) and close to Q_{R0} the density $\phi_1 \sim (Q_R - Q_{R0})^{\beta}$ with the critical exponent $\beta = 1/2$ as in ordinary second-order phase transitions. Higher harmonics proliferate as Q_R is decreased and their relative weight $\phi_m / \sum_{m'} \phi_{m'}$ converge to the harmonic weights of a rectangular profile of alternating $\phi = \pm 1$ layers corresponding to the macroscopically phase separated state at $Q_R = 0$ (the horizontal lines in Fig. 3.7).

The above discussion provides the complete phenomenology of domain pattern formation in isotropic systems. We have shown that the systems never reaches the second-order Gaussian instability line except for a critical point in the phase diagram: the Gaussian instability is preempted by a first-order phase transition [68]. This result shows that the stability of the homogeneous phase ensured at the gaussian level by the finiteness of the charge susceptibility is irreparably undermined when accounting for the non-gaussian cubic and quartic terms of Eq. (3.7). In the next section we will account for anisotropic systems and analyze if the anisotropy leads or not to qualitative changes of the phase diagram Fig. 3.5.

3.2.2 Anisotropic systems

In this section we discuss the phenomenology of domain patterns in systems with intrinsic anisotropic effects due for example to the underlying crystal field. A simple way to account for the latter effects is to introduce an anisotropy in the gradient term of the model Eq. (2.6). We substitute the gradient term by

$$c_\perp \left|\nabla_\perp \phi\left(\mathbf{x}\right)\right|^2 + c_\parallel \left|\nabla_\parallel \phi\left(\mathbf{x}\right)\right|^2$$

where $\mathbf{x} = \left(\mathbf{x}_\perp, \mathbf{x}_\parallel\right)$ is divided into m perpendicular "soft" direction and $D-m$ parallel "hard" directions. The model can be taken in the dimensionless form as before. Here we measure lengths in unit of the bare correlation length in the perpendicular directions $\xi_\perp = \sqrt{2c_\perp/|\alpha|}$ and free energy in unit of $[\alpha^2/(4\beta)]\,\xi_\perp^D$ to get:

$$\widetilde{H}_2^{an} = \int d\mathbf{x} \left|\nabla_\perp \phi\left(\mathbf{x}\right)\right|^2 + \lambda \left|\nabla_\parallel \phi\left(\mathbf{x}\right)\right|^2 + \left[\phi^2\left(\mathbf{x}\right) - 1\right]^2 + \frac{Q_R^2}{2} \int d\mathbf{x}' \frac{\left[\phi\left(\mathbf{x}\right) - \overline{\phi}\right]\left[\phi\left(\mathbf{x}'\right) - \overline{\phi}\right]}{\left|\mathbf{x} - \mathbf{x}'\right|} \tag{3.12}$$

where λ measure the degree of anisotropy and corresponds to the ratio of the stiffness vector parallel component $c_\parallel$ to $c_\perp$. Finally, as for the isotropic case, we introduced the rescaled Coulomb coupling that measures the competition between short- and long-range interactions that in our present anisotropic model reads

$$Q_R^2 = \frac{2e^2}{\varepsilon_0\left|\alpha\right|}\xi_\perp^{D-1} \tag{3.13}$$

In the limit $\lambda \to \infty$, the modulation in the parallel direction are forbidden preserving their translational symmetry and pattern formation can occur only in the soft perpendicular directions. Thus one is left with an effective m-dimensional problem in the perpendicular soft directions. It is worth to mention that the solutions can be given in a different interpretation. Consider a m-dimensional system subject to a fictitious m-dimensional Coulomb interaction defined by:

$$\nabla^2 v_m \left(\mathbf{x}_\perp - \mathbf{x}'_\perp\right) = -4\pi\delta^{(m)} \left(\mathbf{x}_\perp - \mathbf{x}'_\perp\right) \tag{3.14}$$

Then in momentum space we get $v_m(q_\perp) = 4\pi/q_\perp^2$ corresponding to the 3D Coulomb interaction provided one takes $q_\| = 0$ or equivalently $\lambda = \infty$ in Eq. (3.12). Domain pattern formation for this class of systems, has been considered in Ref.[32]. A detailed analysis has been provided for the case of two-dimensional systems embedded in a weak two-dimensional interaction. In the following section, we will generalize this analysis to all regime of couplings.

One "hard" direction

The case of one hard direction and two soft isotropic directions is straightforwardly tractable. Indeed in the strong-coupling regime, our weakly-first-order transition approximation is rigorously valid [4] once one notice that the reciprocal lattice choice is restricted in this case to a triangular lattice alone. From Eq. (3.10) the weakly-first-order transition line is given by:

$$\frac{Q_{R_t}}{Q_{R0}} = 1 - 3\overline{\phi}^2 + \frac{8}{15}\overline{\phi}^2 \tag{3.15}$$

---

[4] We would notice that the isotropic assumption in the "soft" plane is essential to describe via Eq. (3.9) the transition line.

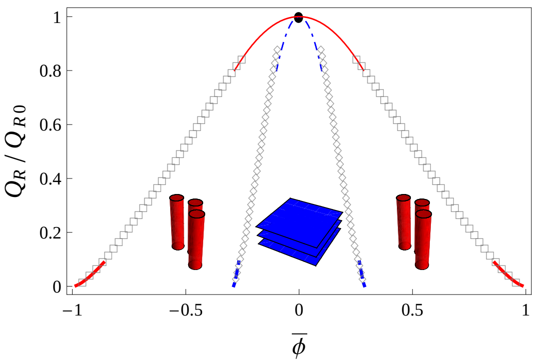

Figure 3.8: The full phase diagram in the $m = 2$ anisotropic case. The full thin and thick lines indicate the first-order transitions to rod-like inhomogeneities respectively in the strong-coupling analysis and in the weak-coupling UDA theory. The □ points indicate the same transition line with numerical minimization method. The dotted-dashed lines and the ◇ points represent the morphological transition to layered structures in the three approximations.

and is shown with the thin full line in Fig. 3.8. Notice that the appearance of a SCDW is restricted to the critical point $(\overline{\phi}, Q_R) = (0, Q_{R0})$ as for the isotropic case. A comparison of Eq. (3.15) with the weakly-first-order transition line for isotropic systems Eq. (3.11) would clarify that anisotropic effects shrinks the region of stability of the inhomogeneous phase. This is clearly due to the constraint imposed in the hard direction. In Fig. 3.8 we show the full phase diagram where the first-order transition to rod-like structures is provided for intermediate and weak couplings by means of discrete numerical minimization method (□ points) and the weak-coupling UDA theory (thick full line). Analogously to the isotropic case, tendency to a morphological change of the inhomogeneities manifests itself in the full range of Q_R. We find indeed both analytically (dot-dashed lines) and numerically (◇ points) a first-order transition leading to layered structures. As emphasized in the previous section, the phase diagram of Fig. 3.8 describes well the phenomenology of two-dimensional systems

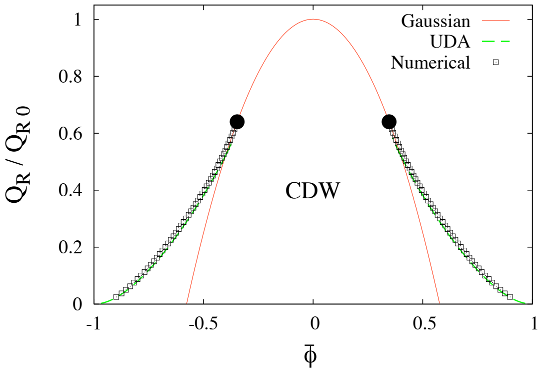

Figure 3.9: The phase diagram for anisotropic three-dimensional systems with a unique soft direction. The thin line is the gaussian instability line that represents the exact second-order transition line for $\overline{\phi} < \overline{\phi}_T$ (the black circle) and the metastability line of the homogeneous phase for $\overline{\phi} > \overline{\phi}_T$. The dashed line is the I-order transition line in the UDA approximation. The $\square$ point are the results of numerical minimization in the first-order region.

subject to a two-dimensional "Coulomb" interaction. In this case rod-like structures would acquire the meaning of droplet-like patterns while layers should be considered as stripe-like objects.

Two "hard" directions

In this section we discuss the more interesting case of only one "soft" direction. Since only one dimensional modulations (layered structures) are allowed, the weakly first-order transition will be replaced at least in the strong-coupling regime by the second-order Gaussian instability line Q_{Rg} shown with the thin full line in Fig. 3.9. The inhomogeneous phase will thus appear in the form of a SCDW in the soft direction with vanishing amplitude at the transition and periodicity $2R_c = 2\pi/k_0$. The question then arises of how this is reconciled with the appearance of the strongly anharmonic inhomogeneous states expected at weak Coulomb couplings. The answer is that this happens trough a tricritical behavior. We find, in fact, a change of regime for $|\overline{\phi}| > \sqrt{3}/5$. In this case the transition is again first-order with tricritical points at $\left(\overline{\phi}, Q_R\right) = \left(\pm\sqrt{3}/5, 16/25 Q_{R0}\right)$. The position of the tricritical points and the behavior of the charge density modulation around it, can be studied retaining only two-harmonics in the density:

$$\phi\left(x\right) = \overline{\phi} + \phi_1 \cos k_0 x + \phi_2 \cos 2k_0 x \tag{3.16}$$

and below we will assume $\phi_2 << \phi_1$. From Eq. (3.7) and retaining only terms up to the ϕ_1^4 the modulated phase energy can be expanded as:

$$\frac{\delta F_{II}}{V} \simeq \frac{3}{8}\phi_1^4 + 3\,\overline{\phi}\,\phi_2\phi_1^2 + \frac{\left(Q_R - Q_{RG}\right)}{Q_{R0}}\left(\phi_1^2 + \phi_2^2\right) + \frac{9}{8}\frac{Q_R}{Q_{R0}}\phi_2^2 + O\left(\phi_1^6\right) \tag{3.17}$$

Near the Gaussian instability line $Q_R \sim Q_{Rg}$, minimization with respect to ϕ_2 implies:

$$\phi_2 = -\frac{4}{3}\frac{Q_{R0}}{Q_R}\,\overline{\phi}\,\phi_1^2 \tag{3.18}$$

Using this condition we can consider Eq. (3.17) as an expansion in ϕ_1 up to ϕ_1^4 thus justifying the order of the next subleading term indicated. Upon reinserting Eq. (3.18) in the expression for the modulated free energy density we finally obtain a Landau-like free energy in the order parameter ϕ_1 that can be put as:

$$\frac{\delta F_{II}}{V} = r\phi_1^2 + u_4\phi_1^4 + u_6\phi_1^6 \tag{3.19}$$

with the quadratic coefficient $r = \left(Q_R - Q_{Rg}\right)/Q_{R0}$ whereas for the coefficient u_4 of the quartic term we get:

$$u_4 = \frac{3}{8} - 2\,\overline{\phi}^2\,\frac{Q_{R0}}{Q_R} \tag{3.20}$$

where we have neglected a term of order $\left(Q_R - Q_{Rg}\right)$. For $u_4 > 0$, the value of the order parameter ϕ_1 can be obtained by minimization of Eq. 3.19 neglecting the sixth

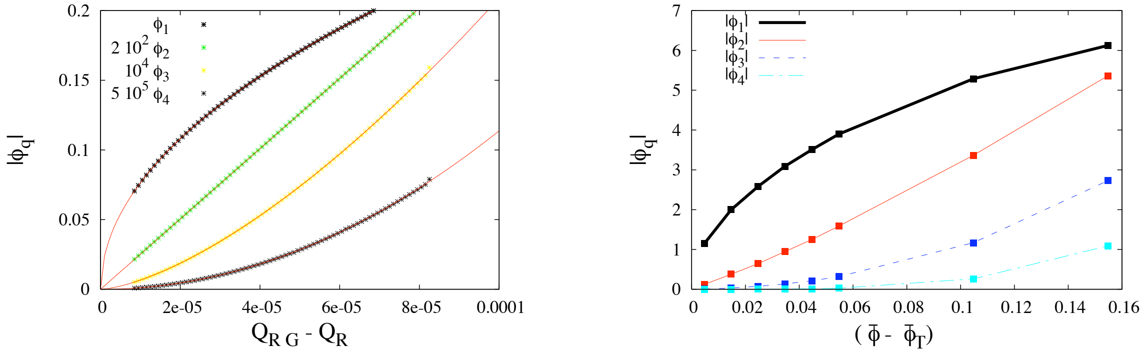

Figure 3.10: Left panel: Evolution of the amplitudes of the first four harmonics for $\overline{\phi} = 0.1$. The dashed lines are fitted lines with critical exponents $\beta_m = m/2$. Right panel: Evolution of the finite harmonic amplitudes of the nucleated layered structure along the first-order transition line starting from the tricritical point. Notice the square root law for the amplitude ϕ_1 as follows from the Landau free energy expansion Eq. (3.19)

order term. Thus the transition is determined by the Gaussian instability line *i.e.* $Q_R = Q_{Rg}$ $(r = 0)$. By following the second-order transition line, we find that the quartic coefficient u_4 vanishes for $\overline{\phi} = \overline{\phi}_T = (\sqrt{3}/5)$ indicating a tricritical point that is shown with the black circle in Fig. 3.9. Thus for $\overline{\phi} > \overline{\phi}_T$ the transition turns out to be first-order like. The analytical determination of the first-order transition line would require knowledge of the subleading terms in our Landau-like free energy expansion since

$$Q_{R_t} - Q_{Rg} = Q_{R0}\frac{|u_4|^2}{u_6} \propto (Q_R - Q_{RT})^2$$

where $Q_{RT} = 16/25 Q_{R0}$ indicates the tricritical Coulomb coupling. In this case we can again take advantage from numerical discrete minimization. The numerically found first-order transition line is shown with the $\square$ points in Fig. 3.9. Almost the full first-order transition line is well depicted (dashed line of Fig. 3.9) by the refined UDA approximation of Chapter 4. In the second-order transition region, the evolution of the SCDW is controlled by a continuous proliferation of harmonics. This is analogous to the behavior found below the critical point in isotopic systems in Sec.3.2.1. The first harmonic grows as $(Q_{Rg} - Q_R)^{1/2}$ as follows for ordinary second-order phase transition. This yields the second-harmonic amplitude to grow linearly by means of Eq. (3.18). By numerically analyzing the behavior of higher order harmonics one finds that, generally, the critical exponents of the order m harmonic amplitude behaves as $\phi_m \propto (Q_{Rg} - Q_R)^{\beta_m}$ where the m-th harmonic critical exponent $\beta_m \sim m/2$ (see left panel of Fig. 3.10). This follows from the fact that the m-order harmonic couples with ϕ_1^m in the cubic term of Eq. (3.7).

In the first-order region, the nucleated layered structure acquire a more prominent anharmonic behavior by deviating from the tricritical point. This is because the finite harmonic amplitudes at the transition progressively grows as shown in Fig. 3.10.

3.3 Temperature-driven transitions to charge inhomogeneous states

As yet emphasized in Chapter 2, the model presented in Sec. 3.1 can be derived by expanding the coarse grained energy of a system around a reference density inside a negative compressibility density range. In general the inverse short-range electronic compressibility α and the bare correlation length ξ will depend upon external parameters like pressure. They can be even taken temperature dependent as in Landau theory where H has to be interpreted like a free energy and the model becomes a mean-field description of a temperature driven transition to an inhomogeneous state which can be useful, for example, to model inhomogeneities appearing below some temperature in manganites [33]. In this section we discuss the case in which the reference density would correspond to a critical liquid-gas point with diverging short-range electronic compressibility at a critical temperature T_c. Close to T_c, the parameter α can be taken as linearly dependent on the temperature as $\alpha = \alpha' (T - T_c)$ with α' constant [71, 42]. It can be useful to obtain the phase diagram as a function of the normalized "temperature" T/T_c and the global density deviation $\Delta\overline{n} = \overline{n} - n_c$. Here we will present the temperature dependent phase diagram for the case of anisotropic three-dimensional systems with one soft direction but a straightforward generalization would yield to derive the phase diagrams in the temperature-density plane for isotropic systems.

We start by considering that the dimensionless density $\overline{\phi}$ and the rescaled Coulomb coupling Q_R^2 are temperature dependent since they have been defined in terms of the inverse short-range compressibility and the bare correlation length. Restoring dimensions and assuming β and the stiffness constant $c_\perp$ constant, one obtains the following equations for the dimensionally correct global density and the bare Coulomb coupling:

$$\overline{\phi}(T) = \frac{\Delta\overline{n}}{\Delta n_0(T=0)} \left[1 - \frac{T}{T_c}\right]^{-1/2} \qquad (3.21)$$

$$\left(\frac{Q_R(T)}{Q_{R0}}\right) = \frac{e^2}{\varepsilon_0} \frac{8\pi\, c}{\alpha' T_c^2} \left[1 - \frac{T}{T_c}\right]^{-2} \qquad (3.22)$$

where we have chosen to measure densities in unit of the Maxwell construction density range at zero temperature $\Delta n_0(T=0) = \sqrt{2\beta/(\alpha' T_c}$. Analogously, we can introduce a dimensionless parameter $Q_0^2 = 8\pi\, c\, e^2/(\alpha' \varepsilon_0 T_c^2)$ that corresponds to the square of the zero temperature renormalized coupling $Q_R(T=0)$ in unit of $Q_{R0} = 1/\sqrt{2\pi}$. All

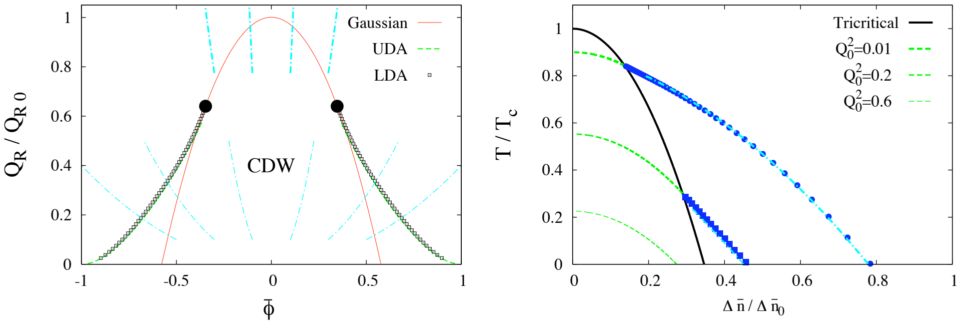

Figure 3.11: Left panel: Behavior of isochoric lines dot-dashed lines for two values of $Q_0^2 = 0.01, 0.2$ in the dimensionless coupling-global density plane. Crossing with the phase diagram determine the transition temperature at fixed global density $\Delta\overline{n}$.Right panel: The phase diagram for $m = 1$ anisotropic systems in the temperature-density plane for different values of the coupling Q_0^2. The full line represents the tricritical line.The dashed lines are the gaussian instability lines. The dot-dashed lines are the UDA first-order transitions. Finally the $\Box$ are the results of the numerical minimization.

the dependence upon the relevant parameters $c\,, \alpha'\,, \varepsilon_0\,, T_c$ that specifies the intrinsic properties of a given system is enclosed in Q_0^2.

The density-temperature phase diagram can be easily found by crossing of the $Q_R - \overline{\phi}$ transition lines of the phase diagram Fig. 3.9 with isochoric trajectories *i.e.* $\Delta\overline{n}/\Delta\overline{n}_0 = const$ at fixed Q_0^2. The behavior of such trajectories is showed in the left panel of Fig. 3.11 and the resulting temperature dependent phase diagram is shown in the right panel of Fig. 3.11. Upon increasing Q_0^2, the maximum transition temperature at $\overline{n} = n_c$ decreases. The change of regime between SCDW and anharmonic inhomogeneous state is expected on a tricritical line. It happens very close to the maximum transition temperature for weak Q_0^2 and progressively drops out by increasing the Coulomb coupling. At strong couplings, nucleation of inhomogeneous states is completely suppressed and the transition is always second-order like.

3.4 A brief discussion of 2D systems

The discussion of an isotropic two-dimensional system subject to the 3D Coulomb interaction is a generalization of 3D systems. In the strong-coupling regime it is easy to recover that the second-order SCDW transition at the Gaussian instability line Eq. (3.5) is preempted by a weakly first-order transition where ordered structures appear. They present in the form inhomogeneities arranged in a triangular lattice and are expected in the full range of global densities $\overline{\phi}$ except at the critical SCDW point $\overline{\phi} = 0$, $Q_R = Q_{R0}$. We thus expect that the phase diagram will be qualitatively similar to the 3D anisotropic case with two soft direction of Fig. 3.8.

The crossing between the energy of the homogeneous phase and the energy of the inhomogeneous phase at the weakly first-order transition implies as a general phenomenon an emergent tendency towards charge segregation since it leads to a cusp singularity of the minimal free energy at the transition density. Thus striped state of the homogeneous phase coexisting with the inhomogeneous state could appear. This feature becomes particularly relevant in two-dimensional systems where we will show [see Chapter 5] that near a cusp singularity, inhomogeneous state are stabilized no matter how big the frustrating effects are.

Now we turn to the anisotropic case and look for the crossover from the SCDW appearing at the Gaussian instability line and the anharmonic inhomogeneous states generally expected at the weak-coupling regime. To obtain the latter change of regime, as for the three-dimensional case, it is enough to retain only the contribution of the first two-harmonics with wave-vectors k_0 and $k_1 = 2k_0$. The free energy density Eq. (3.7) comes out:

$$\begin{aligned}\frac{\delta F_{II}}{V} = &= \frac{3}{8}\left[\phi_1^4+\phi_2^4\right]+\frac{3}{2}\phi_1^2\phi_2^2+3\overline{\phi}\phi_2\phi_1^2-\left(\phi_1^2+\phi_2^2\right)\left[1-3\overline{\phi}^2\right]+\\ &\left(\frac{Q_R^2}{Q_{R0}^2}\right)^{2/3}\left[\left(\phi_1^2+\frac{\phi_2^2}{2}\right)^2\left(\phi_1^2+4\phi_2^2\right)\right]^{1/3}\end{aligned} \tag{3.23}$$

The last term that encloses the effect of surface energy plus charging effect has a different power-law behavior with respect to the 3D case due to the different momentum dependence of the Coulomb interaction. Notice also the period of the charge density wave R_c is obtained as :

$$R_c = \left[\frac{2\pi^2}{Q_R^2}\right]^{1/3}\left[\frac{\phi_1^2+4\phi_2^2}{\phi_1^2+\frac{\phi_2^2}{2}}\right]^{1/3} \tag{3.24}$$

Introducing the dimensionless parameter $\epsilon = \left[Q_R^2/Q_{R0}^2\right]^{2/3}$ with ϵ_g given in terms of Q_{Rg} of Eq. (3.5) and assuming as done for the 3D case $\phi_2 << \phi_1$ from Eq. (3.23) we get

$$\frac{\delta F_{II}}{V} \simeq \frac{3}{8}\phi_1^4+3\overline{\phi}\,\phi_2\,\phi_1^2+(\epsilon-\epsilon_g)\left(\phi_1^2+\phi_2^2\right)+\frac{2}{3}\epsilon\,\phi_2^2+O\left(\phi_1^6\right)$$

where we have retained only term up to ϕ_1^4. By minimizing with respect to $\phi_2 \propto \phi_1^2$ we obtain an effective Landau theory in the density ϕ_1 of the form Eq. (3.19). The quadratic coefficient r becomes negative at the 2D Gaussian instability. Furthermore the quartic coefficient turns out:

$$u_4 = \frac{3}{8}-\frac{27}{8}\frac{1}{\epsilon}\overline{\phi}^2$$

It becomes negative for $\overline{\phi} = 1/(2\sqrt{3})$ predicting a tricritical point. Thus we can anticipate that the phase diagram will look like the 3D one of Fig. 3.9.

Finally we can conclude that pattern formation driven by a negative electronic compressibility in 2D systems behaves similarly to the 3D case of Sec. 3.2. In Chapter 5 we will show that this similarity does not persists in systems with a cusp singularity where the dimensionality plays a key role in Coulomb frustrated phase separation phenomena.

Chapter 4

Surface energy in systems subject to long-range Coulomb interactions

As emphasized in Chapter 2, in a weakly frustrated phase separated state, there is a great separation between the typical domain size and the bare correlation length ξ corresponding to the typical interface width. This allows for approximated sharp interface treatment that are the most economical choice when attempting to analyze the phenomenology of charge inhomogeneous states. Still, a precise computation of the surface energy is needed to make quantitative comparison between the sharp-interface treatment and the results of the exact models introduced in Chapter 2. So far, it is not clear how to correctly define a surface tension in systems subject to Coulomb forces due to the long-range nature of the interaction. Indeed, in previous works the interface free energy was estimated taking into account only short-range effects [32, 4]. In this chapter we will go beyond this approximation and will show how to correctly define the surface energy of a system subject to the long-range

Coulomb interaction. We will restrict to analyze in detail three-dimensional systems where the long-range force effect in the interface scale has a trasparent interpretation, but our analysis could be also extended to two-dimensional systems. In Sec. 4, we will review the Ginzburg-Landau theory of the surface tension for a flat domain wall useful to compute the surface tension in ordinary macroscopic phase separation. Next, starting from the latter theory we discuss how to define a surface tension in systems with long-range Coulomb interaction in the flat interfaces case (Sec. 4.2) including moreover finite curvature effects in Sec. 4.3. Finally in Sec. 4.4 we will show that the simple Uniform-Density-Approximation introduced in Chapter 2 combined with the previous analysis, turns out to make extremely accurate quantitative predictions in all the weak-coupling regime.

4.1 Surface tension: the Ginzburg-Landau theory

Let us begin by considering the negative compressibility model defined in its dimensionless form in Eq. (2.7) and solved in the previous chapter. By minimizing with respect to the charge density profile, one obtains an Euler-Lagrange equation that together with the Poisson equation for the Coulomb interaction yields to the following coupled equations :

$$2\nabla^2\phi + 4\phi - 4\phi^3 + Q_R\psi + \overline{\mu} = 0 \tag{4.1}$$

$$\nabla^2\psi - 4\pi Q_R\left[\phi - \overline{\phi}\right] = 0 \tag{4.2}$$

where ψ is the dimensionless electrostatic potential and $\overline{\mu}$ is a Lagrange multiplier needed to ensure charge neutrality. Eq. (4.1) determines how the charge reacts to

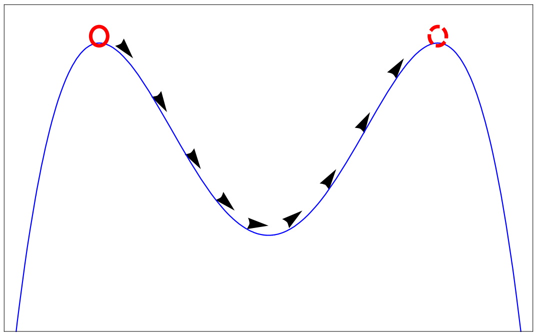

Figure 4.1: Schematic view of a particle moving in the double-well inverted external potential in the z-time. The density ϕ indicates the coordinate in which the particle moves.

the long-range potential while the Poisson equation determines how the long-range potential is generated by the charge. They should be solved self-consistently in order to obtain the charge density profile. Obviously, for $Q_R = 0$, one is left with the simple Ginzburg-Landau equation:

$$2\nabla^2\phi + 4\phi - 4\phi^3 = 0 \tag{4.3}$$

The latter equation leads to the two uniform symmetry-broken solutions $\phi = \pm 1$ of zero energy corresponding to the phase-coexistence values in a macroscopically phase-separated state. In a coexistence state, the ϕ-distribution is ruled by Eq. (4.3) when appropriate boundary conditions are imposed. As an example, in a liquid-gas system gravity determines the appropriate boundary conditions since it “pushes” the liquid to occupy the lower end of a container leaving the gas phase on the top. It can be easily found that at the boundary of the two phases, a thin region of ~ 1 forms where the substance is neither in one phase nor in the other phase but is somewhere in between. Since in this region the spontaneous symmetry breaking is reduced, an higher free energy then either phases is found. This represents the price the system has to pay to form a domain wall and is proportional to its area. The correspondent free energy per unit area is called the surface tension σ.

For a flat interface perpendicular to a z-axis, the appropriate boundary conditions of Eq. (4.3) for a spatially non uniform state read:

$$\lim_{z \longrightarrow \pm\infty} \phi\left(z\right) = \pm 1 \tag{4.4}$$

By considering the density ϕ as a spatial coordinate and z a time coordinate, Eq. (4.3) can be interpreted as the equation of motion $2\phi''(z) = V'(\phi)$ of a classical particle of $m = 2$ mass moving between the maxima $\phi = \pm 1$ of a "inverted" double-well external potential $-V\left(\phi\right) = -\left[\phi^2 - 1\right]^2$ as schematically sketched in Fig. 4.1. Since the potential is "time-independent", the latter equation can be easily integrated and one gets for the "velocity" of the particle $\phi'\left(z\right) = \sqrt{V\left(\phi\right) + E}$, where $E \equiv 0$ for the "velocity" of the particle to vanish at $\phi = \pm 1$ ($z = \pm\infty$). It is thus simple to show that the motion of the particle subject to the boundary condition Eq. (4.4) is ruled by the equation:

$$\phi\left(z\right) = \tanh\left[z - z_I\right]$$

where z_I in the particle motion language would corresponds to the time at which the particle is in the minimum of the inverted potential whereas in the domain wall language indicates the interface location. The behavior of the order parameter profile is shown in the top panel of Fig. 4.2. The surface tension σ is then determined by the free energy excess per unit area of the spatial non-uniform state and thus

$$\sigma_{GL} = \int_{-\infty}^{\infty} dz \left[\left(\frac{d\phi}{dz}\right)^2 + \left(\phi^2 - 1\right)^2\right] = \int_{-\infty}^{\infty} dz f_I\left(z - z_I\right) \tag{4.5}$$

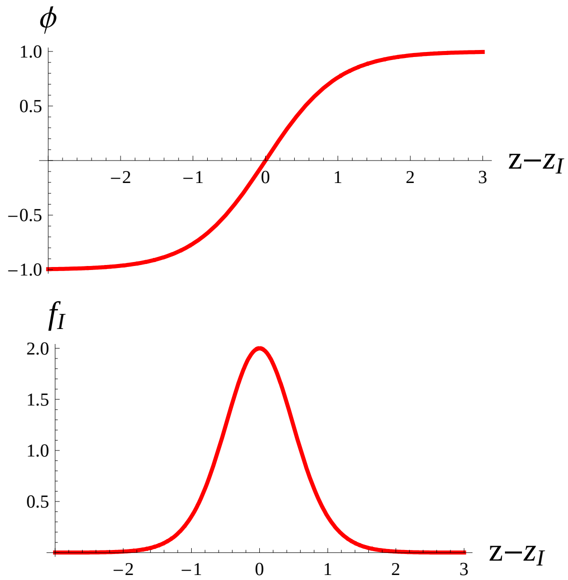

Figure 4.2: The behavior of the order paramter profile (left panel) and the interface free energy density f_I (right panel) for a domain wall in the Ginzburg-Landau theory of neutral systems.

where the terms in the square brackets indicates the ϕ^4-model free energy functional corresponding to the negative compressibility model Eq. (2.7) in absence of the long-range Coulomb interaction. Finally f_I indicates the interface energy density across the interface and is shown in the bottom panel of Fig. 4.2. Two contributions determine the interface energy density of Eq. (4.5). The first one comes from the spatial variation of ϕ ("kinetic energy"). The other is due to the deviations of ϕ from the minima ("potential" energy) . Both terms are equal in magnitude and one then obtains the well-known surface tension $\sigma = 8/3$ of a phase-coexistence state in the Ginzburg-Landau theory. Starting from the latter derivation of the surface tension in neutral system, in the following section we will address a generalization to the case of systems subject to long-range Coulomb interactions.

4.2 Surface energy in charged systems

In charged systems, the order parameter profile is ruled by the coupled equations Eqs. (4.1), (4.2) that can be regarded as a pair of reaction-diffusion equations[86, 87, 88, 89]. In the latter context it has been showed by singular-perturbation method treatments [90, 91] that a strong separation of the typical length scales allows to brake up the solution into an interface solution and a domain solution. The interface solution varies on the length scale of order ~ 1 and describes the variation of ϕ in the vicinity of the domain interfaces whereas the domain solution varies on the length scale l_d of the characteristic size of the domains and describes variation of the order parameter away from the interfaces. The great advantage of the latter separation of the solutions is that the rapid variations of the interface solution near the domain walls, could be integrated out to yield an effective interface free energy. Still, the presence of the long-range Coulomb interaction, makes the definition of an interface free energy a quite difficult job.

In a mesodomain state, domains walls coexist. Albeit this would lead to a system of interacting interface solitons, the strong separation between the interface typical width ξ and the typical domain size l_d ensures that the domain walls would be far apart. Thus in the following we will neglect short range interaction effects among domain walls.

In the following, we will consider the flat interface case leaving a discussion of finite curvature effects in the following section. We thus consider a mesoscopic cell of area Σ and length R_c with two coexisting A-phase ($\overline{\phi} < 0$) and B-phase ($\overline{\phi} > 0$) layers. In addition we will label ϕ_A and ϕ_B the equilibrium densities of the coexisting-phases away from their separating domain wall. This would represent the analog of the boundary conditions Eq. (4.4) for system not subject to long-range forces, necessary to fully determine the density profile. The presence of the "time-dependent" potential ψ in Eq. (4.1) does not allow for an exact solution of the differential equation. Thus we attempt a variational solution with a form for the density profile similar to the one of the neutral case but with variational parameters:

$$\phi_I(z) = \frac{\phi_B + \phi_A}{2} + \frac{\Delta\phi}{2} \tanh \frac{(z - z_I)}{\tilde{\xi}} \tag{4.6}$$

where $\Delta\phi = \phi_B - \phi_A$ to satisfy the boundary conditions introduced above and $\tilde{\xi}$ is the interface thickness in unit of the bare correlation length ξ that can be determined variationally. We assume $\tilde{\xi}$ of order 1 to be much smaller than $\tilde{R}_c \sim \tilde{l}_d$ with $\tilde{R}_c = R_c/\xi$. Thus in the following we will neglect correction of the order $e^{-R_c/\xi}$. Since charge neutrality is needed to avoid a diverging Coulomb cost, we must impose the constraint:

$$\frac{1}{R_c} \int_0^{R_c} d\, z \phi_I(z) = \overline{\phi} \tag{4.7}$$

that fixes the parameter z_I of Eq. (4.6) as a function of R_c, the two equilibrium electronic densities $\phi_{A,B}$ and the background global density $\overline{\phi}$. To proceed further, we will consider the case of three-dimensional systems where by means of the Poisson equation for the dimensionless electric field:

$$\nabla \cdot E(z) = 4\pi Q_R \left[\overline{\phi} - \phi(z)\right] \tag{4.8}$$

we can eliminate the charge density in favor of the electric field in the non-local long-range interaction term of the negative compressibility model Eq. (2.7). Therefore, the dimensionless free energy of an inhomogeneous layered state reads:

$$\Phi = A \int_0^{\tilde{R}_c} dz \left|\nabla\phi(z)\right|^2 + \left[\phi(z)^2 - 1\right]^2 + \frac{\left|E(z)\right|^2}{8\pi} \tag{4.9}$$

Figure 4.3 shows the different components of the free energy density across an interface. The main difference respect to the short range case is that in the latter the free energy density converges to the same constant in the two phases far from the interface. Thus the energy of an interface can be represented as a constant plus the energy localized at the interface without the need to determine precisely the position of the interface. For example in Fig. 4.2 the surface energy is defined by the area between the constant (zero) and the bell shape of f_I. In the present case, the energy density including the long-range Coulomb interaction is not even constant far form the interface. Thus a sharp interface model needs to deal with a discontinuity of the short range part of the free energy at the interface. This is a problem because the difference in free energy between a step distribution and a smooth distribution depends on the relative position between the two steps suggesting that the surface energy is not well defined. We write the density profile of the sharp distributions as:

$$\phi_S\left(z\right) = \frac{\phi_B + \phi_A}{2} + \frac{\Delta\phi}{2} sign\Big(z - \tilde{R}_d\Big) \tag{4.10}$$

where $\tilde{R}_d$ fixes the domain wall location. The problem is how to fix $\tilde{R}_d$ respect to z_I. Fortunately a precise criterion exists because we must require that the long range part of the energy is equal in the two descriptions. Thus we need to impose the equality of the electric field far form the interface. This leads to

$$R_d \equiv z_I$$

In Fig. 4.3 we show the electric fields for the sharp and the smooth distribution ϕ_I. Notice the matching away from the interface. The above discussion leads to a surface

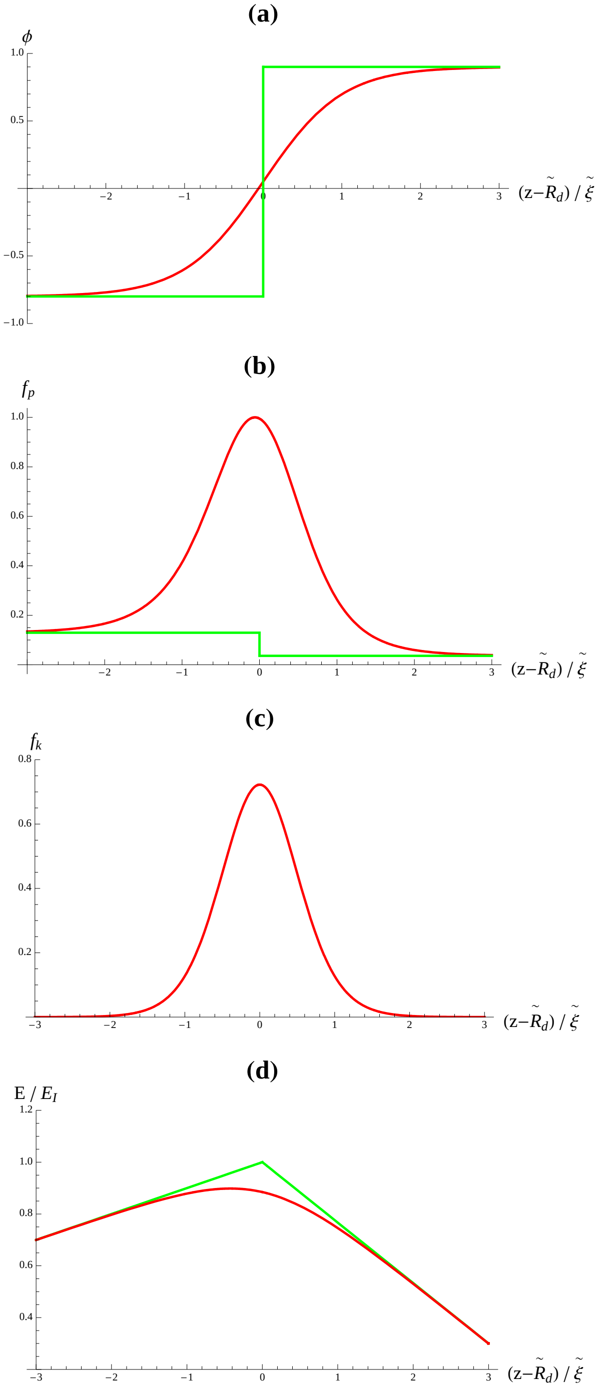

Figure 4.3: (a): The sharp ϕ_S (green line) and the smooth ϕ_I (red line) interface distribution across a domain wall. The two equilibrium values away from the interfaces have been chosen as $\phi_A = -0.8$ and $\phi_B = 0.9$. (b): The double-well potential profile across a domain wall for the latter density distributions. (c): The gradient term free energy contribution in the smooth interface distribution.(d) Behavior of the electric fields E_{ϕ_I} (the red thick line) and $E(\phi_{SH})$ (the green thick line) in unit of E_I for $\nu = 1 - R_d/R_c = 0.3$ and $R_d = 10\xi'$.

tension for charged systems defined by the difference:

$$\begin{aligned}\sigma &= \int_{-\infty}^{\infty} dz \left|\nabla\phi_I(z)\right|^2 + \left[f(\phi_I) - f(\phi_{SH})\right] + \\ &\quad \left[\frac{\left|E_{\phi_I}(z)\right|^2}{8\pi} - \frac{\left|E_{\phi_S}(z)\right|^2}{8\pi}\right] \end{aligned} \tag{4.11}$$

where $f(\phi) = [\phi^2 - 1]^2$ and we have translated the z-axes by $\tilde{R}_d$ to fix the domain wall at $z = 0$. Finally E_{ϕ_I} (E_{ϕ_S}) indicates the macroscopic electric field generated by the interface distribution ϕ_I (ϕ_S) plus the fixed background $\overline{\phi}$.

The first two terms of Eq. (4.11) are analogous to the terms of Eq. (4.5) of the Ginzburg-Landau theory. By computing the integrals in Eq. (4.11) we obtain the density depend surface tension contribution:

$$\sigma'_{GL} = \frac{\Delta\phi^2}{3\tilde{\xi}} + \tilde{\xi}\, g(\phi_B, \phi_A, \Delta\phi) \tag{4.12}$$

where the function g reads:

$$\begin{aligned} g(\phi_B, \phi_A, \Delta\phi) &= 2\log 2\Delta\phi\left(\phi_A^3 - \phi_A - \phi_B^3 - \phi_B\right) + \Delta\phi^2(2\log 2 - 1)\left(-1 + \frac{3}{2}\phi_B^2 + \frac{3}{2}\phi_A^2\right) \\ &\quad + \Delta\phi^4\left(\frac{7}{12} - \log 2\right) \end{aligned}$$

For $\phi_{A,B} = \mp 1$, Eq. (4.12) reduces to the surface tension value for neutral systems upon optimization with respect to the thickness $\tilde{\xi}$.

The third term of Eq. (4.11) represents the novel electrostatic contribution due to the rounding of the cusp singularity of the sharp interface electric field when accounting for the smooth interface distribution $\phi_I(\mathbf{x})$ [see panel (d) of Fig. 4.3]. The difference between the two charge distributions $\delta\phi = \phi_I - \phi_S$ can be accounted by a dipole layer. By using the superposition principle for both the electric field and the density distribution and introducing δE [see Fig. 4.4] as the electric field

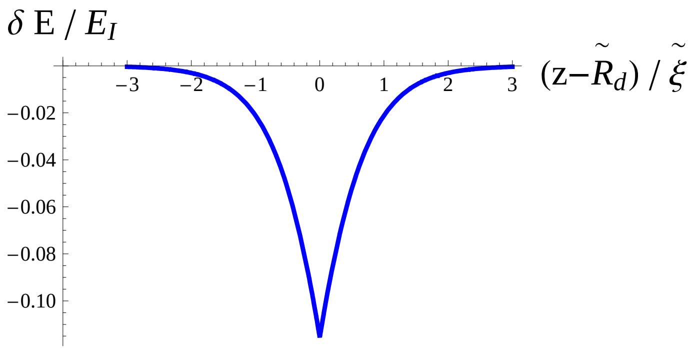

Figure 4.4: The electric field correction δE to the macroscopic electric field due to the presence of the dipole layer at the interface for the same parameters of Fig. 4.3. For convenience δE has been measured in unit of the sharp electric field at the interface $E_{\phi_S}(0) = E_I$.

generated by the interface dipole layer, the electrostatic contribution to the surface tension reads:

$$\sigma_E = \int_{-\infty}^{\infty} dz \frac{1}{8\pi} \left|\delta E(z)\right|^2 + \frac{1}{4\pi} \left[E_{\phi_S}(z) \cdot \delta E(z)\right] \tag{4.13}$$

The first term represents the self-energy of the dipole layer appearing at the interface whereas the second-term accounts for its interaction with the electric field at the interface computed in the sharp interface approximation. The appearance of an electrostatic contribution to the surface tension has been discussed in electron-hole droplets in semiconductors [92, 93] and in two-components liquid of charged particles [94]. In the latter systems, however, away from the interfaces the net charge density goes to zero and the whole electrostatic contribution reduces to the self-energy of the dipole layer. In the present case, the mismatch between the background density and the electronic density at length scales much greater than the interface thickness provide the additional contribution $\delta E \cdot E_{\phi_S}$ due to the presence of a macroscopic electric field.

The electric fields appearing in Eq. (4.13) are straightforwardly found from Gauss theorem:

$$\begin{aligned} E_{\phi_S}(z) &= 4\pi\, Q_R\, \nu\, \Delta\phi\, \tilde{R}_d + 4\pi\, Q_R\, \nu\, \Delta\phi\, z - 4\pi Q_R \Delta\phi\, z\, \theta(z) && (4.14) \\ \delta E(z) &= -2\pi Q_R\, \Delta\phi\; \tilde{\xi}\, f_0\left(\frac{z}{\tilde{\xi}}\right) && (4.15) \end{aligned}$$

where θ, as usual, represents the unit step function, $f_0(y) = \log 2\cosh y - |y|$ and we have introduced the volume fraction of the B-phase $\nu = 1 - R_d/R_c$. As shown in Fig. 4.4 , the electric field δE is peaked at the interface with a broadening of the $\tilde{\xi}$ order. By performing the integrals in Eq. (4.13), we obtain the electrostatic contribution to the surface tension:

$$\sigma_E = -2\pi Q_R^2 (\tilde{\xi})^2 \Delta\phi^2 \nu R_d \int_{-\infty}^{\infty} f_0(y) dy + \pi\, Q_R^2\, \Delta\phi^2\, (\tilde{\xi})^3\, \left[2 \int_0^{\infty} y f_0(y) + \frac{1}{2} \int_{-\infty}^{\infty} f_0^2(y) \right] \tag{4.16}$$

where the first term comes out from the interaction between the dipole layer and the "external" sharp local electric field at the interface $E_{\phi_S}(0) = E_I$. It can be regarded as a dipole energy per unit area $-p \cdot E_I/\Sigma$ once one introduces the dipole moment:

$$p = \frac{1}{2} Q_R \Delta\phi (\tilde{\xi})^2 \Sigma \int_{-\infty}^{\infty} f_0(y) dy \tag{4.17}$$

The most important point is that the interface electric field E_I grows linearly with the domain size $\tilde{R}_d$ and thus the dipole energy above introduced grows with the volume of the mesoscopic cell. This is a quite unexpected behavior since as discussed in Sec. 4.1 the energy that the system has to pay to create a domain wall is proportional to its area in neutral systems. We can interpret this new behavior by considering that the appearance of a long-range term represented by the macroscopic electric field propagates interface effects to the system scale.

It is also interesting to consider the dipole energy per unit volume that comes out:

$$-\frac{p \cdot E_I}{V} = -2\pi\, Q_R^2\, (\tilde{\xi})^2\, \Delta\phi^2\, \nu\, (1-\nu) \int_{-\infty}^{\infty} f_0(y) dy \tag{4.18}$$

Notice that in this form, the dipole energy term is independent on the geometrical parameters R_d and R_c at the mesoscopic scale and takes the same form of a phase separation energy gain depending upon the phase-separated state bulk properties. We thus expect this term to appear also for more complicated domains with finite curvatures as we will verify in the following section.

4.3 Finite curvature effects: the droplet case

Although the results of the previous section are rigorously valid for domain walls with flat interfaces, a straightforward generalization to systems with nearly flat interfaces can be addressed. In this section we will consider the case of spherical droplets that in the weak coupling regime are expected to have a typical radius $R_d >> \xi$ but similar ideas could be applied to rod-like inhomogeneities and to more complicated morphologies. The advantage of considering droplet-like domain is that the spherical symmetry allows to restrict the calculation in the radial direction alone. In addition in the nearly flat interface limit, one can assume the interface distribution to be again described by Eq. (4.6)[32]. The total interface free energy then reads:

$$\begin{aligned} F_I &= \int_0^{\tilde{R}_c} d^3r \left|\nabla \phi_I\,(r)\right|^2 + \left[f\,(\phi_I) - f\,(\phi_S)\right] + \\ & \left[\frac{\left|E_{\phi_I}\,(z)\right|^2}{8\pi} - \frac{\left|E_{\phi_S}\,(z)\right|^2}{8\pi}\right] \end{aligned} \tag{4.19}$$

where $\tilde{R}_c$ indicates the radius of a neutral spherical cell in the Wigner-Seitz approximation [13, 58]. Finally the interface distributions ϕ_{SH} and ϕ_I are ruled respectively by Eqs. (4.10), (4.6) with $z \to r$. As in the previous section, the relative position of the interfaces in the two descriptions is determined by the matching of the electric fields away from the interface. This fixes the domain wall location $\tilde{R}_d = R_d/\xi$ as:

$$\tilde{R}_d = r_I \left[1 + \frac{\pi^2}{4} \frac{\tilde{\xi}^2}{\tilde{R}_d^2}\right]^{1/3} \tag{4.20}$$

where r_I is the analogous of z_I in the flat interface case. An exact computation of the interface free energy Eq. (4.19) requires then numerical exploitation. Still, in the nearly flat interface limit, we can expand Eq. (4.20) in power of $\tilde{\xi}/\tilde{R}_d$ since the variational parameter $\tilde{\xi} \sim 1$. From Eq. (4.20) we thus obtain:

$$r_I \sim \tilde{R}_d \left[1 - \frac{\pi^2}{12} \frac{\tilde{\xi}^2}{\tilde{R}_d^2} + \ldots\right] \tag{4.21}$$

where the ... indicate higher order terms in the expansion parameter. A similar expansion is needed to provide the electric field correction δE to the macroscopic sharp electric field. The leading order term is given by:

$$\delta E\,(r) = -\frac{2\pi Q_R \Delta\phi \tilde{\xi}}{r^2} \tilde{R}_d^2 f_0 \left(\frac{r - \tilde{R}_d}{\tilde{\xi}}\right)$$

where $f_0(y) = \log 2 \cosh y - |y|$ as found for the flat interface case. At this point, the perturbative computation of the interface free energy requires quite lengthy but simple algebra and we will only mention the different term then arises. The leading order is represented by a dipole energy $\propto \tilde{R}_d^3$. As for the flat interface case it is due to the interaction between the local sharp electric field at the interface $E_I = 4\pi/3 Q_R \nu \Delta\phi \tilde{R}_d$ and the dipole electric field δE. As expected, the dipole energy per unit volume $-p \cdot E/V$ assumes the same expression of Sec. 4.2. Similarly for the next-to leading order term one finds a surface energy $\propto \tilde{R}_d^2$ parameterized by the same short-range density dependent surface tension found in the previous section. Finally, the next-to next-to subleading term turns out $\propto \tilde{R}_d$. It corresponds to a curvature energy, and must be taken into account to extend the range of applicability of the weak-coupling theory as we will show in the following section. The energy per unit volume comes out:

$$e_{cur} = \frac{h_c\left(\phi_A, \phi_B, \overline{\phi}\right)}{R_c^2}\left(1-\nu\right)^{1/3}$$

where ν indicates the B-phase volume fraction and $h_c > 0$. As found for the interface free energy in electron-hole droplets [92], the curvature energy has positive sign and represents an additional frustrating term to the phase-coexistence phenomenon.

4.4 The refined Uniform-Density-Approximation

The previous theory of the surface energy in charged systems allows to provide a refined version of the weak coupling Uniform-Density-Approximation discussed in Sec. 2.4 in the case of three-dimensional systems with a short-range negative compressibility density region. By neglecting the curvature energy for rod-like and droplet like inhomogeneities, the free energy of a phase separated state reads:

$$\tilde{f} = \nu\tilde{f}\left(\phi_B\right) + \left(1-\nu\right)\tilde{f}\left(\phi_A\right) + e_{mix} - \frac{p \cdot E_I}{V} \tag{4.22}$$

where the last term indicates the dipole energy term whereas e_{mix} is the mixing energy due to the competition between short-range interface and long-range charging effects. It can be again put as Eq. (2.19) but now the surface tension has an explicit density dependence and an electrostatic contribution. This refinement makes the UDA an extremely powerful tool to describe the domain pattern formation phe-

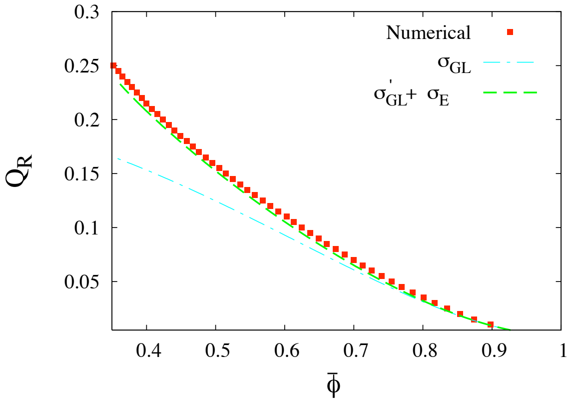

Figure 4.5: The first-order transition line separating the homogeneous phase from layered inhomogeneities in the weak-coupling regime. The □ points represent the result of the numerical minimization method. The long-short dashed line is the result for a UDA with the surface tension of the ordinary GL theory. Finally the dashed line is the result of the refined UDA.

nomenon in the weak-coupling regime. In Fig. 4.5, we compare the transition lines in the density-Coulomb coupling plane from the homogeneous phase to a layered microemulsion phase as obtained in the refined UDA (the dashed line) and in the direct discrete numerical minimization of the model Eq. (2.7) (the □ points) obtained in Chapter 3. At very weak Coulomb couplings $Q_R < 0.05$, the transition line is correctly determined by neglecting the electrostatic contributions to the surface tension and assuming the surface tension of the Ginzburg-Landau theory of neutral systems (the short-long dashed line of Fig. 4.5). Still, by increasing Q_R the dipole energy term and the explicitly density dependence of the surface tension start to cover a prominent role and a huge discrepancy between the two versions of the UDA approximation is observed. Remarkably the transition line in the refined UDA is practically identical to the exact numerical result. It is obvious that for layered structures the refined UDA has an extended range of applicability because of the exact computation of the

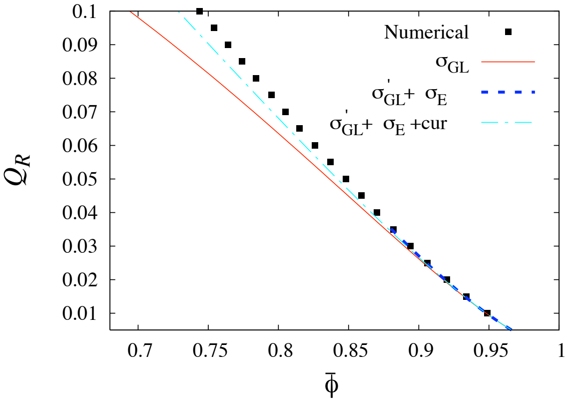

Figure 4.6: First-order transition at weak coupling from homogeneous to droplet-like domain phase. The □ are the exact result of numerical minimization. The full line is the result of the UDA computed at $\sigma = \sigma_{GL}$. The dashed line is the UDA with interface effects neglecting curvature effects. Finally the dotted-dashed line is the result taking also into account the curvature energy.

interface free energy. For non-flat domains, by increasing the Coulomb coupling the curvature term must be at least included to correctly follow the transition line. Indeed, by increasing the effect of the long-range interaction term, the typical domain size R_d in the inhomogeneous phase decreases and the finite curvature effects become important. This is shown in Fig. 4.6 where we report the first-order transition line to droplet-like domains. Notice that also in this case, the UDA with a constant surface tension breaks down at moderate Coulomb couplings showing again the importance of charging effects in the surface energy.

Chapter 5

The cusp singularity model

As remarked in Chapter 2, charge inhomogeneous states are expected to appear with local densities close to the minima of the double-well in the weak-coupling regime and thus the behavior of systems with a cusp singularity is expected to be the same of systems with a negative compressibility density region analyzed in Chapter 3. In the strong coupling regime, instead, the local densities of the coexisting domains approach the maximum of the double well and the specific form of the free energy becomes relevant. In this chapter we will analyze the behavior of systems with a cusp singularity. We will provide the complete phase diagram both in 2D (Sec. 5.2) and in 3D (Sec. 5.3) for electronic systems undergoing a putative electronic first-order phase transition between two homogeneous phases discussing the interplay between the screening and the size of the mixed states. We show the key role of the system dimensionality paying particular attention to the striking behavior of two-dimensional systems that can be even anticipated by means of the Uniform-Density-Approximation Sec. 5.1. Finally in Sec. 5.4 we generalize the 2D behavior by discussing the charge density behavior in metallic-insulating striped phases. The results of Sec. 5.2, 5.3 appeared in Ref. [69] whereas the analysis presented in Sec. 5.4 is a portion of Ref. [52].

5.1 The Uniform Density Approximation close to a cusp singularity

Before analyzing the exact result of the model, we can invoke the Uniform-Density-Approximation keeping in mind that in this case, since we are far from the Maxwell construction limit, the results should be taken with a pinch of salt. Indeed we will see that special care is needed in $D = 2$. We recall that the free energy density of a phase coexistence state in the UDA can be put in dimensionless form as:

$$\tilde{f} = (1-\nu)\,\tilde{f}_A\left(\phi_A\right) + \nu \tilde{f}_B\left(\phi_B\right) + Q_R^{2/D} u(\nu) \delta\phi^{2/D} \tag{5.1}$$

where $\tilde{f}_{A/B} = (\phi \pm 1)^2$, $\delta\phi = \phi_B - \phi_A$ and ν indicates the volume fraction of the B-phase domains. In the following, for simplicity we fix the global density at the crossing point $\overline{\phi} = 0$ and look for the energetic stability of a striped ($D = 2$) or layered ($D = 3$) mixed state. By symmetry $\nu = 1/2$ and the free energy density behaves as

$$\delta f = -|\delta\phi| + \frac{1}{4}\delta\phi^2 + Q_R^{2/D} u(1/2) \delta\phi^{2/D} \tag{5.2}$$

The first term represents the phase separation energy gain, the second term is an energetic cost due to compressibility effects and the last term is the UDA mixing energy. The condition of stability of mixed states reads $\delta\tilde{f} < 0$. In $D = 3$ the last term is dominant at small $\delta\phi$ and combined with the linear term produces an

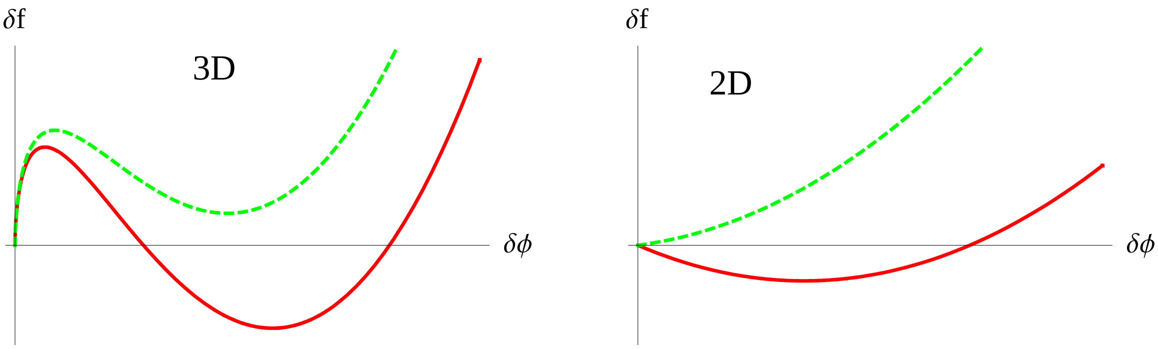

Figure 5.1: Schematic view of the stability condition in the UDA approximation in 3D systems (left panel) and in 2D systems (right panel). The red full lines are for $Q_R < Q_{Rc}$ whereas the green dashed lines indicates unstable inhomogeneous phases.

energetic barrier between the homogeneous state ($\delta\phi = 0$) and the inhomogeneous state ($\delta\phi \neq 0$) [see left panel of Fig. 5.1]. The quadratic term ensures stability for large $\delta\phi$. Clearly the transition will be first order with a critical frustration $Q_{R,c} = \sqrt{27}/[4u(1/2)]^{3/2} \sim 0.7$. We will show that, apart form small numerical corrections, this result coincides with the exact solution. The different power dependence of the phase separation energy gain and the mixing energy cost makes the UDA reliable.

For $D = 2$ there is a delicate balance between the first and the third terms in Eq. (5.2) which are of the same order [see right panel of Fig. 5.1]. The transition looks second order with $Q_{R,c} = 1/u(1/2) \sim 1.2$. However, in this case, we are in a marginal situation [1]. It becomes clear by referring to a long-range interaction $1/r^\alpha$ and looking for the energetic stability of a mixed state. The free energy density behaves in this case as:

$$\delta\tilde{f} = -|\delta\phi| + \frac{1}{4}\delta\phi^2 + \widetilde{Q}_R^{2/(3-\alpha)}\delta\phi^{2/(3-\alpha)} \tag{5.3}$$

---

[1] For a proof of the marginality in D-dimensional systems subject to a $D-1$ dimensional interaction see Appendix D

where we have inserted the mixing energy density dependence for general long-range interactions. Two distinct behaviors than arises. For $\alpha > 1$, the dominant term at small $\delta\phi$ is the phase separation energy gain. No matter how big the frustration degree is, there is an enough small $\delta\phi$ for which the mixed state becomes stable. On the contrary for $\alpha < 1$, we recover the behavior of 3D systems characterized by first-order transitions with a critical frustration. To answer the question of which one of the two latter behaviors the marginal Coulomb case will follow, one has to take into account charge relaxation effects. Fortunately the model Eq. (2.9) is exactly solvable for stripes and layered states that are the expected morphologies close to $\overline{\phi} = 0$.

5.2 The phase diagram of 2D systems

In this section, we consider the cusp singularity model whose Hamiltonian reads:

$$\widetilde{H}_1 = \Sigma + \int d^D x[\phi(\mathbf{x}) - s(\mathbf{x})]^2 + \frac{Q_R^2}{2} \int d^D x \int d^D x' \frac{\left[\phi\left(\mathbf{x}\right) - \overline{\phi}\right]\left[\phi\left(\mathbf{x}'\right) - \overline{\phi}\right]}{|\mathbf{x} - \mathbf{x}'|} \tag{5.4}$$

where $s = \pm 1$ corresponds to a classical Ising spin and we are measuring lengths in unit of the bare correlation length ξ. As emphasized in Chapter 3 an anisotropy of the stiffness constant can favor certain orientations of the interfaces. In the following, we will consider the case in which the modulation of the charge density is restricted to only one “soft” direction. In this case, we will provide the full phase diagram to be compared, for instance, with the anisotropic phase diagram found in Chapter 3. Still, since layered and striped structures are the expected morphologies close to $\overline{\phi} = 0$ even in a isotropic system, we will be able to clarify the behavior of the system at strong frustration .

Since the Hamiltonian Eq. (5.4) is a quadratic function of ϕ, density fluctuations can be easily integrated out to yield an effective model for the spin field alone. Indeed, for each charge inhomogeneous state, the geometry of the domains defines $s(\mathbf{x})$ and its Fourier transform $s(\mathbf{q})$. Uniform phases correspond to the $\uparrow$ and $\downarrow$ ferromagnetic phases in s. Writing the energy in the Fourier space, the $\mathbf{q} = 0$ component of the Coulomb term is canceled to ensure charge neutrality. At $\mathbf{q} \neq 0$, upon minimizing with respect to the charge distribution, one gets:

$$2\phi(\mathbf{q}) - 2s(\mathbf{q}) = \frac{2^{D-1}\pi Q_R^2}{|\mathbf{q}|^{D-1}}\phi(\mathbf{q}) \tag{5.5}$$

Notice that for a fixed domain configuration $s(r)$,

$$\mu\left(\mathbf{r}\right) \equiv 2\phi(\mathbf{r}) - 2s(\mathbf{r})$$

represents the local chemical potential and the electrostatic potential can be put as:

$$\psi\left(\mathbf{r}\right) = \int d\mathbf{r}' v\left(\mathbf{r}-\mathbf{r}'\right)\phi\left(\mathbf{r}'\right).$$

with $v\left(\mathbf{r}\right)$ the Fourier transform of

$$v(\mathbf{q}) \equiv 2^{D-1}\pi Q_R^2/|\mathbf{q}|^{D-1},$$

as follows from Poisson equation in three and two-dimensional systems [see Appendix A] in the presence of the 3D Coulomb interaction playing the role of the “effective” Coulomb interaction. With these definitions Eq. (5.5) states that the local electrochemical potential is constant. The latter condition is the generalization to electronic systems of the Maxwell condition for neutral fluids that is enforced by the constancy of the local chemical potential across different phases.

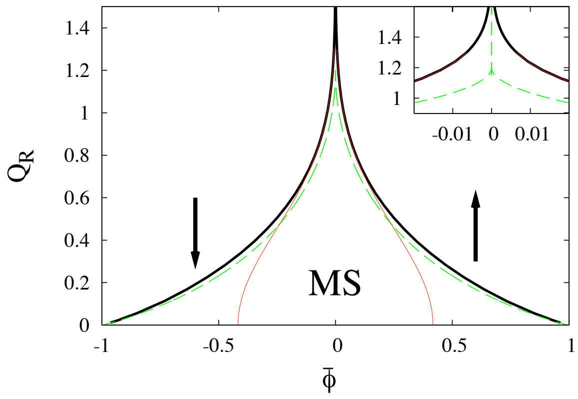

Figure 5.2: The phase diagram for the stripe solution in 2D. The ↑ and ↓ indicate the uniform ferromagnetic phase. The central region corresponds to the mixed state (MS). The thick line is the exact solution of the present model with finite compressibility, the thin full line is the $\kappa \to \infty$ limit taking the short distance cutoff of Ref. [73] equal to the present screening length l_s. The dashed line is the UDA. The inset shows an enlargement near the crossing density n_c where the UDA predicts a critical value of the frustrating parameter.

We can now use Eq. (5.5) to eliminate the charge degrees of freedom from the energy and obtain an effective Hamiltonian depending upon the interface locations:

$$\widetilde{H}_1^{eff} = \Sigma + V\left[\overline{\phi}^2 + 1\right] - 2s_0\overline{\phi} - \frac{1}{V}\sum_{\mathbf{q}\neq 0}\frac{s_{\mathbf{q}}s_{-\mathbf{q}}}{1+\left[\tilde{l}_s^{D-1}|\mathbf{q}|^{D-1}\right]^{-1}} \tag{5.6}$$

where we introduced the dimensionless screening length $\tilde{l}_s$ defined by Eq. (2.15). The first term in Eq. (5.6) is the surface energy of the sharp interfaces. The second and third terms are the $\mathbf{q} = 0$ contribution from the bulk free energy of the competing phases. The last term comes from the $\mathbf{q} \neq 0$ contribution of the last three terms of Eq. (5.4) after eliminating the charge via Eq. (5.5) and represents an interaction term between the coexisting domain walls. It takes the particularly simple form coming back in the real space:

$$-\int\int d\mathbf{x}d\mathbf{x}'\,|\nabla s(\mathbf{x})|\,u\left(\mathbf{x}-\mathbf{x}'\right)|\nabla s(\mathbf{x}')|$$

where $u(\mathbf{x})$ is an effective interaction that for a mixed state of alternating $s = 1$ (↑) stripes of width $2R_d$ and $s = -1$ (↓) stripes of width $2(R_c - R_d)$ can be defined as:

$$u\left(\frac{x}{\widetilde{R_c}}, \frac{R_c}{l_s}\right) \equiv \frac{1}{2\widetilde{R_c}}\sum_{n\neq 0} e^{i\,q_n\,x} u_{q_n} \qquad q_n \equiv \frac{\pi n}{\widetilde{R_c}}$$

with n running over nonzero integers, $\widetilde{R_c} = R_c/\xi$ and for two-dimensional systems

$$u_q \equiv \frac{1}{|q|\left(1 + \widetilde{l_s}|q|\right)}. \tag{5.7}$$

This effective interaction coincides in this case with an effective 3D screened Coulomb interaction in two-dimensional electronic systems. From Eq. (5.6), the energy density of a mixed state can be finally cast as:

$$\widetilde{f} = \pi Q_R^2 \frac{l_s}{R_c} + 1 - 2\overline{\phi}\,(2\nu - 1) + \overline{\phi}^2 - 8\frac{l_s}{2R_c}\left[u\left(0, \frac{R_c}{l_s}\right) - u\left(2\nu, \frac{R_c}{l_s}\right)\right] \tag{5.8}$$

where we introduced the volume fraction $\nu \equiv R_d/R_c$ of the $s = 1$ (↑) phase and we have chosen to measure lengths in unit of the screening length l_s. The dimensionless free energy density, Eq. (5.8), depends upon Q_R, $\overline{\phi}$, ν and R_c/l_s. Minimizing with respect to the volume fraction ν and R_c/l_s, we obtain the phase diagram in the renormalized coupling-density plane shown in Fig. 5.2 with the thick lines. Increasing the frustration, the region of stability of the uniform phases is increased. Noticeably, there is no direct first-order transition between the two homogeneous phases no matter how big the frustration is. Indeed the transition line is logarithmically singular at $\overline{\phi} = 0$ and thus for large Q_R the mixed state is enclosed in the exponentially narrow

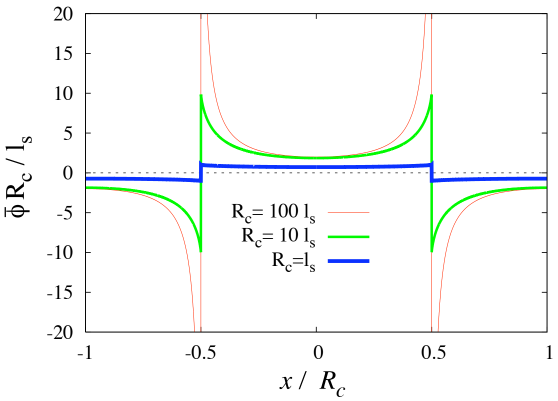

Figure 5.3: Charge density modulation for a cut perpendicular to a stripe in 2D at $\overline{\phi} = 0$, $R_d = R_c/2$ and three different values of the screening length corresponding to $Q_R \sim 0.2$ $(R_c = l_s)$, $Q_R \sim 0.7$ $(R_c = 10 l_s)$ and $Q_R \sim 1.1$ $(R_c = 100 l_s)$. In the case $R_c/l_s \to \infty$ the charge density diverges at the boundary. A finite l_s removes the divergence.

range

$$|\overline{\phi}| < \frac{2}{\pi} e^{-[(\pi Q_R/2)^2 + 1 - \gamma_E]}. \tag{5.9}$$

Here $\gamma_E \sim 0.57$ indicates the Euler gamma constant. As frustration decreases, the range of densities of the mixed state grows and converges to the Maxwell construction range when $Q_R \to 0$.

For high frustration the phase diagram of the exact model is well represented by the "small" screening length limit *i.e.* $R_c >> l_s$ phase diagram (thin full line in Fig. 5.2) where the free energy of a striped phase Eq. (5.8) takes the following simple form:

$$\widetilde{f} = \pi Q_R^2 \frac{l_s}{R_c} + 1 - 2\overline{\phi}\,(2\nu - 1) + \overline{\phi}^2 - 8\frac{l_s}{2\pi R_c}\left[\gamma_E + \log\frac{R_c}{\pi l_s} + \log 2 \sin \pi\nu\right] \tag{5.10}$$

Remarkably, the striped phase free energy Eq. (5.10) coincides with the result obtained by Jamei et al. [73] in the case of infinite compressible $\kappa = \infty$ phases provided

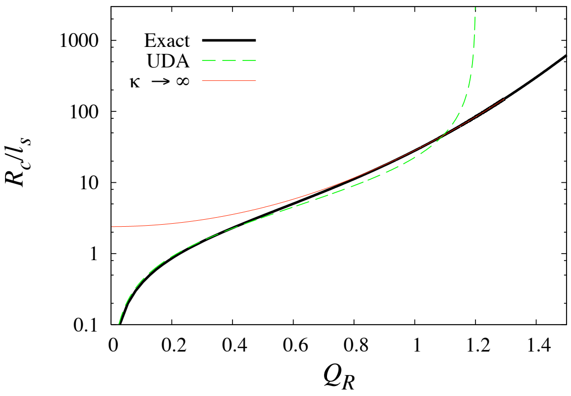

Figure 5.4: Behavior of R_d (log scale) at the crossing density as a function of the frustrating parameter. The thick line is the exact solution of the present model while the thin line is the infinite compressibility limit [73]. The UDA is the dashed line.

one takes the short-distance cutoff, needed to avoid the singularity of the unscreened effective interaction Eq. (5.7), equal to l_s. This agreement is due to the fact that in the highly frustrated regime, the physics is determined by the slow power-law relaxation of the charge (Fig. 5.3) far from the stripe boundary. In fact the stripe width is much larger than the screening length and indeed behaves as (c.f. Fig. 5.4)

$$R_d = \frac{R_c}{2} \sim l_s e^{(\pi Q_R/2)^2+1-\gamma_E} \tag{5.11}$$

whereas the finite compressibility of the present model affects the charge only in a range of order l_s from the boundary. Its effect is to remove the unphysical divergence of the charge density at the stripe boundary arising when $l_s = 0$ (Fig. 5.3). On the contrary, for low Q_R the stripe size is of the order of the screening length $R_d \sim l_s Q_R$ (Fig. 5.4) and the finite compressibility is relevant.

We have compared the exact solution with the uniform density approximation. The phase diagram in this case is plotted in Fig. 5.2 with a dashed line. The UDA

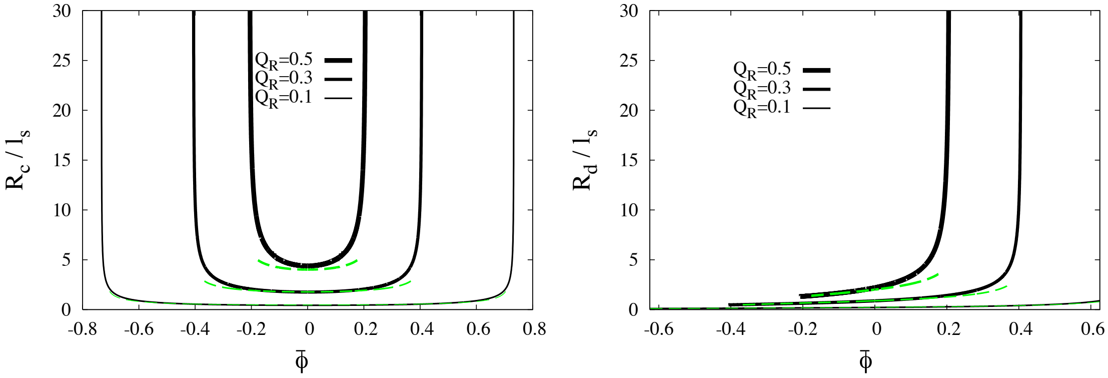

Figure 5.5: Behavior of the width (top panel) and periodicity (bottom panel) of ↑ stripes in 2D systems for different values of $\lambda < 1$. The dashed lines correspond to the uniform density approximation whereas the full line is the exact solution. Notice that the ↑ stripes are the minority phase for $\overline{\phi} < 0$ and the majority phase for $\overline{\phi} > 0$.

gives very accurate results in a wide range of the phase diagram except around the crossing density, where it misses the logarithmic singularity since it predicts a critical value Q_{Rc} of the frustrating parameter (as anticipated in Sec. 5.1) and a first order phase transition among the two homogeneous phases would occur (see the inset of Fig. 5.2). Approaching Q_{Rc} from below, the MS disappears with a divergent stripe size (see Fig. 5.4) in contrast with the exact results where the MS persists with a finite stripe size.

For $Q_R < Q_{Rc}$, at the onset of the mixed state the UDA predicts a first-order transition with the minority phase stripe size and the stripe periodicity that stay finite (see Fig. 5.5). Taking into account the local dependence of the electronic density, the jump in the periodicity of the stripes at the transition is substituted by a square root divergence. Thus the uniform-mixed state transition is characterized by a finite value of the minority phase stripe size and a divergent periodicity which corresponds to a second-order transition. This situation is reminiscent of the transition in a type II superconductor as a function of field at H_{c_1}, which according to Ginzburg-Landau theory is second-order although normal state "drops" (the vortex core) have a finite radius ξ [84].

Although the transition is second order like, for strong frustration, the effect of the mixed state solution is to produce an exponentially small rounding of the singularities in thermodynamic quantities quite hard to distinguish from a first order jump. On the other hand, an important difference from a true first order transition is that the latter shows hysteresis when driven at a finite rate whereas here hysteresis will be absent due to the fact that the surface energy is effectively negative.

Apart from the singularity at the transition between the uniform phase and the stripe phase, the behavior of the mixed state for not so large frustration is very well represented by the UDA (Fig. 5.4, 5.5).

Now we discuss the thermodynamic stability. For finite Q_R the energy vs. density has a negative curvature in the mixed state indicating a negative electronic compressibility [c.f. Fig. 2.4]. For large Q_R, the short-range electronic compressibility in the mixed state corresponds to the inverse of the second derivative of the highly frustrated striped phase free energy Eq. (5.10) optimized with respect to ν and R_c/l_s. We thus get:

$$\kappa_{MS}^{-1} = \kappa_e^{-1}\left[1 - \frac{e^{\left(\pi^2 Q_R^2/4+1-\gamma_E\right)}}{\sqrt{1-\pi^2\overline{\phi}^2/4\,e^{2\left(\pi^2 Q_R^2/4+1-\gamma_E\right)}}}\right] \tag{5.12}$$

where $\kappa_e^{-1} = 2$ indicates the homogeneous phase negative electronic short-range compressibility in dimensionless form. The striped phase electronic compressibility negatively diverges at the uniform-mixed state transition and is exponentially large and negative for $\overline{\phi} \sim 0$. A negative divergence of the compressibility with a 1/2 critical exponent also arises at the uniform-stripe transition for small frustration but with a strength that vanishes when $Q_R \to 0$. In the present model the background is assumed to be incompressible ($k_b = 0$) but real systems will have a small background compressibility $k_b > 0$ and the system will become unstable when the total inverse compressibility $k_b^{-1} + k_e^{-1} < 0$. This will lead to a volume instability [29], substituting the stripe transition with a volume collapse transition and reintroducing hysteresis [95]. This is the most likely behavior to be found in real systems specially for large Q_R where the electronic compressibility is large and negative in the whole mixed state stability range. An incompressible background may seem unphysical according to the above discussion. However in some cases a sufficient separation of energy scales may avoid a volume instability if singularities in the compressibility are rounded by extrinsic effects. For example in ruthanates and in the 2D electron gas the relevant electronic phenomena occurs at temperatures below a tenth of a Kelvin to be compared with melting temperatures of the material of the order of hundreds of Kelvin.

5.3 3D systems and the maximum size rule

In this section we discuss the case of three-dimensional systems. For weak frustration, the behavior of 3D systems is expected to be similar to the one of the negative compressibility model for anisotropic systems analyzed in Chapter 3. From the effective Hamiltonian Eq. (5.6), it is simple to show that the dimensionless energy of a layered mixed state is given by:

$$\widetilde{f} = \frac{1}{\widetilde{R}_c} + 1 - 2\overline{\phi}\left(2\nu - 1\right) + \overline{\phi}^2 - 8\frac{\tilde{l}_s^2}{2\widetilde{R}_c}\left[u\left(0, \widetilde{R}_c, \tilde{l}_s\right) - u\left(2\nu, \widetilde{R}_c, \tilde{l}_s,\right)\right] \tag{5.13}$$

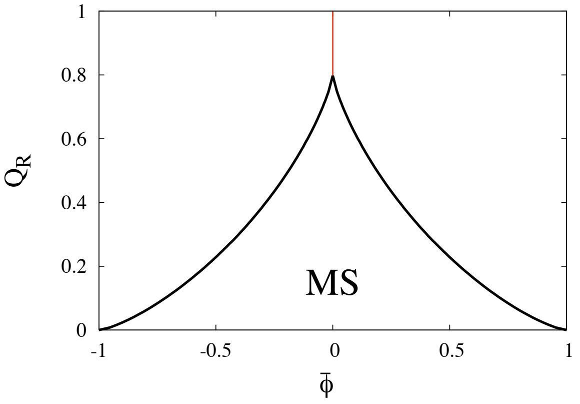

Figure 5.6: The phase diagram in the Q_R-dimensionless density plane for three-dimensional systems. The thick lines correspond to the second-order transitions from the homogeneous phase to the layered phase characterized by a divergent periodicity and a finite minority phase layer size. The thin line represents the first order transition between the two homogeneous phases that occurs for $Q_R > Q_{Rc}$.

where the effective interaction $u\left(q\right)$ is given by

$$u\left(q\right) = (1 + l_s^2 q^2)^{-1}.$$

Notice that the standard 3D screened Coulomb interaction is given by $u\left(q\right)/q^2$. The different nature of the screening in two- and three- dimensional systems affects strongly the properties of the mixed state. At the crossing density $\overline{\phi} = 0$, the exact expression for the energy density of a layered state is minimized for $\nu = R_d/R_c = 1/2$ and takes the following simple form:

$$\tilde{f} = 1 + \frac{1}{\tilde{R}_c}\left[1 - \frac{\sqrt{2}}{\sqrt{\pi}Q_R}\tanh\frac{R_c}{2l_s}\right] \tag{5.14}$$

The energy density of the uniform state is given by $\tilde{f} = 1$, hence for a layered state to be possible, the term in the brackets in Eq. (5.14) must become negative. This condition is equivalent to the existence of a critical frustrating parameter Q_{Rc} as it was derived within the UDA and now showed in an exactly solvable model.

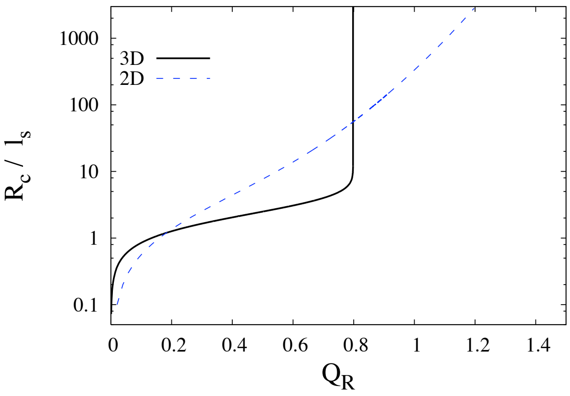

Figure 5.7: Behavior of the period of layers (log scale) vs Q_R at the crossing density in 3D (thick line) and 2D systems (dashed line).

The full exact 3D phase diagram for the layered state in the Q_R-density plane is shown in Fig. 5.6. As expected, it is very similar to the one obtained within the UDA in Refs. [29, 31]. The only difference is that in the UDA the uniform-inhomogeneous transition resulted weakly first order whereas here it is second-order like due to a divergence of R_c/R_d as in 2D.

The main difference with the 2D case is that the two second order transition lines from the homogeneous phase to the mixed state touch each other at $Q_R = Q_{Rc}$. For $Q_R > Q_{Rc}$ the systems has no intermediate state between the uniform phases and a direct first-order transition appears among them. In this case the cusp singularity at $\overline{\phi} = 0$ which produces a Dirac function like negative divergence of the compressibility, leads to a volume instability analogously to two-dimensional systems[29, 95].

Minimizing Eq. (5.14) respect to $\widetilde{R}_c$ one finds that $\widetilde{R}_c$ is smaller than a few screening lengths except in the unphysical case in which Q_R is fine-tuned exponentially close to Q_{Rc}. This is in contrast with the 2D case where R_c is unbounded for a generic

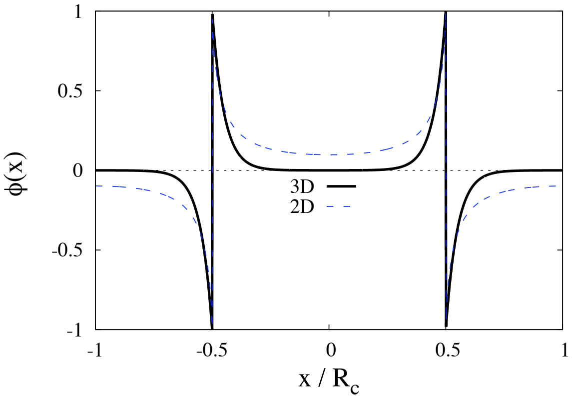

Figure 5.8: Charge density modulation for a cut perpendicular to the layers in 3D systems (thick line) and 2D systems (dashed line) at $\overline{\phi} = 0$ and a layer period $R_c = 20 l_s$.

large Q_R (Fig. 5.7).

This result is due to the different screening effect at strong frustration in three-dimensions with respect to the 2D case. To illustrate this difference we plot in Fig. 5.8, the charge density in 2D and 3D in a cut perpendicular to the stripe/layer for $R_c = 20 l_s$. The electronic charge density behavior inside the domains is dramatically different in 3D with respect to 2D. In the latter case, in fact, the charge density inside one stripe decays with a power-law from the interface and the local electronic charge density differs from the background density (i.e. $n(\mathbf{x}) \neq \overline{n}$) over the entire stripe width. As emphasized in Chapter 2, the phase separation energy gain stems from the regions where the local density $n(x)$ is significantly different from the global $\overline{n}$ value. Thus domains gain phase separation energy in all the region and there is no limitation for their size. This also explains why the mixed state can appear independently on how strong the frustration is.

In 3D the charge density decays exponentially from the interface over a distance of the order of the screening length. Thus the local electronic charge density and the background density are substantially different only in a region of width l_s around the interface. For $Q_R < Q_{Rc}$ the phase separation energy gain from these regions compensates the surface and Coulomb energy cost and makes inhomogeneities possible. Instead the central region in the 3D case of Fig. 5.8 produces an exponentially small phase separation energy gain and therefore one never finds inhomogeneities with $R_c >> l_s$, as in the figure, unless Q_R is exponentially close to Q_{Rc}. Indeed one can check from Fig. 5.7 that this is the case for the present value of R_c/l_s.

As a consequence, the system is forced to satisfy a "maximum size rule"[29, 31] that states that for generic parameters, the inhomogeneities cannot have all linear dimensions much larger than the 3D screening length l_s^{3D}. This allows for arbitrary large inhomogeneities in 2D since one of the dimensions is already smaller than l_s^{3D} as indeed found (Fig. 5.5).

The physics found in this section is not expected to change if the compressibility of the phases is different unless one goes to the extreme case in which one the phases is fully incompressible. The latter case will be analyzed in the following section

5.4 Charge relaxation in 2D metal-insulator striped phases

Because of the importance of the different charge relaxation in 2D systems contrary to 3D ones and the related "maximum" size rule, in this section we analyze the charge density behavior in 2D striped states of a compressible and an incopressible ($\kappa = 0$)

phase. This would correspond to a frustrated phase separation between a metallic and an insulating phase as relevant for example in doped Mott insulators.

Since the insulator is incompressible and thus electrostatiaclly inactive, we must consider only the excess density of mobile electrons counting from the insulating state. Within this scenario, we are thus reduced to study the problem between a metallic phase coexisting with voids.

Without loss of generality we can thus choose $n_A = 0$ and $f_A = 0$ respectively for charge density and the free energy of the insulating phase [see Fig. 5.9].

Indicating with V_B the B-phase domain volume of the compressible "metallic" phase and with V the total system volume, the total free energy of a striped phase can be put within a Local-Density-Approximation approach:

$$\begin{aligned} F \;=\; & \int_{\mathbf{r}\,\epsilon\,\mathbf{B}} f_B\left(n_B\left(\mathbf{r}\right)\right) d^2\mathbf{r} + \sigma \Sigma_{A\,B} + \frac{1}{2\,\varepsilon_0} \iint \frac{e^2}{\left|\mathbf{r_1} - \mathbf{r_2}\right|} \\ & \left[n_B\left(\mathbf{r_1}\right) - \overline{n}\right]\left[n_B\left(\mathbf{r_2}\right) - \overline{n}\right] d^2\mathbf{r}_1 d^2\mathbf{r}_2 \end{aligned} \tag{5.15}$$

where $\overline{n}$ is the global density, while $\Sigma_{A\,B}$ is the total interface surface. We still assume a sharp interface due to short range forces with the parameter σ parameterizing the surface energy. The constraint of charge neutrality of the system reads:

$$\int_{\mathbf{r}\,\epsilon\,\mathbf{B}} n_B\left(\mathbf{r}\right) d^2 r = \overline{n}\, V \tag{5.16}$$

Obviously, by minimizing with respect to the local density we recover the electrochemical potential constancy equation:

$$\mu_B\left(\mathbf{r}\right) - \frac{e}{\varepsilon_0}\phi\left(\mathbf{r}\right) = \mu_e \quad \forall\, \mathbf{r}\,\epsilon\,\mathbf{B} \tag{5.17}$$

where $\phi\left(\mathbf{r}\right)$ indicates the electrostatic potential generated by the charge distribution $\left[n_B\left(\mathbf{r}\right) - \overline{n}\right]$. This equation has to be solved together with the neutrality condition

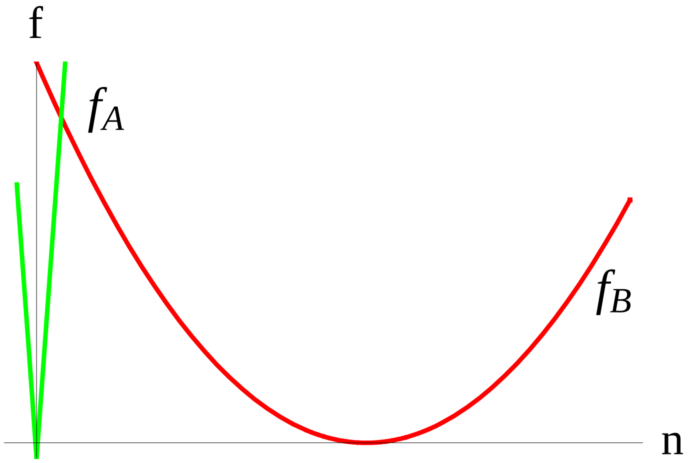

Figure 5.9: Sketch of the free energies of the uniform metallic B-phase in the parabolic approximation (red line) and the insulating A-phase (green line)

Eq. (5.16). Assuming for the metallic B-phase the following free energy expansion :

$$f_B = \mu_0 \left(n_B - n_B^0\right) + \frac{1}{2\kappa}\left(n_B - n_B^0\right)^2$$

shown schematically in Fig. 5.9, one obtains an equation relating the local density to the potential in terms of the compressibility:

$$n_B\left(\mathbf{r}\right) - n_B^0 = \kappa_B \left[\frac{e}{\varepsilon_0}\phi\left(\mathbf{r}\right) - \left(\mu_0 - \mu_e\right)\right] \quad \forall\,\mathbf{r}\,\epsilon\,\mathbf{B} \tag{5.18}$$

or in terms of the screening length

$$\phi\left(\mathbf{r}\right) - \frac{\varepsilon_0}{e}(\mu_0 - \mu_e) = 2\pi e l_s \left[n_B\left(\mathbf{r}\right) - n_B^0\right] \quad \forall\,\mathbf{r}\,\epsilon\,\mathbf{B} \tag{5.19}$$

In the limit of infinite compressibility i.e. zero screening length, the electrostatic potential is constant on the metallic regions and therefore $n_B\left(\mathbf{r}\right)$ corresponds to the distribution of a metal for which the 3D Laplace equation $\nabla^2\phi = 0$ is supplemented by the boundary condition $\phi = const$ on the domains. In this limit, the problem can be solved analytically for the stripes geometry. In fact, the Coulomb potential can

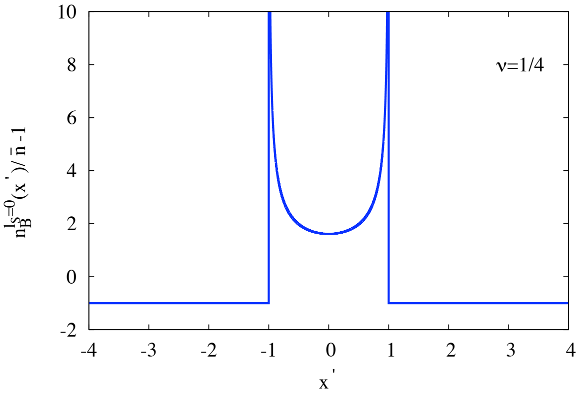

Figure 5.10: The excess charge density profile $n_B^{l_s=0}(x')/\overline{n}-1$ in the direction perpendicular to the stripe for $\nu=1/4$. x' is the component of $\mathbf{r}/\mathbf{R_d}$ perpendicular to the stripe.

be calculated by using the Schwarz-Christoffel conformal transformations [96] in this case. The B-phase density spatial dependence comes out:

$$n_B^{l_S=0}(x') = \overline{n}\,\frac{\left|\cos\dfrac{\pi x'\nu}{2}\right|}{\sqrt{\sin^2\dfrac{\pi\nu}{2}-\sin^2\dfrac{\pi x'\nu}{2}}} \tag{5.20}$$

where x' indicates the x component of the dimensionless coordinate $\mathbf{r}'$ defined by $\mathbf{r}'=\mathbf{r}/\mathbf{R_d}$. In Fig. (5.10) we show the spatial dependence of the excess charge density $n_B^{l_s=0}(x')/\overline{n}-1$ in one unit cell.

Keeping in mind that the charge in the stripe region is undercompensated by the background, one finds that at this level of approximation the metallic stripe behaves as a macroscopic charged metallic strip. The density accumulates on the border of the stripe and decays with the power law $1/\sqrt{x}$ towards the center. Thus one can conclude that the power law charge relaxation in 2D has a general character and depends upon the macroscopic electrostatics.

Of course the divergence of the electronic density at the surface of the stripe [see

Fig. 5.10] is unphysical and will be cutoff by a microscopic length (see below) but this does not affect the behavior of the charge far from the surface that is essential for our argument.

To clarify this point, now we calculate the charge density profile for $l_S \neq 0$. The unphysical divergence of the metallic density will be removed. We restrict to the stripe geometry as above but the same method can be used for other geometries. Using the superposition principle both charge and potential can be written as the sum of the terms evaluated above for infinite compressibility (*i.e.* for $l_s = 0$) plus a correction, which we wish to compute:

$$\phi\left(\mathbf{r}\right) = \phi^{l_S=0}\left(\mathbf{r}\right) + \delta\phi\left(\mathbf{r}\right) \tag{5.21}$$

$$n_B\left(\mathbf{r}\right) = n_B^{l_S=0}\left(\mathbf{r}\right) + \delta n_B\left(\mathbf{r}\right) \tag{5.22}$$

The correction $\delta\phi\left(\mathbf{r}\right)$ satisfy the effective Poisson equation:

$$|q|\delta\phi\left(q\right) = -2\pi e \delta n_B(q) \tag{5.23}$$

as follows from the effective 2D Poisson equation in momentum space. The unknown Lagrange multiplier μ_e has to be determined by fulfilling the neutrality condition and can also change as l_s is increased from zero:

$$\mu_e = \mu_e^{l_s=0} + \delta\mu_e.$$

Eq. (5.19) can be put as

$$\delta n_B\left(\mathbf{r}\right) = \frac{1}{2\pi e\, l_S}\delta\phi\left(\mathbf{r}\right) - n_B^{l_S=0}\left(\mathbf{r}\right) + n_e \qquad \forall\, \mathbf{r} \,\epsilon\, \mathbf{B} \tag{5.24}$$

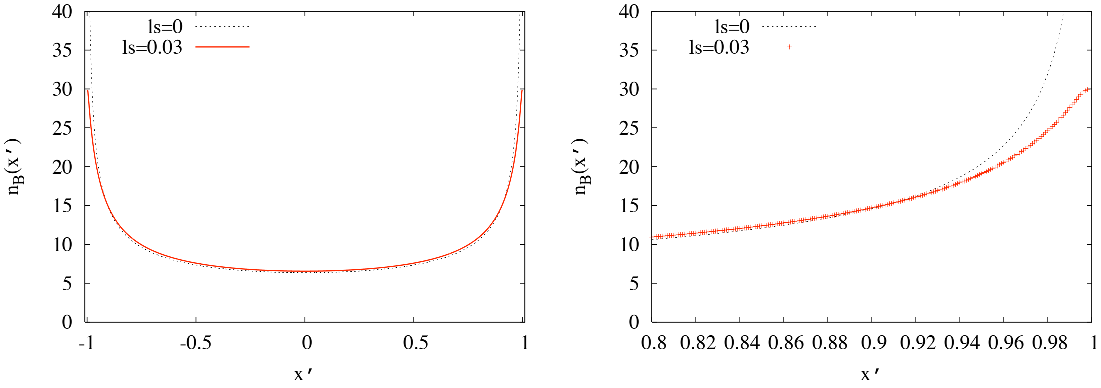

Figure 5.11: Left panel: Comparison between the electronic charge density at $l_S/R_d = 0$ and $l_S/R_d = 0.03$ evaluated at $\nu = 1$ and $\overline{n} = 1$. Right panel: Expansion near the inhomogeneity surface.

where we have absorbed the Lagrange parameter in the constant $n_e = n_B^0 + \frac{\varepsilon_0}{2\pi e^2 l_s}\delta\mu_e$.

In Fourier space we get:

$$\begin{aligned}\delta n_B(q) &= \frac{1}{2\pi e\, l_S R_c}\sum_{q'}\delta\phi(q')\frac{\sin\left[(q-q')R_d\right]}{(q-q')} \\ &- n_B^{l_S=0}(q) + n_e\frac{2\sin(qR_d)}{q}. \end{aligned} \tag{5.25}$$

Eq. (5.23)and Eq.(5.25) are a closed system since the quantities with $l_S = 0$ are known from the previous treatment. In the case $R_c, R_d >> l_S$ one can substitute $\sum_q \to 2R_c\int dq/(2\pi)$ and make the approximation:

$$\frac{2\sin\left[(q-q')R_d\right]}{(q-q')} \to 2\pi\delta(q-q'). \tag{5.26}$$

Using Eq. (5.23) we obtain:

$$\delta n_B(q) = \frac{2n_e\sin(qR_d)/q - n_B^{l_S=0}(q)}{1+1/(l_S|q|)} \tag{5.27}$$

In the limit $q \to 0$ we obtain $\delta n_B \to 0$. The uniform component of the charge does not change and therefore $\delta\mu_e = 0$ and $n_e = n_0^B$. We have evaluated the above expression via a discrete Fourier transform in the limit in which the stripes are far apart ($R_c/R_d \to \infty$ *i.e.* $\nu \to 0$). This corresponds to solve the problem for a single stripe. The electronic density at $l_S = 0$ can be put as:

$$n_B^{l_S=0}(x') = \frac{2\overline{n}}{\pi\nu}\frac{1}{\sqrt{1-(x')^2}}$$

In Fig. 5.11 we show the total electronic charge density for $l_S/R_d = 0.03$. The main difference with respect to the $l_S = 0$ case is that the unphysical divergence of the density at the stripe surface is removed and the density tends to a finite value at the stripe boundary. Notice that at distances from the interface larger than l_S the charge density at $l_S \neq 0$ practically coincides with the one at $l_S = 0$ as expected. Our previous conclusion regarding the absence of upper bounds for the size of the domains remains unchanged. In the entire domain, the local density differs from the average density and therefore the phase separation energy gain comes from the whole domain and not from the electric field penetration depth as it happens in the 3D case.

Chapter 6

Anomalous dimensions of $N = 4$ SYM from the Hubbard model

The $N = 4$ super Yang-Mills (SYM) theory has a well-known duality to strings in a $AdS_5 \times S^5$ background. [100, 101, 102, 103, 104]. In particular, the anomalous dimensions of long composite operators in the planar limit correspond to masses of string states with large angular momentum. The calculation of anomalous dimensions in specific sectors of the $N = 4$ theory can be cast in algebraic form by computing the loop corrected dilatation operator [105]. At one-loop, the dilatation operator can be identified with the Hamiltonian of the integrable XXX spin 1/2 lattice model [106]. As the loop order increases, the dilatation operator can be identified with the Hamiltonian of a spin chain with an increasing range of the spin interaction. Since the spin model is nothing but the strong coupling expansion of an itinerant fermion model , it has been proposed [107] the one-dimensional (twisted) Hubbard model hamiltonian as the correct all loops dilatation operator of the $N = 4$ SYM. The analysis of the

Hubbard states can be performed via the Lieb-Wu equations which encode integrability (Sec. 6.1). We will explore these equations for the case of two particular states , the so-called antiferromagnetic state (AF) [108] (Sec. 6.2) and the folded-string state (FS) (Sec. 6.3) [109]. A large portion of this chapter appeared in Refs. [110, 111].

6.1 The twisted Hubbard model

The correspondence between the Hamiltonian of a spin-chain model and the dilatation operator of the $N = 4$ SYM allows for the knowledge of the anomalous dimensions in the gauge theory. In the SU(2) sector, the Hubbard model should predict at all loops and non-perturbatively the anomalous dimensions of gauge operators of fixed length L [107]. In the following we will consider an half-filled Hubbard Hamiltonian :

$$H = H_0 + \frac{\sqrt{\lambda}}{4\pi} H_1$$

where $\lambda = g_{\mathrm{YM}}^2 N$ indicates the 't Hooft coupling, H_0 contains the on-site Coulomb-type interaction:

$$H_0 = L - \sum_{i=1}^{L} n_{\uparrow,i}\, n_{\downarrow,i}, \qquad n_{\sigma,i} = c^{\dagger}_{\sigma,i}\, c_{\sigma,i}$$

while H_1 is the free fermion part:

$$H_1 = \sum_{\sigma=\uparrow,\downarrow} \left(\sum_{i=1}^{L-1} c^{\dagger}_{\sigma,i}\, c_{\sigma,i+1} + e^{i\phi} c^{\dagger}_{\sigma,L}\, c_{\sigma,1} \right) + \text{h.c.}$$

The parameter $\phi = \pi/2$ arises from an Aharonov-Bohm flux which is needed to reproduce the Bethe-Ansatz multiloop BDS equations [112] . In addition, the introduction of the twisting phase makes the Hamiltonian invariant under the shift:

$$\begin{aligned} c_{\sigma,j} &\rightarrow e^{i\phi/L} \quad c_{\sigma,j+1}, \qquad j = 1, \ldots, L-1, \\ c_{\sigma,L} &\rightarrow e^{i\phi(L+1)/L}\, c_{\sigma,1}, \end{aligned} \tag{6.1}$$

and related transformations for annihilation operators. Information about composite operators anomalous dimensions can be derived from the analysis of the full Hubbard model spectrum. The coupling dependent spectrum flow has been evaluated numerically through direct diagonalization method for lattices from $L = 4$ [113] to $L = 8$ [110] by considering only states with total spin zero and invariant under the shift Eq.(6.1). The latter assumption reduces the Hilbert space. For example it has been shown that in a half-filled $L = 8$ lattice the total dimension is reduced from 4900 to 226 [110]. Several crossings of the coupling dependent levels have been observed. This apparent violation of the Wigner-Von Neumann non-crossing rule follows directly from nontrivial coupling dependent conservation laws and is a characteristic signature of the one-dimensional Hubbard model quantum integrability [114].

Notice that the fermion Hubbard model introduces states with double occupancy that do not have a direct correspondence with the gauge theory composite operators. Below, we will consider the coupling dependent behavior of states that at $\lambda = 0$ reduces to states with no double occupancy, *i.e.* the states that have classical anomalous dimensions $\Delta(\lambda = 0) = L$ (the perturbative multiplet in Ref [110]). Nevertheless as the 't Hooft coupling increases, these states will mix with all the *extra* states with double occupancy. We assume an optimistic attitude, waiting for a better understanding of the role of the Hubbard model.

The direct diagonalization method is clearly turning off for large dimensions of the

Hilbert space. Nevertheless it is possible to investigate longer composite operators using the integrability of the one-dimensional Hubbard model shown in Ref.[115].

After working out the S-matrix, one needs to diagonalize the multi-particle system by a nested Bethe Ansatz. The result of this procedure, generalized to the case with the twisting phase, yields the following Lieb-Wu equations for an half-filled lattice:

$$\begin{aligned} L\, q_n &= 2\pi\, I_n + 2\sum_{j=1}^{L/2} \tan^{-1}\left[2(u_j - \frac{\sqrt{\lambda}}{2\pi}\sin(q_n+\phi))\right], \qquad (6.2) \\ 2\pi\, J_k &= 2\sum_{j=1}^{L/2} \tan^{-1}(u_k - u_j) - 2\sum_{m=1}^{L} \tan^{-1}\left[2(u_k - \frac{\sqrt{\lambda}}{2\pi}\sin(q_m+\phi))\right], \end{aligned}$$

where $\phi \equiv \pi/(2L)$ and the I_n, J_k are the Bethe quantum numbers. The quantum numbers q_n are the Bethe momenta of the particles while the u_i are the spin rapidities (Bethe roots) and describe the spin state. At $\lambda = 0$, the Lieb-Wu equations simplify since the equations for the momenta and the spin rapidities decouple and can be solved successively. Together with this decoupling, there is a decoupling of the wave function into a charge and a spin part that is determined by the Bethe Ansatz of a Heisenberg spin chain. Once the spin rapidities of a particular state are determined in the Heisenberg model, it is possible to follow the evolution as the 't Hooft coupling increases, and finally to determine the strong-coupling behavior of any state.

6.2 The AF operator

At $\lambda = 0$ the state with highest anomalous dimensions corresponds to the ground state of the one-dimensional Heisenberg antiferromagnet. The Bethe-Ansatz solution in the thermodynamic limit has been found by Hulthén in 1938 [116]. Instead, we determine the Bethe roots for L finite and then follow the evolution as the 't Hooft

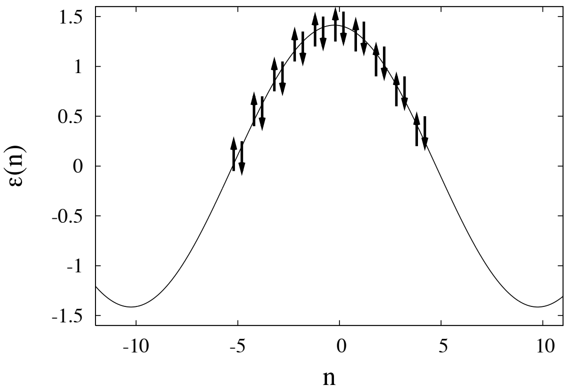

Figure 6.1: Asymptotic free fermion state for the AF operator at $L = 20$.

coupling increases by solving step by step the Lieb-Wu equations. From the knowledge at every step of the Bethe momenta, we can determine the weak-strong coupling flow of the anomalous dimensions for the antiferromagnetic operator. In particular by determining the asymptotic free fermion state at strong coupling, we can provide a series expansion in inverse powers of λ:

$$\Delta^H_{\mathrm{AF}}(\lambda, L) = a_0(L)\sqrt{\lambda} + a_1(L) + a_2(L)\frac{1}{\sqrt{\lambda}} + \dots \tag{6.3}$$

We find that the asymptotic free fermion state corresponds to the ground state of the Hubbard hopping term shown in Fig.6.1. This is the state where all positive energy levels are doubly occupied and thus we have:

$$|\psi_0^{AF}\rangle = \prod_{n=1}^{L-1} \prod_{\sigma=\uparrow,\downarrow} a^\dagger_{\sigma,p_n}|0\rangle$$

where $a^\dagger_{\sigma,p_n}$ is the canonical creation operator in the momentum space. Since the dispersion relation for the hopping term :

$$\varepsilon_n = 2\,\cos\left(\frac{2\pi n}{L} + \frac{\pi}{2L}\right),$$

we can easily obtain the function $a_0(L)$ of the expansion Eq.(6.3):

$$a_0(L) = \frac{1}{2\pi} \sin^{-1} \frac{\pi}{2L}$$

In addition, we can compute analytically $a_1(L)$ from first-order perturbation theory. Expressing the Coulombian term H_0 of the Hubbard hamiltonian in momentum space, we obtain:

$$a_1(L) \equiv \langle \psi_0^{AF} | L - \frac{1}{L} \sum_{n,n',m,m'} \delta\left(n - n' + m - m'\right) a^\dagger_{\uparrow,n} a_{\uparrow,n'} a^\dagger_{\downarrow,m} a_{\downarrow,m'} | \psi_0^{AF} \rangle$$

It is easy to verify that the latter expression reduces to:

$$a_1(L) \equiv \langle \psi_0^{AF} | L - \frac{1}{L} \sum_{n,m} a^\dagger_{\uparrow,n} a_{\uparrow,n} a^\dagger_{\downarrow,m} a_{\downarrow,m} | \psi_0^{AF} \rangle = L - \frac{1}{L}\left(\frac{L}{2}\right)^2 = \frac{3}{4} L$$

Finally the next-to next-to leading order coefficient can be put as:

$$a_2(L) = 2\sqrt{2}\pi \, \delta_{\mathrm{AF,L}} \, L$$

with $\delta_{\mathrm{AF,L}}$ numerically evaluated for finite $L \in 4\mathbb{N}$ up to $L = 32$ (see Fig.6.2) It is interesting to compare our expansion with the prediction of the AF state anomalous dimensions calculated via the BDS multi-loops Bethe Ansatz equations. In this case a series expansion in inverse power of L is available. Thus:

$$\Delta^{BDS}_{\mathrm{AF}}(\lambda, L) = b_0(\lambda) L + b_1(\lambda) + b_2(\lambda) \frac{1}{L} + \dots \tag{6.4}$$

The leading order coefficient corresponds to the solution of the BDS Bethe Ansatz in the thermodynamic limit $L \to \infty$ [108]. It reads:

$$b_0(\lambda) = 1 + \frac{\sqrt{\lambda}}{\pi} f\left(\frac{\pi}{\sqrt{\lambda}}\right)$$

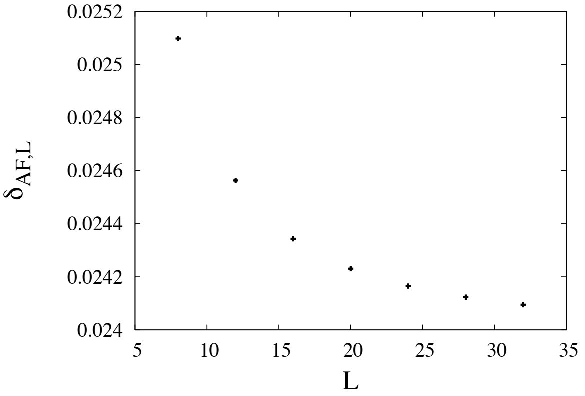

Figure 6.2: Behavior of the next-to subleading term coefficient at strong coupling and finite $L \in 4\mathbb{N}$.

where

$$f(x) = \int_0^\infty \frac{dk}{k} \frac{J_0(k)\, J_1(k)}{1 + e^{2\,k\,x}},$$

and the $J_\nu(x)$ are the Bessel functions of the first kind. In order to obtain the next-to and the next-to next-to leading order of the expansion Eq.(6.4), one has to take into account finite size correction to the thermodynamic limit. It has been showed [117, 111] that the subleading order

$$b_1(\lambda) \equiv 0$$

whereas the next-to subleading order coefficient results:

$$b_2(\lambda) = \frac{\sqrt{\lambda}}{12} \frac{I_1\left(\frac{\sqrt{\lambda}}{2}\right)}{I_0\left(\frac{\sqrt{\lambda}}{2}\right)},$$

where $I_\nu(x)$ are the modified Bessel functions of the first kind. We can match the two expressions in the double limit $\lambda, L \to \infty$. Within the Hubbard formulation, the anomalous dimensions Eq.(6.3) can be expanded at large L to obtain:

$$\Delta^H_{\mathrm{AF}} = \left[\frac{L}{\pi^2} + \frac{1}{24\,L} + o\left(\frac{1}{L}\right)\right] \sqrt{\lambda} + \frac{3}{4} L + (\delta_{\mathrm{AF},\infty} + \ldots)\, \frac{2\sqrt{2}\pi}{\sqrt{\lambda}}\, L \qquad (6.5)$$

where the coefficient $\delta_{\mathrm{AF},\infty} \sim 0.0240(1)$ has been found from a simple polynomial extrapolation of $\delta_{\mathrm{AF,L}}$. On the other hand, the BDS prediction can be computed in the strong coupling limit. The subleading order coefficient can be expanded asymptotically as [118]:

$$f(x) = \frac{1}{\pi} - \frac{x}{4} + \sum_{m=1}^{N} \mu_m x^{2m} + O(x^{2N+2}),$$

where

$$\mu_m = \frac{(2m-1)(2^{2m+1}-1)\left[(2m-3)!!\right]^3}{2^{3m-1}(m-1)!} \frac{\zeta(2m+1)}{\pi^{2m+1}}, \qquad (-1)!! \equiv 1.$$

and ζ is the Riemann zeta function. In addition, it is easy to verify that the asymptotic value of the next-to subleading order coefficient is given simply by:

$$b_2\left(\lambda \to \infty\right) = \frac{\sqrt{\lambda}}{12}$$

Inserting the latter expansions in Eq.(6.4), we find that the two Ansatz have a perfect matching in the terms $\propto L$ but a discrepancy of a factor 2 arises in the term $\sqrt{\lambda}/L$. This shows that only in the thermodynamic limit, the two different approaches give the same results. The discrepancy in the finite size term may be due both to the uncontrolled effect of the *wrapping* interactions which start to contribute at the perturbation order $o(\lambda^L)$ in the BDS description and to the different order of limits $\lambda, L \to \infty$. More interestingly the leading behavior at strong coupling in both descriptions of the anomalous dimensions scales as $\lambda^{1/2}$. It seems difficult to recover the generic Gubser-Klebanov-Polyakov (GKP) law [104]:

$$\Delta \sim 2\sqrt{n}\,\lambda^{1/4}$$

It has been thus proposed to identify the dual string state of the antiferromagnetic state with *slow-moving* string solutions [119] that have the same scaling behavior.

However such string states scale as:

$$\Delta \sim \sqrt{\lambda} L$$

This implies that the string solution has a numerical discrepancy $1/\pi^2$ in the numerical prefactor with the dual gauge operator. Along a different route, one can start from the classical string theory at large λ and derive string Bethe Ansatz equations which are expected to match string calculations including leading quantum corrections. The latter approach has been recently studied and the leading behavior at large λ for the antiferromagnetic operator has been shown to reproduce the GKP law.

6.3 The FS state

It is well known that Bethe solution of the Heisenberg antiferromagnet admits the existence of states with spin rapidities that acquire an imaginary part. In this case the Bethe wave function is made up of plane waves with complex wave vector. These states are usually named 'Bethe string solution' and can be identified with quantum Bloch wall state [120, 121]. We consider the state with complex spin rapidities that corresponds to the state with lowest anomalous dimensions in the perturbative multiplet *i.e.* the lightest state. For this state, it has been shown that the Bethe roots (the spin rapidities) condense in the thermodynamic limit in two symmetrical curves in the complex plane [122] and it is thus named the *double contour* solution. Its string state dual is nothing but the folded string state described in Ref.[109]

As for the antiferromagnetic operator, we determine at $g = 0$ the spin rapidities considering lattices with $L = 12, 20$ and determined step by step the evolution at

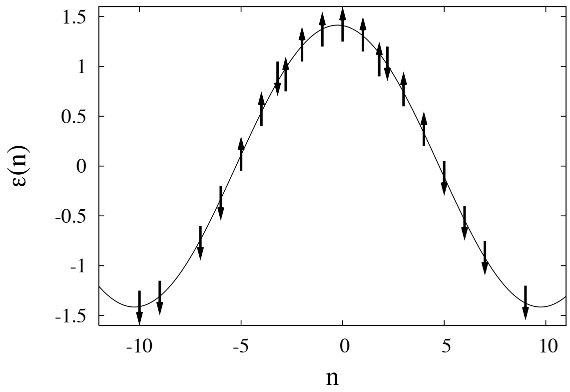

Figure 6.3: Free fermion state for the FS. The modes $n = \pm 8$ are empty. We show only a particular spin configuration for the singly occupied levels.

strong coupling of u_i as well as of the Bethe momenta q_n. For both lattices we find that in the limit $g \to \infty$, the Bethe momenta flow to a state, shown in Fig.(6.3), where the positive energy levels with mode numbers $n = k, L-k-1$ are doubly occupied and the negative mirror levels are empties. The other positive levels are singly occupied as well as their negative mirror levels, thus they do not contribute to the leading term of the state energy. Since the results are completely identical for the two lattices we conjecture that for all $L = 4(2k+1)$ the pattern will be identical. From the dispersion relation for the hopping term of the Hamiltonian the leading term of the anomalous dimensions at strong coupling results:

$$\Delta^0_{\rm FS}(\lambda, L) = \frac{\sqrt{2}}{\pi} \cos\frac{\pi}{2L}\sqrt{\lambda} \tag{6.6}$$

The next-to leading term is computed from perturbation theory. It is easy to verify that the non-vanishing matrix elements of $\langle\psi_0^{FS}|H_0|\psi_0^{FS}\rangle$ can be cast as:

$$\Delta^1_{\rm FS}(g, L) = \langle\psi_0^{FS}|L - \frac{1}{L}\sum_{n,m} a^\dagger_{\uparrow,n}a_{\uparrow,n}a^\dagger_{\downarrow,m}a_{\downarrow,m} - \frac{1}{L}\sum_{n,m} a^\dagger_{\uparrow,n}a_{\uparrow,m}a^\dagger_{\downarrow,m}a_{\downarrow,n}|\psi_0^{FS}\rangle \tag{6.7}$$

The first two terms have been computed for the AF operator. The third term, contrary is a spin-flip that gives non zero contribution only between singly occupied mirror levels. Thus we have:

$$\Delta^1_{\rm FS}(g, L) = L - \frac{1}{L}\left[\left(\frac{L}{2}\right)^2 + \left(\frac{L}{2} - 2\right)\right] \tag{6.8}$$

Finally the series expansion for the folded string anomalous dimensions can be put as:

$$\Delta_{\rm FS}(g, L) = \frac{\sqrt{2}}{\pi}\cos\frac{\pi}{2L}\sqrt{\lambda} + \frac{3L^2 - 2L + 8}{4L} + \delta_{\lambda,L}\,\frac{2\sqrt{2}\pi}{\sqrt{\lambda}}\,L + \cdots\,, \tag{6.9}$$

Similarly to the antiferromagnetic state, the next-to next-to leading order coefficient $\delta_{\lambda,L}$ can be computed from the numerical exploration of the Lieb-Wu equation. We find:

$$\begin{aligned} \delta_{\lambda,12} &= 0.597(1) \\ \delta_{\lambda,20} &= 0.953(1) \end{aligned}$$

Similarly to the AF state, a different scaling behavior in λ is expected in the string side [123, 111]. This feature suggests that it seems dangerous to rely on the gauge Bethe Ansatz equations to estimate the strong coupling limit of general states.

Chapter 7

Conclusions

In this thesis, we analyzed the main aspects of frustrated phase separation in charged systems considering two kind of compressibility anomalies that generally occur in strongly correlated systems. For the different coarse-grained models that have been introduced, the outcome of long-range forces can be measured by a dimensionless parameter that defines the amount of frustrating effects. Frustration tends to reduce the range of density where a mixed state appears. Thus uniform phases are possible at densities where, in the absence of long-range forces, phase separation would occur. This situation is in accord with capacitive measurements [48, 49] in the uniform two-dimensional electron gas that have revealed the stability of a homogeneous phase with negative compressibility.

In the presence of frustration, the mixed state consists of domains of mesoscopic size with various structures depending on the control parameters. A sequence of morphological transitions occurs resembling the evolution of domain patterns in other systems [1, 4].

When frustrating effects are a small perturbation upon the phase separation mechanism, a universal picture of frustrated phase separation can be achieved. We have shown that the properties of frustrated phase separated states can be captured by a simple approximation in which the density inside the domains is assumed constant. It gives very accurate results once the effect of the long-range Coulomb interaction upon interface effects is considered. We have shown that this can be easily reached in three-dimensional systems. The price to pay is that new long-range terms appear due to the interaction of the field at the interface with the dipole layer. However the new term is tractable leading to a useful theory.

Upon increasing frustrating effects, the situation is more complex and the properties of mixed states strongly depends upon the particular form of the free energy. Thus, the two compressibility anomalies represent two different universality classes.

In systems with a cusp singularity, we found the system dimensionality to play a key role in frustrated phase separation. Two-dimensional systems display a prominent tendency towards charge inhomogeneous states. No matter how strong the frustrating effects are, an inhomogeneous state always preempts a direct first-order transition between two homogeneous phases in accord with Ref.[73]. This result is due to the macroscopic electrostatic of two-dimensional systems that allows for a charge imbalance in all the domain size. The system gain phase separation energy in the entire region leading to arbitrary large domains. An opposite feature is instead expected in three-dimensional systems. Screening effects are dominant and the typical domain size is bounded by the screening length.

The computation in the exactly solvable model of Chapter 5 confirms the "maximum" size rule [29] that states that inhomogeneities cannot have all linear dimensions much larger than the three-dimensional screening length l_s^{3D} independently of the frustration degree. Therefore mesoscopic domains can be expected in systems with small compressibility as bad metals or systems close to metal-insulator transitions or systems with very anisotropic electronic properties which makes them effectively two-dimensional (i.e. are nearly insulating in one direction).

Systems with a short-range negative electronic compressibility represent a different universality class. A critical value of the frustration Q_{R0} exists for both two- and three-dimensional systems. Close to Q_{R0}, the inhomogeneous state are generally expected as sinuisoidal charge density waves occurring at a charge susceptibility divergence. We have found that an isotropic system never reaches the Gaussian instability line except for a critical point. The second-order phase transition to sinuisoidal charge density waves is always preempted by a first-order phase transition to ordered structures. Using an approach similar to the mean-field theory of the liquid-crystal theory [83] we were able to determine the competition between all the expected structures close to the critical point. The inhomogeneous states appears in the form of a BCC crystal near Q_{R0} which is followed by a triangular lattice of inhomogeneities reminiscent of the Abrikosov vortex lattice in type II superconductors above the lower magnetic critical field H_{c_1}. A subsequent morphological transition can lead to a layered state corresponding to a smectic electronic liquid phase [41]. More complicated structures as an icosahedral quasicrystal have been found to never become favorable. At weak couplings, the same structures above discussed appear but in this case they present in the form of sharply defined droplet, rods, and layered inhomogeneities.

In solid-state systems an anisotropy in the underlying crystal field can favor certain orientations of the interfaces that, in turn, can change dramatically the nature of the transition to mixed states. Indeed it can become second order with a tricritical point separating the second-order transition line at strong coupling from the first-order transition line at weak coupling. This is important for theories of metallic systems where the existence of a second order quantum critical point separating an homogeneous phase from an inhomogeneous one, can destroy the Fermi liquid behavior [16].

In two dimensional systems, the phase diagram resembles the phase diagram of an anisotropic three-dimensional system. However, for a truly two-dimensional system, a new effect will arise. Indeed, close to the transition from the homogeneous phase to the inhomogeneous one, a new state is expected to appear. It will be formed by stripes which have inside smaller inhomogeneities alternated with homogeneous stripes.

Charge inhomogeneities seems to be related to a number of interesting phenomena in systems as colossal magnetoresistance manganites, high-temperature superconductors and other strongly correlated materials. As discussed in the Introduction, the situation in manganites is quite complex. In layered cuprates one finds striped charge and spin density waves at small doping and a Fermi liquid at large doping. From the behavior of the mean-field energy[37], it is quite natural to expect phase separation among the stripe state and the overdoped Fermi liquid crossing at some density. To make a rough estimate of the typical size of the domains, we identify the stripe state as the pseudogap phase. If we assume that the surface energy is of order $\sigma \sim J/a$, with J the superexchange constant and a the lattice constant, the typical size of the domains can be written as [c.f. Chapter2]:

$$l_d \sim \frac{a}{\Delta x}\left(\frac{\epsilon_0 a J}{2a_0 Ry}\right)$$

where a_0 is the Bohr radius, $\Delta x \sim 0.1$ is the range of doping where one expects phase separation according to Maxwell construction. Using $J = 0.01Ry$, $a = 7.2a_0$, $\epsilon_0 = 5$, one gets $2R_d \ \sim 8a \sim 30\mathring{A}$ which compares well with the inhomogeneities found in Ref.[21]. Although several indirect manifestation of mesoscopic phase separation are evident in the literature as discussed in the Introduction, it has been difficult to make more detailed comparison with experiments. This is mainly because specific probes of the electronic distribution in the bulk are lacking. Thus one can infer the effects of mesoscopic phase separation only indirectly by what happens in the surface and by the anomalous response (often gigantic) to external fields. We hope that our study stimulates further experimental and theoretical work in this regard.

Appendix A

Effective Poisson equation in two-dimensional systems

In this appendix, we derive the effective Poisson equation in two-dimensional systems subject to the three-dimensional Coulomb interaction. Let us begin by considering the three-dimensional Poisson equation

$$\nabla^2 \psi^{3D}\left(\mathbf{r}, z\right) = -4\pi Q_R \left[\overline{\phi}(z) - \phi\left(\mathbf{r}, z\right)\right] \tag{A.1}$$

where $\mathbf{r}$ is a two-dimensional vector in the plane of the system while z measures the distance from the plane. In order to keep the notation consistent, we are referring here to the renormalized Coulomb coupling Q_R and the dimensionless charge density ϕ. Finally the dimensionless electrostatic potential ψ^{3D} is defined as:

$$\psi^{3D}(\mathbf{r}, z) = Q_R \int \frac{\left[\overline{\phi}(z') - \phi(\mathbf{r}, z')\right]}{\left[(\mathbf{r} - \mathbf{r'})^2 + (z - z')^2\right]}$$

The 3D charge density can be defined as $\overline{\phi}(z) - \phi\left(\mathbf{r}, z\right) = \left[\overline{\phi} - \phi(\mathbf{r})\right] \delta\left(z\right)$ with $\phi(\mathbf{r})$ the 2D in plane electronic charge density and $\overline{\phi}$ its average value. To solve

Eq.(A.1), we perform a partial Fourier transform in the plane coordinates and define the Fourier decomposition of the charge density as:

$$\phi^{3D}\left(\mathbf{r},z\right)=\frac{1}{V}\sum_{\mathbf{k}}e^{i\mathbf{k}\cdot\mathbf{r}}\,\phi^{3D}\left(\mathbf{k},z\right) \tag{A.2}$$

where the $\mathbf{k}=0$ term $\phi^{3D}\left(\mathbf{k},z\right)=\overline{\phi}(z)$ to fulfill neutrality of the system. A similar Fourier decomposition holds for the electrostatic potential. By restricting to one-dimensional charge modulation, the Poisson equation is then:

$$\frac{\partial^2\psi^{3D}\left(k,z\right)}{\partial z^2}-k^2\psi^{3D}\left(k,z\right)=+4\pi Q_R\phi(k)\delta\left(z\right) \qquad k\neq 0 \tag{A.3}$$

with $\phi(k)$ defined as the Fourier transform of the in plane electronic charge density For $z\neq 0$ the solution for the potential is $\psi^{3D}\left(k,z\right)=\psi^{3D}(k,0)e^{-|k||z|}$. Integrating Eq. (A.3) in a small interval around $z=0$, one obtains the boundary condition:

$$|k|\psi(k)=-2\pi Q_R\phi(k) \tag{A.4}$$

with the Fourier transform of the in-plane electrostatic Coulomb potential defined as $\psi(k)\equiv\psi^{3D}\left(k,0\right)$. This 3D boundary condition Eq. (A.4) corresponds to the effective 2D Poisson equation. It is also interesting to compare the effective 2D Poisson equation in momentum space with the 3D analog. In three-dimensional systems, the momentum space version of the Poisson equation easily reads $\psi(\mathbf{k})=-4\pi Q_R\phi(\mathbf{k})/|\mathbf{k}|^2$ at finite momentum, thus one can conclude that for $D=2,3$:

$$\psi(\mathbf{k})=-\frac{2^{D-1}\pi Q_R}{|\mathbf{k}|^{D-1}}\phi(\mathbf{k}) \tag{A.5}$$

Appendix B

Mixing energy in the Uniform Density Approximation

In this appendix, we compute the morphological dependence of the mixing energy Eq.(2.19) in two- and three-dimensional systems subject to the three-dimensional Coulomb interaction. In the following, we will limit to explicitly consider cylindrical rods in 3D and disk in 2D but the method can be used for the other relevant geometries addressed in Chapter[3].

- **Three-dimensional systems**

We assume cylindrical rods of radius $\tilde{R}_d$ in unit of ξ and height $\tilde{H}$ with charge density ϕ_B of the B-phase embedded in a homogeneous matrix of the A-phase at charge density ϕ_A. Within the Wigner-Seitz-Approximation, we can divide the system in neutral cylindrical cells of volume $\pi \tilde{R}_c^2 h = V/N_r$ with V the system volume and N_r the number of rods. Finally $\tilde{R}_c$ is the radius of the cell in unit of the bare correlation length ξ. Next we compute the electrostatic energy. The cells are globally neutral by construction and only the charge density inside the cell contributes to the electric field in the cell. For the purpose of computing the electrostatic energy, it is convenient to consider an electronic charge density $\delta\phi = \phi_B - \phi_A$ inside the cylindrical rod and a background in the entire cell of positive charge density $\overline{\phi} - \phi_A$. We will call the former "rod" contribution and the latter "background" contribution.

The total electric field inside the cell can be written as $\mathbf{E} = \mathbf{E_r} + \mathbf{E_b}$ where $b(r)$ refers to the background (rod) contributions that are related to the charge densities by the dimensionless Poisson equation for the electric field

$$\begin{aligned}\nabla \cdot \mathbf{E_r}\,(r) &= -4\pi Q_R \delta\phi \\ \nabla \cdot \mathbf{E_b}\,(r) &= 4\pi Q_R \left[\overline{\phi} - \phi_A\right]\end{aligned}$$

Obviously the electric fields depend only upon the radial direction due to the cylindrical symmetry. Integrating the square of the electric field inside one cell, we obtain three different contributions to the electrostatic energy $F_{lr} = F_d + F_b + F_{d-b}$, with

$$F_d = \frac{1}{8\pi}\int d^2\mathbf{r}\mathbf{E}_d(\mathbf{r})$$

and a similar equation for the background contribution F_b. Finally the interaction energy can be put as:

$$F_{d-b} = \frac{1}{4\pi}\int d^2\mathbf{r}\mathbf{E}_r \cdot \mathbf{E}_b$$

The electric fields can be easily evaluated with Gauss theorem. The total electrostatic energy per unit cell volume can be finally put as:

$$f_{lr} = -\delta\phi^2 \tilde{R}_c^2 \left[-\pi\nu^2 \log\sqrt{\nu} - \frac{\pi}{2}\nu^2 + \frac{\pi}{2}\nu^3\right]$$

where we have eliminated $\tilde{R}_d = \sqrt{\nu}\tilde{R}_c$ and the "background" charge density $\overline{\phi} - \phi_A = \nu\delta\phi$ to ensure charge neutrality.

The total surface energy is given by:

$$f_\sigma = 2\pi \tilde{R}_d^2 h \frac{N_r}{V} = \frac{2\sqrt{\nu}}{\tilde{R}_c}$$

By optimizing with respect to the cell radius R_c, one finally obtains the mixing energy in the form Eq.(2.19) with the function $u\left(\nu\right)$ given by:

$$u\left(\nu\right) = 3\nu^{1/3}\left[-\pi\nu^2 \log\sqrt{\nu} - \frac{\pi}{2}\nu^2 + \frac{\pi}{2}\nu^3\right]^{1/3}$$

mentioned in Chapter[3]. With the same methods discussed above, it is possible to easily compute $u\left(\nu\right)$ also for droplets-like inhomogeneities and alternating layers. A detailed derivation has been provided in Ref.[29]

• Two-dimensional systems

In the evaluation of the electrostatic energy in two-dimensional systems with the full 3D Coulomb interaction, Gauss theorem is not useful and one should in principle compute the Coulomb potential ψ generated by the inhomogeneities of all neutral Wigner-Seitz cells and the electrostatic potential generated by the whole background charge density. The latter corresponds to the Coulomb potential of an infinite uniformly charged plane and can be taken as constant in the plane. Because of the global neutrality, the value of the constant does not affect the electrostatic energy and can be put to zero. The inhomogeneity Coulomb potential is the sum of the N contributions from each cell. It is easy to show that one can separate the total electrostatic energy in a self-energy contribution (f_{lr}^{Σ}) and an interaction contribution among different inhomogeneities f_{lr}^{int}. For disks inhomogeneities of size $\tilde{R}_d$ in unit of ξ, the latter contribution can be easily found in the limit in which the domains are far apart *i.e.* $\tilde{R}_d << \tilde{R}_c$, with $\tilde{R}_c$ representing, analogously to three-dimensional systems, the radius of the neutral circular cell. Indeed the disks can be considered as negative point charges at distances $\tilde{R}_c$ and will arrange in a Wigner crystal. The electrostatic energy is given by:[77]

$$F_{lr}^{int} \propto -\alpha \frac{\left[Q_R \, \tilde{R}_d^2 \, \delta\phi^2\right]^2}{\tilde{R}_c} \tag{B.1}$$

Since $\nu = \tilde{R}_d^2/\tilde{R}_c^2$ for the disk geometry and referring to the energy per unit volume one has:

$$f_{lr}^{int} \propto -Q_R^2 \delta\phi^2 \tilde{R}_c \, \alpha \nu^2 \tag{B.2}$$

The Coulomb self-energy of a cell of radius $\tilde{R}_d$ can be evaluated noticing that the cell charge density can be written in the Fourier space as [97]:

$$\delta\phi\left(k\right) = 2\pi\delta\phi\tilde{R}_d^2 \left(\frac{J_1\left(k\tilde{R}_d\right)}{k\tilde{R}_d} - \frac{J_1\left(k\tilde{R}_c\right)}{k\tilde{R}_c} \right)$$

The electrostatic energy per unit volume is then:

$$f_{lr}^{\Sigma} = \frac{Q_R^2}{2\,\pi\,\tilde{R}_c^2} \int \frac{d^2k}{\left(2\,\pi\right)^2} \, \delta\phi(k)^2 \, \frac{2\,\pi}{k}$$

Computing the coulombic self-energy per unit volume in the Fourier-space one obtains:

$$f_{lr}^{\Sigma} = Q_R^2 \delta\phi^2 \tilde{R}_c \, \frac{8}{3} \left[\nu^{\frac{3}{2}} + o\left(\nu^2\right)\right] \tag{B.3}$$

where we have kept the dominant contribution when $\nu \to 0$ ($\tilde{R}_d << \tilde{R}_c$). Comparing with Eq. (B.2), we see that in this limit, the self-energy term dominates the electrostatic energy and the intercell interaction can be neglected. Since the surface energy for a disk is given by:

$$f_\sigma = \frac{2\sqrt{\nu}}{\tilde{R}_c}$$

the geometrical factor of the mixing energy is readily found as:

$$u\left(\nu\right)=\frac{8}{\sqrt{3}}\nu$$

The evaluation of the latter function for stripes inhomogeneities is more complicated and requires a numerical analysis that has been provided in Ref.[52, 53]. Here we would notice that at enough low volume fractions the intercell interaction can be neglected and the mixing energy is again well represented by considering the self-energy of an isolated stripe.

Appendix C

Negative compressibility model in the weak-coupling limit

In Chapter 2, we emphasized that for weak frustration a universal picture can be achieved since the negative compressibility model Eq.(2.7) is formally equivalent to the cusp singularity model once the free energy of the homogeneous phases are expanded quadratically around the two dimensionless densities of the ordinary Maxwell construction. In this appendix we study the validity of the latter expansion. Since for $Q_R << 1$, there is a strong separation between the typical domain size l_d and the bare correlation length ξ, in the following we will refer to a sharp-interface version of the model Eq. (2.7) that can be put as:

$$\widetilde{H}_2^{SH} = \sigma\Sigma + \int d\mathbf{x} \left[\phi^2\left(\mathbf{x}\right) - 1\right]^2 + \frac{Q_R^2}{2} \int d\mathbf{x}' \frac{\left[\phi(\mathbf{x}) - \overline{\phi}\right] \left[\phi(\mathbf{x}') - \overline{\phi}\right]}{|\mathbf{x} - \mathbf{x}'|} \tag{C.1}$$

where σ represents the short-range surface tension of an isolated domain wall. A straightforward minimization of Eq. (C.1) with respect to the dimensionless charge density profile provide the electrochemical constancy equation:

$$-4\phi\left(\mathbf{x}\right)+4\phi\left(\mathbf{x}\right)^{3}-Q_{R}\psi(\mathbf{x})=\overline{\mu} \tag{C.2}$$

where we defined the dimensionless electrostatic potential

$$\psi(\mathbf{x})=Q_{R}\int d\mathbf{x}'\,\frac{\left[\overline{\phi}-\phi(\mathbf{x}')\right]}{|\mathbf{x}-\mathbf{x}'|}$$

and $\overline{\mu}$ is a global chemical potential representing a Lagrange multiplier needed to ensure charge neutrality. To provide an approximated solution of Eq. (C.2), it is convenient to brake up the dimensionless density profile $\phi(\mathbf{x})$ as a distribution $\phi_{MC}(\mathbf{x})=\pm1$ corresponding to the Maxwell construction plus a correction $\delta\phi(\mathbf{x})$ which we wish to compute. Linearizing the cubic term of the chemical potential, one obtains the simple equation:

$$\delta\phi(\mathbf{x})=\kappa_{R}Q_{R}\psi(\mathbf{x})-\overline{\mu} \tag{C.3}$$

where $\kappa_R Q_R$ is basically the coefficient of the linear response for the local theory [32]. κ_R corresponds to the short-range electronic compressibility in dimensionless units evaluated at the Maxwell construction density $\kappa_R=1/8$ reflecting the fact that the linearization in the chemical potential would correspond to a quadratical expansion of the homogeneous phase free energy around the minima of the double-well.

Eq. (C.3) must be solved together with the Poisson equation for the dimensionless electrostatic potential:

$$\nabla^{2}\psi\left(\mathbf{x}\right)=4\pi Q_{R}\left[\phi\left(\mathbf{x}\right)-\overline{\phi}\right] \tag{C.4}$$

A solution of Eq. (C.3) in D-dimensional systems subject to a D-dimensional interaction has been proposed by Muratov [32]. Here both 3D and 2D systems embedded in a 3D-Coulomb interaction will be considered. For simplicity we look for a

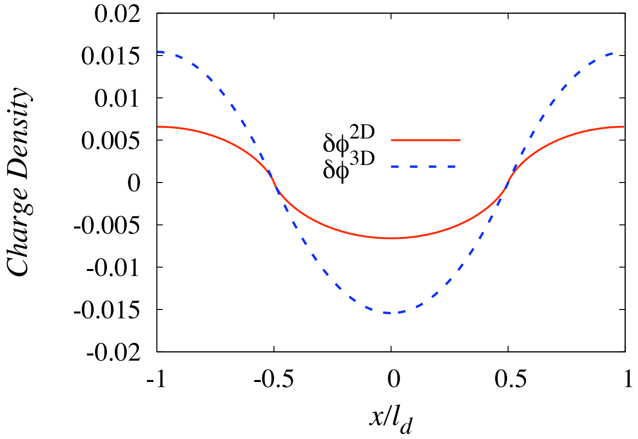

Figure C.1: Behavior of the correction to the Maxwell density profile ϕ_{MC} for $Q_R \sim 0.02$. The dashed blue line is for 3D systems for which $l_s \sim 2l_d$. The red full line indicates the behavior for two-dimensional systems for which the domain size turns out to be $l_d \sim l_s/28$.

layered in 3D and a striped in 2D charge inhomogeneous state and assume the two coexisting phases to have an equal size region that we fix as the typical domain size $\tilde{l}_d$ defined in Chapter [2]. We thus define the Fourier decomposition of the charge density as:

$$\delta\phi(\mathbf{x}) = \frac{1}{2\tilde{l}_d} \sum_{k_n} e^{i\, k_n\, x} \delta\phi_{k_n} \qquad\qquad k_n = \frac{\pi n}{\tilde{l}_d} \tag{C.5}$$

where we recall that lengths are measured in unit of the bare correlation length ξ. In Fourier space the $k = 0$ component in the electrostatic potential can make to vanish by a proper choice of the origin of the potential. At finite momenta it is determined by the "effective" Poisson equation in 2D [see Appendix A] and 3D and reads:

$$\psi(k_n) = -\frac{2^{D-1}\pi Q_R}{|k_n|^{D-1}}\phi(k_n)$$

Finally, one obtains the following momentum space version of Eq. (C.4):

$$\delta\phi(k_n) = \frac{-\phi_{MC}(k_n)}{1 + 2\tilde{l}_s^{D-1}|q_n|^{D-1}} \tag{C.6}$$

where we have inserted the screening length definition in systems with a negative compressibility Eq. (2.16).

In Fig. C.1, we show the correction to the Maxwell density profile at a Coulomb coupling $Q_R \sim 0.02$. For both two- and three-dimensional systems $\delta\phi << 1$ that justifies the linearization of the chemical potential. By requiring $\delta\phi < 0.5 \times 10^{-2}\phi_{MC}$, we find that the approximation is very accurate for $Q_R \sim 0.21$ in two-dimensional systems ($l_d \sim l_s/3$) and $Q_R \sim 0.18$ in three-dimensional systems ($l_d \sim l_s$), thus making the phenomenology of inhomogeneous states in systems with a negative compressibility density region practically identical to systems with a cusp singularity in all the weak coupling regime.

Appendix D

Mesophase separation in systems with long-range forces

In this appendix, we depict qualitatively the effect of general long range forces upon the phase separation mechanism. We consider the free energy expansion introduced in Chapter 2:

$$f_\gamma = \alpha|n - n_c|^\gamma + \beta(n - n_c)^{2\gamma}$$

To address qualitatively, the effect of long-range forces upon the phase coexistence phenomenon on general perspectives it is convenient to fix the global density $\overline{n}$ to the reference density n_c for both $\gamma = 1$ and $\gamma = 2$ where the volume fraction $\nu = 1/2$ and consider the Uniform-Density-Approximation. For a system subject to a general long-range force, the free energy of a mixed state reads:

$$f_{MS} = \frac{1}{2}\left[f_A\left(n_c - \Delta n\right) + f_B\left(n_c + \Delta n\right)\right] + f_\sigma + f_{lr} \tag{D.1}$$

where the density in the coexisting phases have been rearranged in such a way that Δn represents the deviation of the local densities from the average one. In Eq. (D.1), the first term represents what would have been the gain from phase separation without long range forces. Indeed for $\overline{n} = n_c$ the uniform phase f_A and f_B have been defined in such a way that they have zero energy ($f_A(n_c) = f_B(n_c) = 0$). The second term of Eq. (D.1) is the short-range contribution due to the surface energy:

$$f_\sigma = \frac{\sigma}{L} \tag{D.2}$$

where L indicates the typical size of the A, B-phase region $L = V_{A,B}^{1/D}$ being D the system dimensionality. Finally the last term of Eq. (D.1) is the long-range interaction term :

$$f_{lr} = \frac{1}{L^D} g^2 \int d\mathbf{r} d\mathbf{r}' V\left(\mathbf{r} - \mathbf{r}'\right) \Delta n(\mathbf{r}) \Delta n(\mathbf{r}') \tag{D.3}$$

where the interaction kernel $V(\mathbf{r}) = 1/|\mathbf{r}|^x$ and g^2 is a coupling strength. In addition, for the system to have global density n_c we must require $\int \Delta n(\mathbf{r}) = 0$. Finally $\Delta n(\mathbf{r}) = \pm \Delta n$ depending whether one is in a A or B portion of the system. Although the case $x = 1$, corresponding to the Coulomb interaction, and $x = 3$ for which the dipole-dipole interaction affects the phase-coexistence phenomenon are the most interesting, physically, here we will consider a generic x. The long-range interaction term Eq. (D.3) has a very different character depending on whether x is greater or less than the system dimensionality D.

- **The case** $x < D$

In the case $x < D$ the integral Eq. (D.3) can be estimated assuming Δn constant as

$$f_{lr} = g^2 (\Delta n)^2 L^{D-x}$$

In the $L \to \infty$ case the long-range free energy density diverges reflecting the fact that macroscopic phase separation is avoided analogously to the Coulomb interaction. Thus domain patterns on the mesoscopic scale appears. The characteristic scale for meso-phase separation is determined by the competition that arises between the surface cost proportional to the number of domain walls and the long-range effect. It can be put as:

$$L_0 = \left[\frac{\sigma}{g^2(\Delta n)^2}\right]^{1/(D-x+1)}$$

The combined effect of the surface and the long-range effect can be recast in the "mixing" energy term:

$$e_{mix} = 2\left[g^2 \sigma^{D-x}\right]^{1/(D-x+1)} (\Delta n)^{2/(D-x+1)} \tag{D.4}$$

It is an additional energy term to the mixed state free energy that introduces frustration in the phase-coexistence phenomenon.

- **The case** $x > D$

In this situation both the long and short-distance contribution to the integral Eq. (D.3) are singular. This requires the introduction of an additional short-range distance cut-off, with the consequence that the long-range contribution to the free energy comes out:

$$f_{lr} = g^2(\Delta n)^2 \left[c'\, \xi^{D-x} - c\, L^{D-x}\right] \tag{D.5}$$

In this case, macroscopic phase separation is not avoided but it is possible that a mixed state with finite L has lower energy.

D.0.1 The $\gamma = 1$ case

For systems with $\gamma = 1$ the mixed state free energy for "frustrated" systems can be recast as [see Eq. (D.1), (D.4)]:

$$f_{MS}^{\gamma=1} = -\frac{\Delta\mu_c}{2}\Delta n + \frac{1}{2\kappa}\Delta n^2 + 2\left[c\, g^2 \sigma^{D-x}\right]^{1/(D-x+1)} (\Delta n)^{2/(D-x+1)} \tag{D.6}$$

The first term represents the phase separation energy gain, the second term is an energetic cost due to compressibility effects and the last term is the mixing energy. The condition of stability of mixed states reads $f_{MS} < 0$. Depending on whether $x < D-1$ as for example in the case of three-dimensional systems subject to the three-dimensional Coulomb interaction or $D-1 < x < D$, a different behavior occurs. In the case $x < D-1$ indeed, the last term is dominant at small ϕ and combined with the linear term produces an energetic barrier between the homogeneous state ($\Delta n = 0$) and the inhomogeneous state ($\Delta n \neq 0$). The quadratic term ensures stability for large Δn. The transition will be first order with a critical value of the frustrating parameter λ_c.

Antithetically, for $D-1 < x < D$, the absence of the mixing barrier allows for an energetically mixed state no matter how big is the frustration degree. The question that arises is what would be the behavior in the marginal case $x \equiv D-1$. In this situation, indeed, there is a delicate balance between the first and the third terms in Eq. (D.6) which are of the same order. Thus a more involved analysis that accounts for the local variation of the density inside the phase-coexistence region is needed as discussed for the Coulomb interaction case in two-dimensional systems [see Chapter 5].

For long-range interactions with $x > D$ the free energy of a mixed state for the

$\gamma = 1$ case reads:

$$f_{MS}^{\gamma=1} = -\frac{\Delta\mu_c}{2}\Delta n + \frac{1}{2\kappa}\Delta n^2 + \frac{1}{L}\left[\sigma - c\,g^2\,\Delta n^2 L^{D-x+1}\right]$$

where the compressibility κ has been renormalized by the inclusion of the short-distance cutoff term of Eq. (D.5), $\kappa^{-1} \to \kappa^{-1} + 2g^2\,c'\,\xi^{D-x}$. For $x < D+1$ a macroscopic phase separation $L \to \infty$ is not avoided. Still, it is easy to find [98] that a mixed state with large but finite domains of size L, have lower free energy no matter how large is g^2. For $x = D+1$ we are again in a marginal situation. This is realized for two-dimensional systems with dipolar interactions. A detailed analysis of the latter case has been addressed in Ref.[99].

D.0.2 The $\gamma = 2$ case

A straightforward analysis can be provided also for the $\gamma = 2$ case. For the mixed state free energy in the frustrated case $x < D$ we get:

$$f_{MS}^{\gamma=2} = -\frac{|a|}{2}\Delta n^2 + \frac{b}{4}\Delta n^4 + 2\left[c\,g^2\sigma^{D-x}\right]^{1/(D-x+1)}(\Delta n)^{2/(D-x+1)}$$

The mixing energy term is dominant for small Δn and combined with the negative quadratic term produces an energetic barrier similarly to the $\gamma = 1$ case but now it will present independently upon the power law of the long-range force. This separates, in a certain sense, the $\gamma = 1$ and the $\gamma = 2$ case into two distinct classes with different behaviors. This is also evident when referring to the case of $x > D$. Indeed the short-distance cutoff term of Eq. (D.5) adds to the negative compressibility term a that produce the tendency towards phase separation. This leads to a renormalized parameter:

$$a' = a - c' \, g^2 \, \xi^{D-x}$$

that implies a weakening of the tendency towards charge segregation due to long-range forces effects.

Appendix E

Negative compressibility model in the strong coupling limit

In this appendix, we derive the free energy of the modulated phase in the strong-coupling regime. We start by considering the Fourier decomposition of the free energy of a modulated phase introduced in Sec. 3.2:

$$\begin{aligned}\frac{\delta F}{V} &= \frac{1}{V^2}\sum_{\mathbf{k}\neq 0}\phi_{\mathbf{k}}\,\chi^{-1}\left(\mathbf{k}\right)\phi_{-\mathbf{k}} + \\ &+\frac{1}{V^3}\sum_{\mathbf{k}_1,\mathbf{k}_2,\mathbf{k}_3\neq 0} 4\overline{\phi}\phi_{\mathbf{k}_1}\phi_{\mathbf{k}_2}\phi_{\mathbf{k}_3}\delta\left(\mathbf{k}_1+\mathbf{k}_2+\mathbf{k}_3,0\right) + \\ &+\frac{1}{V^4}\sum_{\mathbf{k}_1,\mathbf{k}_2,\mathbf{k}_3,\mathbf{k}_4\neq 0}\phi_{\mathbf{k}_1}\phi_{\mathbf{k}_2}\phi_{\mathbf{k}_3}\phi_{\mathbf{k}_4}\delta\left(\mathbf{k}_1+\mathbf{k}_2+\mathbf{k}_3+\mathbf{k}_4,0\right)\end{aligned} \tag{E.1}$$

Now consider a given set of primitive reciprocal vectors $\{\mathbf{k}\}$, made up of m vectors of magnitude k_0. As discussed in Chapter 3, $m = 2$ for inhomogeneities with charge modulation in one direction, $m = 6$ for a rod-like structure with a triangular reciprocal lattice in the modulation plane and $m = 12$ for a face-centered-cubic reciprocal lattice.

For any set $\{\mathbf{k}\}$ the quadratic term $\propto \phi_{\mathbf{k}}\phi_{-\mathbf{k}}$ of Eq. (E.1) is trivially proportional to $m\,\phi_{k_0}^2$. The evaluation of the third-order term is formally identical to the analysis of the same contribution in the liquid-solid transition [42]. Thus we can follow Chaikin and Lubensky to obtain the latter term. It is clear that the third-order term gives a non-vanishing contribution if triads of vectors that add to zero can be constructed. In the present approximation, the latter triads would correspond to closed equilatelar triangles. Suppose now that in a given set $\{\mathbf{k}\}$, p would be the number of triangles to which each vector belongs. In $\phi_{\mathbf{k}_1}\phi_{\mathbf{k}_2}\phi_{\mathbf{k}_3}$, we have m-choices for $\mathbf{k}_1$, $2p$-choices for $\mathbf{k}_2$ and one choices for $\mathbf{k}_3$ thus yielding a contribution $2\,p\,m\,\phi_{k_0}^3$. The evaluation of the quartic term is more complicated and requires a detailed analysis. For the quartic term one has to evaluate two distinct contributions. The first one, hereafter $f_{4\,1}$, comes from the sets of two and opposite equal vectors while the second one, hereafter $f_{4\,2}$, comes out from the contribution of the non planar diamonds in the reciprocal lattices.

Let us first discuss the first term: for the "diagonal" sets of one and its opposite vector, there are m choices for $\mathbf{k}_1$. Once $\mathbf{k}_1$ is fixed we have 2 choices for both $\mathbf{k}_2$ and $\mathbf{k}_3$ that corresponds to $\mathbf{k}_{2,3} = \pm\mathbf{k}_1$ and a single choice for $\mathbf{k}_4$. However the set with $\mathbf{k}_2 = \mathbf{k}_3 = \mathbf{k}_1$ is avoided by the Kronecker delta. Thus the "diagonal" sets yield a contribution $3m\phi_{k_0}^4$.

The evaluation of the off-diagonal terms is more complicated. In a single set of two $\mathbf{k}$'s with $\mathbf{k}_1$ fixed, one has 3 possible choices for $\mathbf{k}_2$, 2 choices for $\mathbf{k}_3$ and one for $\mathbf{k}_4$ thus yielding a multiplicity 6. The total number of the above sets is given by $m\,(m-2)\,/2$ since $\mathbf{k}_1$ can run over the m vectors while $\mathbf{k}_2$ runs over $(m-2)/2$

vectors. This is because we have to exclude the "diagonal" terms $\mathbf{k}_2 = \pm\mathbf{k}_1$ and have to include the factor 1/2 in order to avoid double-counting. Thus the off-diagonal part yields a contribution $3m\,(m-2)\,\phi_{k_0}^4$ and finally:

$$f_{4\,1} = [3m + 3m\,(m-2)]\,\phi_{k_0}^4$$

The evaluation of $f_{4\,2}$ follows as for the cubic term. We have m-choices for $\mathbf{k}_1$, $3\,q$ choices for $\mathbf{k}_2$ where q is the number of non-planar diamonds to which each vector belongs, 2 choices for $\mathbf{k}_3$ and a single choice for $\mathbf{k}_4$ thus yielding a contribution $6\,q\,m\,\phi_{k_0}^4$. Finally we can write down the free energy of modulated phase in the k_0 approximation and from Eq. (E.1) together with the above arguments, we obtain:

$$\frac{\delta F}{V} = \chi^{-1}\,(k_0)\,m\phi_{k_0}^2 + 8\overline{\phi}\,p\,m\phi_{k_0}^3 + \phi_{k_0}^4\,[3m\,(m-1) + 6qm] \tag{E.2}$$

Bibliography

[1] M. Seul and D. Andelman, Science **267**, 476 (1995).

[2] C. Kittel, Phys. Rev. **70**, 965 (1946).

[3] L. Landau and E. Lifshitz, *Electrodynamics of Continuous Media* (Pergamon, New York, 1984).

[4] T. Ohta and K. Kawasaki, Macromolecules **19**, 2621 (1986).

[5] E. N. Thomas and T. Witten, Phys. Today **21**, 27 (1990).

[6] J. C. Bacri and D. Salin, Endeavor New Ser. **12**, 76 (1988).

[7] L. Landau and E. Lifshitz, Physic. Zeits. Sowjetunion **8**, 153 (1935).

[8] E. L. Nagaev, A. I. Podel'shchikov, and V. E. Zil'bewarg, J. Phys.: Condens. Matter **10**, 9823 (1998).

[9] C. P. Lorenz, D. G. Ravenhall, and C. J. Pethick, Phys. Rev. Lett. **70**, 379 (1993).

[10] *Phase separation in cuprate superconductors*, edited by K. A. Muller and G. Benedek (World Scientific, Singapore, 1992).

[11] *Phase separation in cuprate superconductors*, edited by E. Sigmund and K. A. Muller (Springer-Verlag, Berlin, 1993).

[12] A. Moreo, S. Yunoki, and E. Dagotto, Science **283**, 2034 (1999).

[13] E. L. Nagaev, *Physics of magnetic semiconductors* (MIR, Moscow, 1983).

[14] M. Hennion, F. Moussa, G. Biotteau, J. Rodriguez-Carvajal, L. Pinsard, and A. Revcolevschi, Phys. Rev. Lett. **81**, 1957 (1998).

[15] U. Löw, V. J. Emery, K. Fabricius, and S. A. Kivelson, Phys. Rev. Lett. **72**, 1918 (1994).

[16] C. Castellani, C. Di Castro, and M. Grilli, Phys. Rev. Lett. **75**, 4650 (1995).

[17] S. Ilani, A. Yacoby, D. Mahalu, and H. Shtrikman, Phys. Rev. Lett. **84**, 3133 (2000).

[18] S. Ilani, A. Yacoby, D. Mahalu, and H. Shtrikman, Science **292**, 1354 (2001).

[19] S. H. Pan, J. P. O'neal, R. L. Badzey, C. Chamon, H. Ding, J. R. Engelbrecht, Z. Wang, H. Eisaki, S. Uchida, A. K. Gupta, K.-W. Ng, E. W. Hudson, K. M. Lang, and J. C. Davis, Nature (London) **413**, 282 (2001).

[20] K. McElroy, R. W. Simmonds, J. E. Hoffman, D.-H. Lee, J. Orenstein, H. Eisaki, S. Uchida, and J. C. Davis, Nature (London) **422**, 592 (2003).

[21] K. M. Lang, V. Madhavan, J. E. Hoffman, E. W. Hudson, H. Eisaki, S. Uchida, and J. C. Davis, Nature (London) **415**, 412 (2002).

[22] T. Becker, C. Streng, Y. Luo, V. Moshnyaga, B. Damaschke, N. Shannon, and K. Samwer, Phys. Rev. Lett. **89**, 237203 (2002).

[23] V. J. Emery, S. A. Kivelson, and H. Q. Lin, Phys. Rev. Lett. **64**, 475 (1990).

[24] S. A. Kivelson, V. J. Emery, and H. Q. Lin, Phys. Rev. B **42**, 6523 (1990).

[25] N. Cancrini, S. Caprara, C. Castellani, C. Di Castro, M. Grilli, and R. Raimondi, Europhys. Lett. **14**, 597 (1991).

[26] M. Grilli, R. Raimondi, C. Castellani, C. Di Castro, and G. Kotliar, Phys. Rev. Lett. **67**, 256 (1991).

[27] P. G. J. van Dongen, Phys. Rev. Lett. **74**, 182 (1995).

[28] S. Okamoto, S. Ishihara, and S. Maekawa, Phys. Rev. B **61**, 451 (2000).

[29] J. Lorenzana, C. Castellani, and C. Di Castro, Phys. Rev. B **64**, 235127 (2001).

[30] J. Lorenzana, C. Castellani, and C. Di Castro, Phys. Rev. B **64**, 235128 (2001).

[31] J. Lorenzana, C. Castellani, and C. Di Castro, Europhys. Lett. **57**, 704 (2002).

[32] C. B. Muratov, Phys. Rev. E **66**, 066108 (2002).

[33] L. Zhang, C. Israel, A. Biswas, R. L. Greene, and A. de Lozanne, Science **298**, 805 (2002).

[34] N. M. R. Peres, J. M. P. Carmelo, D. K. Campbell, and A. W. Sandvik, Z. Phys. B **103**, 217 (1997).

[35] S. Larochelle, A. Mehta, N. Kaneko, P. K. Mang, A. F. Panchula, L. Zhou, J. Arthur, and M. Greven, Phys. Rev. Lett. **87**, 095502 (2001).

[36] S. Larochelle, A. Mehta, L. Lu, P. K. Mang, O. P. Vajk, N. Kaneko, J. W. Lynn, L. Zhou, and M. Greven, Phys. Rev. B **71**, 024435 (2005).

[37] J. Lorenzana and G. Seibold, Phys. Rev. Lett. **89**, 136401 (2002).

[38] S. Wakimoto, K. Yamada, J. M. Tranquada, C. D. Frost, R. J. Birgeneau, and H. Zhang, Phys. Rev. Lett. **98**, 247003 (2007).

[39] R. A. Borzi, S. A. Grigera, J. Farrell, R. S. Perry, S. J. S. Lister, S. L. Lee, D. A. Tennant, Y. Maeno, and A. P. Mackenzie, Science **315**, 214 (2007).

[40] M. P. Lilly, K. B. Cooper, J. P. Eisenstein, L. N. Pfeiffer, and K. W. West, Phys. Rev. Lett. **83**, 824 (1999).

[41] S. A. Kivelson, E. Fradkin, and V. J. Emery, Nature (London) **393**, 550 (1998).

[42] P. M. Chaikin and T. C. Lubensky, *Principles of Condensed Matter Physics* (Cambridge University Press, Cambridge, 1995).

[43] C. Honerkamp, Phys. Rev. B **72**, 115103 (2005).

[44] A. A. Koulakov, M. M. Fogler, and B. I. Shklovskii, Phys. Rev. Lett. **76**, 499 (1996).

[45] S. V. Kravchenko, G. V. Kravchenko, J. E. Furneaux, V. M. Pudalov, and M. D'Iorio, Phys. Rev. B **50**, 8039 (1994).

[46] S. V. Kravchenko, W. E. Mason, G. E. Bowker, J. E. Furneaux, V. M. Pudalov, and M.D'Iorio, Phys. Rev. B **51**, 7038 (1995).

[47] M. Y. Simmons, A. R. Hamilton, M. Pepper, E. H. Linfield, P. D. Rose, D. A. Ritchie, A. K. Savchenko, and T. G. Griffiths, Phys. Rev. Lett. **80**, 1292 (1998).

[48] J. P. Eisenstein, L. N.Pfeiffer, and K. W. West, Phys. Rev. Lett. **68**, 674 (1992).

[49] J. P. Eisenstein, L. N. Pfeiffer, and K. W. West, Phys. Rev. B **50**, 1760 (1994).

[50] S. C. Dultz and H. W. Jiang, J. Phys. Soc. Jpn. **72**, 674 (2003).

[51] S. C. Dultz and H. W. Jiang, Phys. Rev. Lett. **84**, 4689 (2000).

[52] C. Ortix, J. Lorenzana, and C. Di Castro, Phys. Rev. B **73**, 245117 (2006).

[53] C. Ortix, *Thesis Laurea* (Rome, University "La Sapienza", 2003).

[54] E. Dagotto, T. Hotta, and A. Moreo, Phys. Rep. **344**, 1 (2001).

[55] J. Burgy, M. Mayr, V. Martin-Mayor, A. Moreo, and E. Dagotto, Phys. Rev. Lett. **87**, 277202 (2001).

[56] M. Fäth, S. Freisem, A. A. Menovsky, Y. Tomioka, J. Aarts, and J. A. Mydosh, Science **285**, 1540 (1999).

[57] J. Schmalian and P. G. Wolynes, Phys. Rev. Lett. **85**, 836 (2000).

[58] G. D. Mahan, *Many Particle Physics, Third Edition* (Plenum, New York, 2000).

[59] J. K. Freericks, E. H. Lieb, and D. Ueltschi, Phys. Rev. Lett. **88**, 106401 (2002).

[60] R. S. Markiewicz, Journal of Physics: Condensed Matter **2**, 665 (1990).

[61] E. L. Nagaev, JETP Lett. **6**, 18 (1967).

[62] M. Y. Kagan, D. I. Khomskii, and M. V. Mostovoy, Eur. Phys. J. B **12**, 217 (1999).

[63] K. I. Kugel, A. L. Rakhmanov, and A. O. Sboychakov, Phys. Rev. Lett. **95**, 267210 (2005).

[64] R. S. Fishman, F. A. Reboredo, A. Brandt, and J. Moreno, Phys. Rev. Lett. **98**, 267203 (2007).

[65] D. M. Ceperley and B. J. Alder, Phys. Rev. Lett. **45**, 566 (1980).

[66] J. van den Brink, G. Khaliullin, and D. Khomskii, Phys. Rev. Lett. **83**, 5118 (1999).

[67] C. Ortix, J. Lorenzana, and C. Di Castro, arXiv:0707.1265 .

[68] C. Ortix, J. Lorenzana, and C. Di Castro, arXiv:cond-mat:0801.0955 .

[69] C. Ortix, J. Lorenzana, M. Beccaria, and C. Di Castro, Phys. Rev. B **75**, 195107 (2007).

[70] A. B. Pippard, *Classical thermodynamics* (University Press, Cambridge, 1964).

[71] L. Landau and E. Lifshitz, *Statistical physics* (Pergamon, New York, 1969).

[72] B. V. Fine and T. Egami, Phys. Rev. B **77**, 014519 (2008).

[73] R. Jamei, S. Kivelson, and B. Spivak, Phys. Rev. Lett. **94**, 056805 (2005).

[74] T. Mertelj, V. V. Kabanov, J. Miranda, and D. Mihailovic, Phys. Rev. B **76**, 054523 (2007).

[75] M. Tarzia and A. Coniglio, Phys. Rev. Lett. **96**, 075702 (2006).

[76] Z. Nussinov, J. Rudnick, S. A. Kivelson, and L. N. Chayes, Phys. Rev. Lett. **83**, 472 (1999).

[77] E. Wigner, Phys. Rev. **46**, 1002 (1934).

[78] P. Schiffer, A. P. Ramirez, W. Bao, and S.-W. Cheong, Phys. Rev. Lett. **75**, 3336 (1995).

[79] C. Zener, Phys. Rev. **82**, 403 (1951).

[80] P. W. Anderson and H. Hasegawa, Phys. Rev. **100**, 675 (1955).

[81] P. G. de Gennes, Phys. Rev. **118**, 141 (1960).

[82] T. Ando, A.B.Fowler, and F.Stern, Rev. Mod. Phys. **54**, 437 (1982).

[83] S. Alexander and J. McTague, Phys. Rev. Lett. **41**, 702 (1978).

[84] M. Tinkham, *Introduction to superconductivity* (McGraw-Hill, New York, 1975).

[85] E. Fradkin and S. A. Kivelson, Phys. Rev. B **59**, 8065 (1999).

[86] R. E. Goldstein, D. J. Muraki, and D. M. Petrich, Phys. Rev. E **53**, 3933 (1996).

[87] D. M. Petrich and R. E. Goldstein, Phys. Rev. Lett. **72**, 1120 (1994).

[88] T. Ohta, A. Ito, and A. Tetsuka, Phys. Rev. A **42**, 3225 (1990).

[89] C. B. Muratov, Phys. Rev. Lett. **78**, 3149 (1997).

[90] B. Kerner and V. V. Osipov, *Autosolitons: A New Approach to Problems of Self-Organization and Turbolence* (Kluwer, Dordrecht, 1994).

[91] C. B. Muratov and V. V. Osipov, Phys. Rev. E **53**, 3101 (1996).

[92] H. Buttner and E. Gerlach, Journal of Physics C Solid State Physics **6**, L433 (1973).

[93] R. K. Kalia and P. Vashishta, Phys. Rev. B **6**, 2655 (1978).

[94] G. Senatore and M. P. Tosi, Il Nuovo Cimento B **56**, 169 (1980).

[95] S. Bustingorry, E. Jagla, and J. Lorenzana, Acta Mater. **53**, 5183 (2005).

[96] W.R.Smythe, *Static and dynamic electricity* (McGraw-Hill, New York, 1975).

[97] J. Shi, S. He, and X. C. Xie, Phys. Rev. B **60**, R13950 (1999).

[98] B. Spivak and S. A. Kivelson, Annals of Physics **321**, 2071 (2006).

[99] B. Spivak and S. A. Kivelson, Phys. Rev. B **70**, 155114 (2004).

[100] E. Witten, Adv. Theor. Math. Phys. **2**, 253 (1998)

[101] V. A. Kazakov, A. Marshakov, J. A. Minahan and K. Zarembo, JHEP **0405**, 024 (2004)

[102] I. R. Klebanov, arXiv:hep-th/0009139.

[103] J. M. Maldacena, Adv. Theor. Math. Phys. **2**, 231 (1998) [Int. J. Theor. Phys. **38**, 1113 (1999)]

[104] S. S. Gubser, I. R. Klebanov and A. M. Polyakov, Phys. Lett. B **428**, 105 (1998)

[105] N. Beisert, C. Kristjansen and M. Staudacher, Nucl. Phys. B **664**, 131 (2003)

[106] J. A. Minahan and K. Zarembo, JHEP **0303**, 013 (2003)

[107] A. Rej, D. Serban and M. Staudacher, JHEP **0603**, 018 (2006)

[108] K. Zarembo, Phys. Lett. B **634**, 552 (2006)

[109] S. Frolov and A. A. Tseytlin, Phys. Lett. B **570**, 96 (2003)

[110] M. Beccaria and C. Ortix, JHEP **09**, 016 (2006),

[111] M. Beccaria, C. Ortix Theor. Math. Phys. **152**, 1060 (2007)

[112] N. Beisert, V. Dippel and M. Staudacher, JHEP **0407**, 075 (2004)

[113] J. A. Minahan, arXiv:hep-th/0603175.

[114] E. A. Yuzbashyan, B. L. Altshuler, B. S. Shastry, J. Phys. A **35**, 7525-7547 (2002),

[115] E.H. Lieb and F.Y. Wu, Phys. Rev. Lett. **20**, 1445 (1968); *Erratum*, ibid. **21**, 192 (1968).

[116] L. Hulthén, Über das Austauschproblem eines Kristalles, Arkiv för Matematik, Astronomi och Fysik **26A**, 1 (1938).

[117] G. Feverati, D. Fioravanti, P. Grinza and M. Rossi, JHEP **0605**, 068 (2006)

[118] W. Metzner and D. Vollhardt, Phys. Rev. B **39**, 4462 (1989).

[119] R. Roiban, A. Tirziu and A. A. Tseytlin, Phys. Rev. D **73**, 066003 (2006)

[120] A. Dhar and B. Shastry, Phys. Rev. Lett. **85**, 2813 (2000).

[121] B. Sutherland, Phys. Rev. Lett. **74**, 816 (1995);

[122] N. Beisert, J. A. Minahan, M. Staudacher and K. Zarembo, JHEP **0309**, 010 (2003)

[123] J. Plefka, arXiv:hep-th/0507136.

Publications

- **"Frustrated phase separation in two-dimensional charged systems"**
  C. Ortix, J. Lorenzana and C. Di Castro ;
  Phys. Rev. B **73**, 245117 (2006), Virtual Journal of Nanoscale Science and Technology **14**, 2 (2006)
- **"Strong coupling anomalous dimensions in $N = 4$ super Yang-Mills"**
  M. Beccaria and C. Ortix ;
  Journal of High Energy Physics **09**, 025 (2006)
- **"Screening effects in Coulomb frustrated phase separation"**
  C. Ortix, J. Lorenzana, M. Beccaria and C. Di Castro ;
  Phys. Rev. B **75**, 195107 (2007)
- **"Ads/CFT duality at strong coupling"**
  M. Beccaria and C. Ortix ;
  Theoretical and Mathematical Physics **152**, 1060 (2007)
- **"Coarse grained models in Coulomb-frustrated phase separation"**
  C. Ortix, J. Lorenzana and C. Di Castro ;
  arXiv:0707.1265 (*submitted to Journal of Physics: Condens. Matter*)
- **"Phase diagram for Coulomb-frustrated phase separation in systems with negative short-range compressibility"**
  C. Ortix, J. Lorenzana and C. Di Castro ;
  arXiv:0801.0955 (*submitted to Phys. Rev. Lett.*)

Acknowledgments

Completing this doctoral work has been a rich experience and I would like to express my gratitude to my advisors Prof. Matteo Beccaria, Prof. Carlo Di Castro and Dr. José Lorenzana. for guiding my first steps in scientific research, for always having time for discussions and for the great deal of physics I learned from. I wish also to acknowledge Prof. Walter Metzner for his co-report on this thesis.

There are countless others I wish to express my gratitude to but I owe particular thanks to all my "roman" friends, especially to my housemate Valerio. My mother and my brother Francesco are my guiding lights. They provided me constant encouragement and advices particularly during my hardest time. Finally, a special thank to Marcella. She has seen my best and my worst and she always supported me to the end.